SAPIENZA
UNIVERSITÀ DI ROMA

Department of Physiology and Pharmacology “Vittorio Erspamer”

DOCTOR OF PHILOSOPHY IN PHARMACOLOGY AND TOXICOLOGY

XXXVII cycle

New Strategies Leveraging ALIAmides in Acute and Chronic Anti-inflammatory Therapies

Ph.D candidate:

IRENE PALENCA

Ph.D supervisor:

Prof. GIUSEPPE ESPOSITO

2021-2024

SUMMARY

ABBREVIATIONS

5-ASA, 5-aminosalicylic-acid

ACE2, Angiotensin-Converting Enzyme 2

Ade, Adelmidrol

AEA, anandamide

ALIAmides, (Autacoid Local Injury Antagonist)mides

AOM, azoxymethane

APCs, antigen-presenting cells

ARDS, Acute respiratory distress syndrome

BALF, Broncho-alveolar lavage fluid

CB1, cannabinoid receptors 1

CB2, cannabinoid receptors 2

CD, Chron's Disease

CMC, carboxymethylcellulose

COX-2, cycloxigenase-2

CRC, Colorectal Cancer

DAB, 3,30-diaminobenzidine

DAI, Disease Activity Index

DMEM, Dulbecco-Modified Eagle's Medium

DNBS, dinitrobenzene sulfonic acid

DSS, dextran sodium sulfate

DTT, dithiothreitol

EIS, endoscopic injury score

ELISA, Enzyme-linked immunosrbent Assay

EtOH, Ethanol

GI, Gastrointestinal

H&E, Hematoxylin & Eosin

HA, Hyaluronic Acid

HEPES, 4-(2-hydroxyethyl)-1-piperazineethanesulfonic acid

HRP, horseradish peroxidase

HYAL-1, Hyaluronidase-1

IBD, Istinal Bowel Disease

IC/PBS, interstitial cystitis/painful bladder syndrome

ICAM1, Intercellular Adhesion Molecule 1

IFN-γ, Interferon- γ

IL-1β, Interleukin-1β

IL-6, Interleukin-6

iNOS, Inducible nitric oxide synthase

LPS, Lipopolysaccharide

m-PGA, micronized- N-palmitoyl-D-glucosamine

MDA, Malonyl dialdehyde

MERS-CoV, Middle East respiratory syndrome coronavirus

MPO, Myeloperoxidase

NAPE, N-acylphosphatidylethanolamine phospholipase D

NAPE-PLD, N-Arachidonoyl-phosphatidylethanolamine phospholipase D

NFκB, Nuclear factor kappa-light-chain-enhancer of activated B cells

NLRP3, NOD-, LRR- and pyrin domain-containing protein 3

NO, Nitrix oxide

PBS, Phosphate buffer saline

PEA, Palmitoylethanolamide

PFA, Paraformaldehyde

PGE_2 Prostaglandin E2

pLP, Lactobacillus paracasei subsp. paracasei F19

pNAPE-LP, engineered NAPE-PLD-expressing Lactobacillus paracasei F19

PPARs, Peroxisome proliferator-activated receptors

ROS, Reactive oxygen species

RT, Room Temperature

SARS-CoV-2, Severe acute respiratory syndrome coronavirus 2

SDS, Sodium-dodecylsulfate

SP, Spike Protein

TLR4, Tool like receptor 4

TNF-α, Tumor necrosis factor - α

UC, Ulcerative Colitis

VEGF, Vascular Endothelial Growth Factor

ZO-1, Zonula Occludens one

GENERAL ABSTRACT

This thesis examines innovative approaches to enhance the anti-inflammatory and antiproliferative potential of ALIAmides, bioactive lipids with promising roles in modulating physiological and pathological inflammatory responses. ALIAmides, particularly Palmitoylethanolamide (PEA) and novel compounds like N-palmitoyl-D-glucosamine (PGA) and adelmidrol, exert significant anti-inflammatory effects primarily through PPAR-α activation, which suppresses pro-inflammatory cytokines and enhances anti-inflammatory and antioxidant gene expression. However, pharmacokinetic limitations, including poor bioavailability, restrict their therapeutic application. This research addresses these challenges by investigating novel delivery systems and synthetic alternatives in murine models of inflammatory bowel disease (IBD), colorectal cancer (CRC), and SARS-CoV-2-induced lung inflammation. To optimize ALIAmide administration, micronized PGA (m-PGA) and adelmidrol were formulated to improve absorption and efficacy, with m-PGA tested in a DNBS (dinitrobenzene sulfonic acid)-induced colitis model to evaluate its impact on inflammation during both acute and resolution phases. In addition, m-PGA was investigated for its antiproliferative properties in a colorectal cancer model induced by AOM + DSS (azoxymethane + dextran sodium sulfate), focusing on its effects on inflammatory markers, tumor size, and cellular proliferation. To further enhance targeted delivery, an engineered strain of Lactobacillus paracasei F19 (pNAPE-LP) was developed, capable of biosynthesizing PEA at the site of inflammation in response to palmitate supplementation, with its efficacy assessed in a murine model of SARS-CoV-2-induced lung inflammation. A novel adelmidrol-hyaluronic acid rectal gel was also evaluated in a murine colitis model and ex vivo in human biopsy samples for its potential to reduce inflammation and protect mucosal integrity. The m-PGA demonstrated significant anti-inflammatory effects in the colitis model, reducing cytokine expression and improving histological scores in both acute and resolution phases. In the CRC model, m-PGA inhibited tumor proliferation, reduced inflammation, and showed marked improvements in tissue integrity. The adelmidrol-hyaluronic acid gel (Ade/HA) produced similar anti-inflammatory effects, effectively reducing pro-inflammatory markers and preserving mucosal integrity. Notably, pNAPE-LP in the lung inflammation model showed

promising results in mitigating inflammatory cell infiltration, preserving alveolar structure, and downregulating ACE-2 expression, indicating its potential as an adjunctive therapy for SARS-CoV-2-related respiratory distress.

The results underscore the potential of ALIAmides as versatile agents for managing inflammation through both oral and topical formulations. The findings support the hypothesis that m-PGA and adelmidrol can provide effective anti-inflammatory and antiproliferative benefits in IBD and CRC by modulating PPAR-α pathways, offering therapeutic advantages with fewer side effects than traditional treatments. The engineered pNAPE-LP strain represents a groundbreaking approach to in situ drug delivery, capable of enhancing bioavailability while minimizing systemic exposure.

This research suggests exciting directions for optimizing ALIAmide-based therapies through pharmaceutical and biotechnological innovations and contributes to advancing anti-inflammatory strategies, positioning ALIAmides as promising candidates for novel therapies in chronic inflammation and cancer.

INTRODUCTION

1. Aliamides: new therapeutic and adjuvants perspectives with anti-inflammatory and antiproliferative properties

ALIAmides (Autacoid Local Injury Antagonist), represent a class of bioactive lipids that play a significant role in modulating physiological and pathological responses in our body. These molecules are derived from the biosynthesis of a lipid precursor known as N-acylphosphatidylethanolamine phospholipase D (NAPE), which is primarily produced by cellular membranes in response to inflammatory or injurious stimuli (D'Amico R. et al., 2020).

The key enzyme involved in this biosynthesis is N-Arachidonoyl-phosphatidylethanolamine phospholipase D (NAPE-PLD), which catalyzes the hydrolytic cleavage of NAPE, ultimately releasing ALIAmides as the final product.

When an inflammatory response is triggered, cells such as macrophages, mast cells, and endothelial cells become activated, leading to the enhanced expression of inflammatory mediators. The mechanism of action of ALIAmides operates primarly as a response to inflammatory or injurious stimuli. These lipid-derived signaling molecules are generated in the body under conditions of stress, particularly when tissues are compromised or inflamed (D'Amico R. et al., 2020; Della Rocca G, Re G. et al., 2022).

These molecules exert their effects through specific receptors, predominantly the peroxisome proliferator-activated receptors (PPARs) (Lo Verme J. et al., 2005) and indirectly activates cannabinoid receptors 1 and 2 (CB1 and CB2) through inhibiting the degradation of the endocannabinoid, anandamide (AEA), a phenomenon known as the '*entourage effect'* (Re G. et al., 2007; Di Marzo V. et al., 2001; Rankin L, Fowler C.J., 2020; Baggiato S. et al., 2019) PPARs, particularly PPAR-α and PPAR-γ, mediate various metabolic and inflammatory responses (Korbecki J. et al., 2019; Yang XY et al., 2008).

Activation of PPARα initiates a cascade of molecular events that suppress pro-inflammatory cytokine production and promote the expression of genes associated with anti-inflammatory and antioxidant effects. This modulation is particularly relevant in the context of chronic inflammatory diseases, where excessive inflammation contributes to tissue damage and tumorigenesis. Furthermore, PPARα agonism has been implicated in inhibiting cell cycle progression and inducing apoptosis in various cancer cell lines, underlining its potential as a therapeutic target in oncology. Anti-inflammatory effects of PPAR-α agonists involve the trans-repression of pro-inflammatory transcription factors such as NFκB, leading to an inhibition of the release of inflammatory cytokines such as tumor necrosis factor α (TNF-α) and interleukins 1β and 6 (Grabacka M. et al., 2021; Clayton P. et al., 2021). Palmitoylethanolamide (PEA, *N*-hexadecanoylethanolamide) is an endogenous and widely investigated compound belonging to the family of ALIAmides. PEA exerts a wide range of anti-inflammatory effects, downregulating inducible nitric oxide synthase (iNOS), cycloxigenase-2 (COX-2), tumor necrosis factor-α (TNF-α) expression, NFκB and Tool like receptor 4 (TLR4) signaling pathways, with downstream regulation of pro-inflammatory cytokines and immune cell infiltration in inflamed tissues (Clayton P. et al., 2021; Del Re A. et al., 2021). PEA anti-inflammatory effects have been tested in several *in vitro* and *in vivo* models of colitis, as well as gastrointestinal biopsies from human patients with inflammatory bowel disease (IBD) and functional dyspepsia (Esposito G. et al., 2021; Sarnelli G. et al., 2021). ALIAmides, especially PEA, have exhibited an excellent safety profile across various preclinical and clinical studies, with few reported adverse effects. As a result, these molecules stand out as promising candidates for diverse therapeutic applications.

2. Pharmacokinetic Limits of ALIAmides and Optimization of Formulations

The pharmacokinetic limitations of ALIAmides, specifically their poor absorption and limited bioavailability due to their high lipophilicity, present challenges in maximizing their therapeutic potential. Moreover, the first-pass metabolism can significantly dimmish the compound's systemic availability, leading to reduced therapeutic effects (Bilia A.R. et al., 2017; Petrosino S. et al., 2018). Despite demonstrating favorable pharmacological properties, these compounds struggle to enter systemic circulation efficiently. The

suboptimal absorption rates are attributable to various factors, including molecular structure, solubility, and gastrointestinal stability. As a result, the limited bioavailability necessitates the administration of higher doses to attain effective physiological responses, which may not only increase the risk of adverse effects but also elevate healthcare costs. Furthermore, the inefficacy in achieving adequate plasma concentrations means that the anticipated therapeutic benefits might remain unfulfilled, leading to a potential misunderstanding of the compounds' effectiveness in clinical settings. Higher required dosages can also complicate treatment regimens and patient adherence, as individuals may be reluctant to engage in prolonged therapeutic measures that appear ineffective or burdensome (Petrosino S. et al., 2018).

Two primary approaches can be explored to overcome these pharmacokinetic limitations: (1) the development of novel pharmaceutical formulations that improve the delivery and absorption of ALIAmides, and (2) the design of synthetic or semi-synthetic molecules with similar therapeutic effects but superior pharmacokinetic properties.

2.1 Novel Pharmaceutical Formulations

Innovative drug delivery technologies offer an opportunity to enhance the pharmacokinetics of ALIAmides without altering their chemical structure. Techniques such as micronization, nanoencapsulation, or the use of advanced drug delivery systems like liposomes and solid lipid nanoparticles can improve the solubility and absorption of ALIAmides (Leleux J, Williams R.O., 2014; Takano R. et al., 2008; Rao S. et al., 2011; Petrosino S. et al., 2018; Del Re A. et al., 2021). These strategies could enhance bioavailability, allowing for more efficient drug uptake and prolonged therapeutic action, especially in inflammatory tissues. By optimizing the formulation, the therapeutic potential of ALIAmides can be maximized, reducing the frequency of dosing and improving patient compliance. Among the various techniques available to enhance drug pharmacokinetics, micronization has emerged as a superior choice for improving the properties of aliamides, offering distinct advantages over other methods. By breaking down the particles to a finer scale, micronization allows for more efficient absorption in the gastrointestinal tract, thus potentially improving the therapeutic efficacy of aliamides in both acute and chronic inflammatory states. Compared to alternative approaches, such as nanoparticle formulation or the use of solubilizing agents, micronization is a simpler, more cost-effective technique. While

nanotechnology-based strategies may offer further improvements in drug delivery, they often involve complex processes, higher production costs, and potential issues related to stability and toxicity. On the other hand, micronization offers a balance between feasibility and effectiveness, enhancing the pharmacokinetics without introducing significant formulation complexities. Additionally, micronization retains the integrity of aliamides, ensuring that their functional properties remain intact while improving their pharmacokinetic performance. This makes micronization particularly suitable for aliamides, whose anti-inflammatory effects rely on maintaining their bioactive structure.

Another particularly promising approach involves leveraging bacterial engineering to develop genetically modified bacteria capable of biosynthesizing ALIAmides directly at the site of inflammation (Fooladi S. et al., 2023). By engineering bacteria to produce ALIAmides in situ, this approach could ensure localized drug delivery, thus improving therapeutic efficacy while minimizing systemic exposure and side effects. The bacteria could be designed to colonize inflamed tissues, releasing ALIAmides where they are most needed, thereby enhancing bioavailability and reducing the need for high systemic doses. This biotechnological innovation represents a groundbreaking method for improving the pharmacokinetics of ALIAmides while simultaneously ensuring targeted therapeutic action (Leyang W. et al., 2022).

2.1.1 engineered NAPE-PLD-expressing Lactobacillus paracasei F19 (pNAPE-LP)

By engineering Lactobacillus paracasei subsp. paracasei F19 (pLP) with the human N-acylphosphatidylethanolamine-specific phospholipase D (NAPE-PLD) gene, we aimed to develop an in situ probiotic drug-delivery system capable of selectively releasing PEA in the gastrointestinal (GI) tract, activated by ultra-low doses of exogenous palmitate (Esposito G. et al., 2021; Esposito G. et al., 2021). Previous *in vivo* studies demonstrated that Lactobacillus F19 survived effectively throughout the human GI tract and was found in significant numbers in stool samples from 100% of the subjects (Mättö J. et al., 2006;Crittenden R. et al., 2002). Lactobacilli can survive the GI tract and colonize the large intestine, where they are part of the endogenous microflora. Recognized as safe (GRAS) for human consumption, they are ideal carriers for delivering therapeutic molecules to the large intestine.

2.2 Synthetic or Semi-synthetic Molecules

The design and synthesis of new synthetic or semi-synthetic molecules that mimic the therapeutic actions of ALIAmides while possessing enhanced pharmacokinetic properties is a promising avenue for addressing the limitations of natural ALIAmides. By modifying their molecular structure, these compounds can improve solubility, metabolic stability, and overall bioavailability, leading to better absorption and controlled distribution. This can result in more predictable and sustained therapeutic effects while retaining the anti-inflammatory benefits of ALIAmides. Such modifications allow for fine-tuning of pharmacokinetics without compromising the ability to modulate key inflammatory pathways. As a result, these engineered analogs can offer more effective treatments with fewer side effects and more convenient dosing regimens. The exploration of synthetic and semi-synthetic molecules represents a significant opportunity for developing next-generation anti-inflammatory therapies. By leveraging modern medicinal chemistry techniques, researchers can design compounds that maintain the efficacy of ALIAmides while addressing their pharmacokinetic challenges, ultimately leading to more effective and better patients compliance for inflammatory diseases.

2.2.1 N-palmitoyl-D-glucosamine (PGA)

N-palmitoyl-D-glucosamine (PGA) is a naturally occurring fatty acid amide derived from glucosamine and palmitic acid. This molecule has garnered significant attention due to its potential therapeutic applications. PGA exhibits promising anti-inflammatory properties by modulating various pathways involved in the inflammatory response. It is known to inhibit the production of pro-inflammatory cytokines and chemokines, thus reducing inflammation in various tissues. Moreover, PGA's ability to interact with cellular signaling pathways positions it as a potential candidate for managing chronic inflammatory diseases such as arthritis, inflammatory bowel disease, and others (Iannotta M. et al., 2021; Della Rocca G. et al., 2023; Cordaro M. et al., 2019; Palenca I. et al., 2022; Palenca I. et al., 2024).

2.2.2 Adelmidrol

Adelmidrol is an N-acyl derivative of palmitic acid. The structural modification includes a hydroxethyl group that enhances its solubility and bioavailability. This unique structure is key to its interaction with biological membranes and cellular targets. Adelmidrol has been shown to downregulate the expression of pro-inflammatory cytokines such as TNF-α, IL-1β, and IL-6. By inhibiting these mediators, it reduces the inflammatory response, which is particularly beneficial in chronic inflammatory diseases. 2. It also inhibits inducible nitric oxide synthase (iNOS), leading to reduced nitric oxide (NO) production. Elevated levels of NO are associated with inflammatory processes, and its reduction helps mitigate tissue damage. The anti-inflammatory properties of adelmidrol make it a potential candidate for treating diseases like rheumatoid arthritis, inflammatory bowel disease, and chronic pain syndromes (Guida F. et al., 2022; Fusco R. et al., 2020; Di Paola R. et al., 2016; Impellizzeri D. et al., 2024; Del Re A. et al., 2022; Palenca I. et al., 2023).

During my doctoral journey, I focused on testing new synthetic and semi-synthetic molecules, in particular micronized PGA (m-PGA) and Adelmidrol, with the potential for pharmacological efficacy and an improved pharmacokinetic profile compared to endogenous ALIAmides. In addition to exploring synthetic alternatives, I also investigated an innovative formulation derived from the bacterial engineering of NAPE-PLD-expressing Lactobacillus paracasei F19 (pNAPE-LP), able to produce PEA under the boost of ultra-low palmitate supply. This approach aimed to enable effective and efficient biosynthesis of ALIAmides directly at the site of action. By leveraging the unique properties of this engineered bacterium, it was possible to create a targeted delivery system that could enhance the local concentration of ALIAmides in inflamed tissues. In particular, these formulations were tested in the context of acute and chronic inflammatory conditions in the intestinal and pulmonary systems. This research not only sought to develop compounds with superior pharmacological profiles but also aimed to explore novel biotechnological strategies

that could revolutionize the delivery and efficacy of ALIAmides in clinical practice. Through this dual approach, I aimed to contribute to the advancement of anti-inflammatory therapies, offering more effective and patient-friendly treatment options for individuals suffering from inflammatory diseases.

EXPERIMENTAL STUDIES

Background (i)

1 Acute and Chronic Inflammatory Bowel Diseases (IBDs)

1.1 Epidemiology

Intestinal bowel diseases (IBD) encompass a range of gastrointestinal disorders characterized by inflammation of the digestive tract. These conditions can be broadly classified into acute and chronic forms, with acute intestinal bowel diseases typically presenting with sudden onset symptoms, such as diarrhea, abdominal pain, and fever, while chronic intestinal bowel diseases, including Crohn's disease and ulcerative colitis, are marked by persistent or recurrent inflammation leading to long-term complications. The prevalence of IBD is rising globally, with significant variations based on geographic location, age, and ethnicity. In developed countries, the incidence rates of IBD are among the highest, with estimates suggesting that over 1.6 million individuals in the United States and approximately 2.5 million in Europe are affected. Acute intestinal bowel diseases, often related to infections or inflammatory processes, can affect individuals of any age, while chronic forms typically manifest in young adults, usually between the ages of 15 and 35 (Windsor J.W., Kaplan G.G., 2022; Agrawal M., Jess T., 2022). Emerging trends indicate an alarming increase in cases among children and adolescents, necessitating a closer examination of environmental and genetic factors contributing to these disorders.

1.2 Current treatments

Treatment strategies for intestinal bowel diseases aim to induce and maintain remission, alleviate symptoms, and prevent complications. For acute intestinal bowel disease, particularly those caused by infections, treatment often focuses on hydration, electrolyte replacement, and, in some cases, antibiotics or antiparasitics. Dietary modifications may also play a critical role in managing acute symptoms. Management of chronic IBD includes a combination of medications such as: Aminosalicylates (5-ASA): Primarily

used for mild to moderate ulcerative colitis, these agents help reduce inflammation in the bowel. Corticosteroids: Effective in controlling acute flare-ups, they are not recommended for long-term use due to potential side effects. Immunomodulators: Drugs like azathioprine and methotrexate work by suppressing the immune response to reduce inflammation. Biologic therapies: Targeted biologic agents, including anti-TNF and integrin inhibitors, have transformed the treatment landscape for moderate to severe IBD, providing significant symptom relief and promoting mucosal healing (Pithadia A.B., Jain S., 2011). Surgical intervention: In severe cases of chronic IBD, surgical options such as resections or colectomy may be necessary to alleviate symptoms and prevent complications (Maggiori L., Panis Y., 2013).

2 Colorectal Cancer (CRC)

2.1 Epidemiology

Colorectal cancer (CRC) is one of the most common malignancies worldwide, representing a significant public health challenge due to its high incidence and mortality rates. Globally, CRC ranks as the third most diagnosed cancer and the second leading cause of cancer-related deaths, affecting both men and women. The disease primarily arises from the epithelial cells lining the colon or rectum and typically progresses over several years from benign polyps to invasive carcinoma. CRC incidence varies widely across regions, with higher rates observed in developed countries, which is often attributed to lifestyle factors such as diets high in red and processed meats, sedentary behavior, obesity, and alcohol consumption. However, recent trends indicate that CRC rates are rising in younger populations in many parts of the world, particularly in high-income countries, shifting the traditional understanding of risk demographics. Age remains the most significant risk factor, with the majority of cases occurring in individuals over the age of 50. However, screening programs have played a crucial role in early detection and prevention, contributing to declining mortality rates in some populations (Baidoun F. et al., 2021; Patel S.G. et al., 2022).

2.2 Current treatments

Pharmacological treatments play a central role in the management of CRC, especially for patients with advanced or metastatic disease. Over recent decades, the CRC

treatment landscape has evolved significantly, integrating traditional chemotherapeutic agents with targeted therapies, immunotherapies, and adjuvant pharmacological strategies aimed at reducing side effects and enhancing treatment efficacy. These advances have markedly improved survival rates and quality of life, particularly when treatments are tailored to the molecular characteristics of the tumor. Chemotherapy remains a cornerstone in the pharmacological treatment of CRC. Common regimens such as FOLFOX (fluorouracil, leucovorin, and oxaliplatin) and FOLFIRI (fluorouracil, leucovorin, and irinotecan) work by disrupting cancer cell division and inducing apoptosis (Labianca R. et a., 2013; Van Cutsem E. et al., 2014; Kuipers et al., 2015). Targeted therapies have also revolutionized CRC treatment by focusing on specific molecular pathways that drive tumor growth and metastasis. Monoclonal antibodies such as bevacizumab (anti-VEGF) and cetuximab (anti-EGFR) are frequently combined with chemotherapy, allowing for lower doses of chemotherapeutic agents while maintaining or even enhancing efficacy (Willett C.G. et al., 2004; Labianca R. et al., 2013). However, the non-selective nature of chemotherapy often results in significant side effects, including gastrointestinal toxicity, myelosuppression, and neuropathy. This has driven the development of adjuvant pharmacological therapies that can reduce chemotherapy dosages and mitigate these adverse effects. Adjuvant therapies, such as anti-inflammatory agents, probiotics, and antioxidants, are increasingly being studied for their potential to reduce chemotherapy-induced toxicity. For example, the use of PEA and ALIAmides, which act as endogenous anti-inflammatory agents, has shown promise in reducing the inflammatory side effects of chemotherapy, allowing for lower chemotherapeutic dosages without compromising efficacy (Sarnelli G. et al., 2016; Pagano E. et al., 2021).

Aims (i)

The aim of these studies was to evaluate the anti-inflammatory potential of m-PGA administered orally in a mouse model of colitis induced by DNBS (dinitrobenzene sulfonic acid). The aim was to assess its effects during both the acute and resolution phases of inflammation. Additionally, we investigated the effects of PGA in an AOM + DSS (azoxymethane + dextran sodium sulfate)-induced colorectal cancer model, with a focus on its anti-inflammatory and antiproliferative properties, and how these mechanisms influence tumor growth and proliferation. Inflammation plays a critical role in the pathogenesis of both colitis and colorectal cancer, with chronic inflammatory conditions like colitis being a major risk factor for the development of colorectal cancer. Thus, addressing inflammation not only in the acute phase but also during the resolution phase is crucial for reducing disease progression and potential malignant transformation. PGA, as an ALIAmide with known anti-inflammatory properties, offers promise in modulating the inflammatory response and potentially inhibiting tumor proliferation in colorectal cancer models. Furthermore, to explore the broader potential of ALIAmides in treating inflammatory bowel diseases, we assessed the efficacy of a rectally administered gel composed of adelmidrol and hyaluronic acid. This gel was tested in both a murine model of colitis and in an ex-vivo culture of biopsy samples. The objective was to evaluate its anti-inflammatory effectiveness and its protective barrier effect on the mucosal lining, which is crucial in maintaining the integrity of the gastrointestinal tract during inflammation. By investigating both oral and topical formulations of ALIAmides, these studies aim to provide a comprehensive understanding of their therapeutic potential in both inflammation-driven diseases like colitis and colorectal cancer. The findings may support the development of novel, targeted therapies that reduce inflammation, promote mucosal healing, and potentially inhibit tumor growth, with fewer side effects than traditional treatments.

N-Palmitoyl-D-Glucosamine Inhibits TLR-4/NLRP3 and Improves DNBS-Induced Colon Inflammation through a PPAR-α-Dependent Mechanism

Irene Palenca , Luisa Seguella , Alessandro Del Re , Silvia Basili Franzin , Chiara Corpetti , Marcella Pesce , Sara Rurgo , Luca Steardo , Giovanni Sarnelli , and Giuseppe Esposito.

Abstract: Similar to canine inflammatory enteropathy, inflammatory bowel disease (IBD) is a chronic idiopathic condition characterized by remission periods and recurrent flares in which diarrhea, visceral pain, rectal bleeding/bloody stools, and weight loss are the main clinical symptoms. Intestinal barrier function alterations often persist in the remission phase of the disease without ongoing inflammatory processes. However, current therapies include mainly anti-inflammatory compounds that fail to promote functional symptoms-free disease remission, urging new drug discoveries to handle patients during this step of the disease. ALIAmides (ALIA, autacoid local injury antagonism) are bioactive fatty acid amides that recently gained attention because of their involvement in the control of inflammatory response, prompting the use of these molecules as plausible therapeutic strategies in the treatment of several chronic inflammatory conditions. N-palmitoyl-D-glucosamine (PGA), an under-researched ALIAmide, resulted in being safe and effective in preclinical models of inflammation and pain, suggesting its potential engagement in the treatment of IBD. In our study, we demonstrated that micronized PGA significantly and dose-dependently reduces colitis severity, improves intestinal mucosa integrity by increasing the tight junction proteins expression, and downregulates the TLR-4/NLRP3/iNOS pathway via PPAR-α receptors signaling in DNBS- treated mice. The possibility of clinically exploiting micronized PGA as support for the treatment and prevention of inflammation-related changes in IBD patients would represent an innovative, effective, and safe strategy.

Keywords: micronized N-palmitoyl-D-glucosamine; ulcerative colitis; IBD; intestinal inflammation; toll-like receptors; PPARs; NLRP3; intestinal barrier

1. Introduction

Inflammatory Bowel Disease (IBD) is a complex of chronic and relapsing diseases of the gastrointestinal (GI) tract that converges environmental, microbial, immunological, and genetic factors both in humans [1] and dogs [2]. In humans, these heterogeneous GI disor- ders present as two major clinical phenotypes, ulcerative colitis (UC) and Crohn's disease (CD), which are characterized by periods of remission and flare-ups of the disease, in which diarrhea, visceral hypersensitivity, and fever are commonly referred [3]. Acute inflamma- tion markedly impairs intestinal physiology and function, and persistent alterations are often observed after the resolution of intestinal inflammation, consistently suggesting a role for inflammatory effects in generating the symptoms that occur during remission in patients with IBD. These long-term changes involve motility, abnormal secretion, and altered visceral sensation, and no effective treatments are currently available to handle this phase of the disease. In recent decades, IBD has alarming emerged in Western countries, predominantly UC, suggesting that this epidemiological evolution is likely related to the westernization of lifestyle associated with changes in diet, antibiotic use, hygiene status, and microbial exposures [4]. UC primarily involves confluent inflammation of the colonic mucosa and im- pairs the epithelial barrier integrity, and intestinal homeostasis. The consequent abnormal translocation of luminal microbes and their products across the impaired intestinal barrier leads to robust activation of resident macrophages and antigen-presenting cells (APCs), and the massive release of Tumor Necrosis Factor- α (TNF-α), Interleukin-1β (IL-1β), IL-13, IL-9, IL-23, IL-36, and other pro-inflammatory mediators [5]. This acute inflammation is responsible for most alterations in intestinal functions that often persist following the resolution of the acute inflammation process and are frequently observed during remis- sion in patients with IBD. Currently, there are no effective treatments for UC that prevent the inflammation-related acute and long-term intestinal dysfunctions, but only combined pharmacological and nutritional therapies, which encompass assessment of daily caloric intake and periodic measurement of functional capacities. 5-aminosalicylic acid is the first therapeutic approach with corticosteroids and thiopurines. However, the high incidence of side effects,

including hypersensitivity reactions, liver toxicity, immunosuppression, and pancreatitis [5] associated with the increasing number of corticosteroids/thiopurines-resistant UC led to the development of alternative therapeutical strategies that include anti-TNF-α, anti-IL-12/23 p40, and anti-integrin or JAK inhibitors [6]. Biological therapies, such as infliximab and adalimumab, also have limitations mainly related to the reduced compliance for parenteral administration, immunogenicity, and high costs that reduce their clinical application. N-palmitoyl-D-glucosamine (PGA) is a natural amide of palmitic acid and glucosamine that shares the anti-inflammatory properties with its endogenous analog palmitoylethanolamide (PEA) and those of glucosamine [7]. PGA belongs to the ALIAmide family (ALIA, autacoid local injury antagonism), a class of both synthetic and endogenous fatty acid amides that display a wide range of homeostatic effects in response to increased oxidative stress and cell damage, including anti-inflammatory and pain-relieving effects [8]. In particular, PEA has repeatedly been shown to improve clinical and histological signs of colitis in different murine models [9,10]. In line, micronized PGA resulted in being safe (LD50 ≥ 2000 mg/kg) and effective in preclinical models of inflammation and osteoarthritis (OA) pain, taking advantage of particle size reduction that enhances its anti-inflammatory activity [7]. To note, the anti-inflammatory action of PGA might derive from both the amide and monosaccharide portions [11]. In fact, glucosamine improved colitis symptoms in DSS- treated mice by preventing intestinal epithelial cell activation and tight junction proteins expression decrease, with a parallel decrease in the nuclear factor-kappa B (NF-kB) activity and reduced TNF-α and IL-1β release [11,12]. Moreover, oral glucosamine and chondroitin compositions positively impact microbiota composition in the intestine of healthy adults, supporting PGA similar acitivity [13]. Iannotta et al. also reported that micronized PGA acts as a toll-like receptor (TLR)-4 antagonist, thanks to its structural similarity to the lipid A component of lipopolysaccharide (LPS). TLR-4 is involved in activating the nucleotide-binding oligomerization domain leucine-rich repeat and pyrin domain-containing protein 3 (NLRP3) inflammasome complex, which is overactivated in several inflammatory syndromes, including intestinal inflammation, neurodegenerative, and metabolic diseases [14]. NLRP3 inflammasome plays a critical role in inflammatory response as a major component of innate immunity and is involved in exacerbating the mucosal immune response and intestinal epithelial barrier damage during colitis [15]. ALIAmide-mediated

activation of the peroxisome proliferator-activated receptors-α (PPAR- α) counters the NLRP3 activity [16], although whether PGA exerts its anti-inflammatory effects via PPAR-α receptors is still unknown.

In this study, we investigated the effectiveness and the mechanisms of action of micronized PGA in a murine model of colitis induced by the 2,4-dinitrobenzene sulfonic acid (DNBS) and assessed the *in vivo* effects of orally administered micronized PGA on (i) colitis severity, (ii) mucosal inflammation and immune cells infiltration, (iii) release of pro-inflammatory cytokines, and (iv) NLRP3 and TLR-4 intestinal activation in a resolution phase of intestinal inflammation.

2. Materials and Methods

2.1. Animals and Experimental Design

Eight-week-old male C57BL/6J mice (Charles River, Lecco, Italy) (*n* = 50) have been used for the experiments. The procedures included in the experimental plan have been approved by Sapienza University's Ethics Committee. Animal care followed the (Inter- national Association for the Study of Pain) IASP and European Community (EC L358/1 18/12/86) guidelines on the use and protection of animals in experimental research. Colitis groups received a single intracolonic administration of 4 mg DNBS (Sigma Aldrich, St. Louis, MO, USA) in 100 µL of 50% ethanol (Sigma Aldrich, St. Louis, MO, USA) and saline (Thermo Fisher Scientific, Waltham, MA, USA), whereas the vehicle group received a single intracolonic administration of saline and ethanol as described below. Overnight-fasted mice were treated with DNBS on day 0 through a soft cannula (Hugo-Sachs Elektronik, March, Germany) quickly inserted around 3cm away from the anus without anesthetization. DNBS solution was slowly administrated into the colon-rectal tract, and animals were maintained slightly sloped for the entire procedure. Thus, mice were placed back into their cages and kept overnight on a heating pad to aid recovery. Disease activity index (DAI) parameters were daily recorded from day 0 to day 7 to assess colitis severity. Micronized PGA was suspended in carboxymethylcellulose (CMC) (Thermo Fisher Scientific, Waltham, MA, USA) and 1X PBS (Sigma Aldrich, St. Louis, MO, USA), and 200 µL of 30 mg/kg and 100 mg/kg PGA suspension were daily given by a single gavage from days 1 to 6 based on the experimental design [7]. PGA was used in the micronized formulation kindly provided by Epitech Group S.p.A

(Saccolongo, Italy). Micronized formulation of PGA with a smaller particle size overcomes the low water-solubility issue of this compound, increasing its oral absorption and bioavailability. In fact, drug solubility is strongly related to particle size and its reduction leads to an increase in the specific surface area with enhanced solubility and potentially higher bioavailability. PPAR-α antagonist MK886 (Selleck Chemicals, Houston, TX) was dissolved in 1X PBS and given daily at the dose of 10 mg/kg by a single intraperi- toneal (IP) administration (150 µL) from days 1 to Mice were randomly divided into the following groups (*n* = 10 each): (1) vehicle group receiving single intracolonic administra- tion of saline; (2) colitis group; (3) colitis group receiving a daily gavage with 30 mg/kg micronized PGA; (4) colitis group receiving a daily gavage with 100 mg/kg micronized PGA; (5) colitis group receiving a daily gavage with 100 mg/kg micronized PGA associated with daily intraperitoneal administration of 10 mg/kg PPAR-α antagonist MK886. Animals in the vehicle and colitis groups also received a daily gavage of CMC solution in 1X PBS (200 µL) and a daily IP with 1X PBS (150 µL) from days 1 to day 6. Mice were euthanized on day 7 by cervical dislocation; thus, spleen weight and colon length were measured, and blood samples, as well as colon tissues, were collected to conduct histochemical and biochemical analyses as described below. Each experimental group included *n* = 10 mice. All the experiments were performed in triplicate on the distal colon by randomly using N = 5 colon for histological staining and N = 5 colon for immunofluorescence analysis.

2.2. Disease Activity Index (DAI)

The DAI score was used to evaluate the colitis severity and progression during the 7 days of the experimental protocol, according to the criteria developed by Cooper et al. [17]. The scored parameters were: (i) changes in body weight; (ii) stool consistency; (iii) rectal bleeding. DAI score was recorded daily (from day 0 to 7), scores were given depending on the severity of the symptoms, and the results were expressed as cumulative average scores in each experimental group. ZO-1 Mouse Occludin Rabbit NLRP3 Rabbit TLR-4 Rabbit iNOS Mouse

2.3. Histopathological Analyses

Colonic tissues were fixed in 4% paraformaldehyde (PFA) (Thermo Fisher Scientific, Waltham, MA, USA) and cryo-sectioned in 15 µm slices. Slices were stained with

hema- toxylin and eosin (H&E) (Sigma Aldrich, St. Louis, MO, USA) to evaluate the histopatho- logical damage score according to Li et al. [18]. Criteria included: (i) distortion and loss of crypt architecture; (ii) inflammatory cells infiltration; (iii) muscle thickening; (iv) goblet cells depletion; (v) crypts absence.Slices were analyzed with a microscope Nikon Eclipse 80i by Nikon Instruments Europe (Nikon Corporation, Tokyo, Japan), and images were captured at 10× magnification by a high-resolution digital camera (Nikon Digital Sight DS- U1). Cumulative damage scores obtained from each experimental group were expressed as average scores.

2.4. Immunofluorescence Analysis on Colonic Sections

Immunofluorescence analyses were performed on 15 µm colonic slices fixed in ice-cold 4% PFA. Sections were blocked with a solution composed of 1X PBS, 4% Normal Donkey Serum, 0.4% (Merk Millipore, St. Louis, MO, USA) TRITON-100 (Sigma Aldrich, St. Louis, MO, USA), and 1% Bovine Serum Albumin (BSA) (Sigma Aldrich, St. Louis, MO, USA) for 45 min and subsequently incubated at +4 ◦C overnight with primary antibody (Table 1). Slices were then washed with 1X PBS and incubated in the dark at +4 ◦C with fluorescein isothiocyanate-conjugated anti-rabbit (1:1000 dilution *v*/*v*; Abcam, Cambridge, UK) or Texas Red-conjugated anti-mouse (1:500 dilution *v*/*v*, mouse; Abcam, Cambridge, USA). Sections were analyzed with a microscope Nikon Eclipse 80i, and images were captured at 20× and 40× magnification by a high-resolution digital camera (Nikon Digital Sight DS-U1). Results were expressed as relative fluorescence units (RFU) and fluorescence intensity percentage (FI%).

Antibody	**Host**	**Clonality**	**Dilution**	**Brand**
ZO-1	Mouse	Monoclonal	6 microgram w/v	Invitrogen, Thermo Fisher, Waltham, MA, USA
Occludin	Rabbit	Polyclonal	1:100 v/v	Bioss Antibodies, Boston, MA, USA

NLRP3	Rabbit	Polyclonal	1:1000 v/v	Invitrogen, Thermo Fisher, Waltham, MA, USA
TLR-4	Rabbit	Polyclonal	1:150 v/v	Bioss Antibodies, Boston, MA, USA
iNOS	Mouse	Monoclonal	1:1000 v/v	Novusbio, Centennial, CO, USA

Table 1. Primary antibodies used in immunofluorescence analyses on cryo-sectioned colon slides.

2.5. Enzyme-Linked Immunosorbent Assay (ELISA) for IL-1β and PGE2

Enzyme-linked immunosorbent assay (ELISA) for PGE2 and IL-1β (Thermo Fisher Sci- entific, Waltham, MA, USA) was carried out on mouse plasma isolated from blood samples according to the manufacturer's protocol. Absorbance was measured on a microtiter plate reader. PGE2 and IL-1β levels were determined using standard curve methods.

2.6. Statistical Analyses

Results were expressed as the mean ± SD. Statistical analysis was performed using parametric one-way analysis of variance (ANOVA) and multiple comparisons were performed by Bonferroni's post hoc test. *p*-values < 0.05 were considered statistically significant. Data were analyzed by using Graphpad Prism and ImageJ software.

3. Results

3.1. Micronized PGA Improves the Disease Spectrum and Macroscopic Signs of Colitis in a Dose-Dependent Manner through PPAR-α Involvement

The DAI score was significantly increased in the colitis group during the 7 days that followed DNBS administration (7.9 ± 0.141, $p < 0.0001$; Figure 1A), with a parallel colonic shortening (3.83 ± 0.543 cm, $p < 0.0001$; Figure 1B,D) and spleen weight increase (0.153 ± 0.0269 g, $p < 0.05$; Figure 1C) in comparison to the vehicle group. PGA resulted in a dose-dependent improvement of overall colitis hallmarks, leading to a significant decrease in DAI score (4.65 ± 0.354, $p < 0.001$ and 3.07 ± 0.305, $p < 0.0001$ for the 30 mg/kg and 100 mg/kg dose, respectively; Figure 1A), increase in colon length (5.82 ± 0.676 cm and 7.55 ± 0.572 cm, $p < 0.0001$ for 30 mg/kg and 100 mg/kg dose, respectively; Figure 1B), and reduction of spleen weight (0.0897 ± 0.011 g, $p < 0.05$ for 100 mg/kg m-PGA, Figure 1C) as compared to DNBS-treated mice. DAI score, colon length, and spleen weight were com- parable to those in DNBS mice treated with 100 mg/Kg um-PGA and PPAR-α antagonist MK886 (10 mg/kg), suggesting that PGA exerts its beneficial effects on colitis through the selective involvement of PPAR-α receptors.

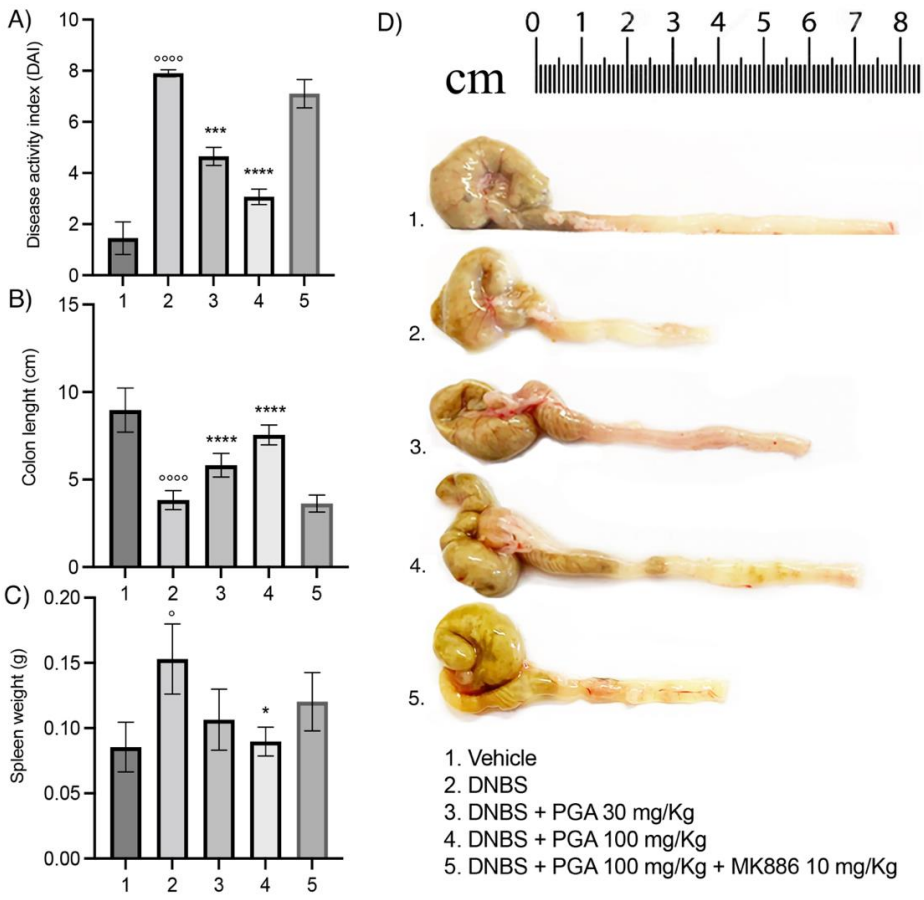

Figure 1. Micronized PGA significantly improves colitis hallmarks in PPAR-α-dependent manner. The effects of oral administration of micronized PGA on (A) DAI score, (B, D) colonic length and (C) spleen weight in DNBS-treated mice. Results are expressed as the mean ± SD of n=5 experiments. ° p< 0.05 *vs*. vehicle; °°°° p< 0.0001 *vs*. vehicle; * p< 0.05 *vs.* DNBS; *** p< 0.001 *vs.* DNBS; **** p< 0.0001 *vs*. DNBS.

3.2. Micronized PGA Ameliorates Mucosal Integrity and Prevents Colonic Histological Damage in DNBS-Treated Mice

DNBS-treated mice maintained a significant impairment of colonic mucosal integrity on day 7 following colitis induction, as demonstrated by the decreased expression of the two tight junction proteins, zonula occludens-1 (ZO-1) and occludin, compared to the vehicle group (25.08 ± 3.196 FI%, $p < 0.0001$ for ZO-1 and 18.23 ± 1.322 FI%, $p < 0.0001$ for occludin; Figure 2A–C). The loss of ZO-1 and occludin was partially prevented by PGA at 30 mg/kg dose (37.4 ± 2.507 FI%, p <0.0001 for ZO-1 and

33.97 ± 2.217 FI%, $p < 0.0001$ for occludin; Figure 2A–C), whereas a marked restoration was observed in colitis mice treated with 100 mg/kg PGA in comparison to the DNBS group (87.8 ± 2.579 FI% and 94.75 ± 3.988 FI%, $p < 0.0001$ for ZO-1 and occludin, respectively; Figure 2A–C). The effects of PGA (100 mg/kg) were reverted by MK886 (10 mg/kg) in colitis mice, further demonstrating the involvement of PPAR-α receptors. Histopathological scores revealed extensive damage in the colonic mucosal barrier of DNBS-treated mice with marked neutrophil infiltration and damaged mucosal integrity compared to vehicle (8.2 ± 0.9189, $p < 0.0001$; Figure 2D,E). Micronized PGA (30 mg/kg) preserved mucosal integrity and counteracted the neutrophil infiltration within the mucosa, although the number of crypts was lower in comparison to the DNBS group (5.5 ± 0.9718, $p < 0.0001$; Figure 2D,E). At the higher dose (100 mg/kg), PGA widely restored mucosal integrity, significantly reducing the neutrophil infiltration, and preserving the architecture and number of the crypts in comparison to the DNBS group (2.5 ± 0.8498, $p < 0.0001$; Figure 2D,E). Co- administration of PGA and MK886 resulted in colonic histological damage comparable to DNBS-group, further supporting that PGA preserves the intestinal mucosal integrity by PPAR-α engagement.

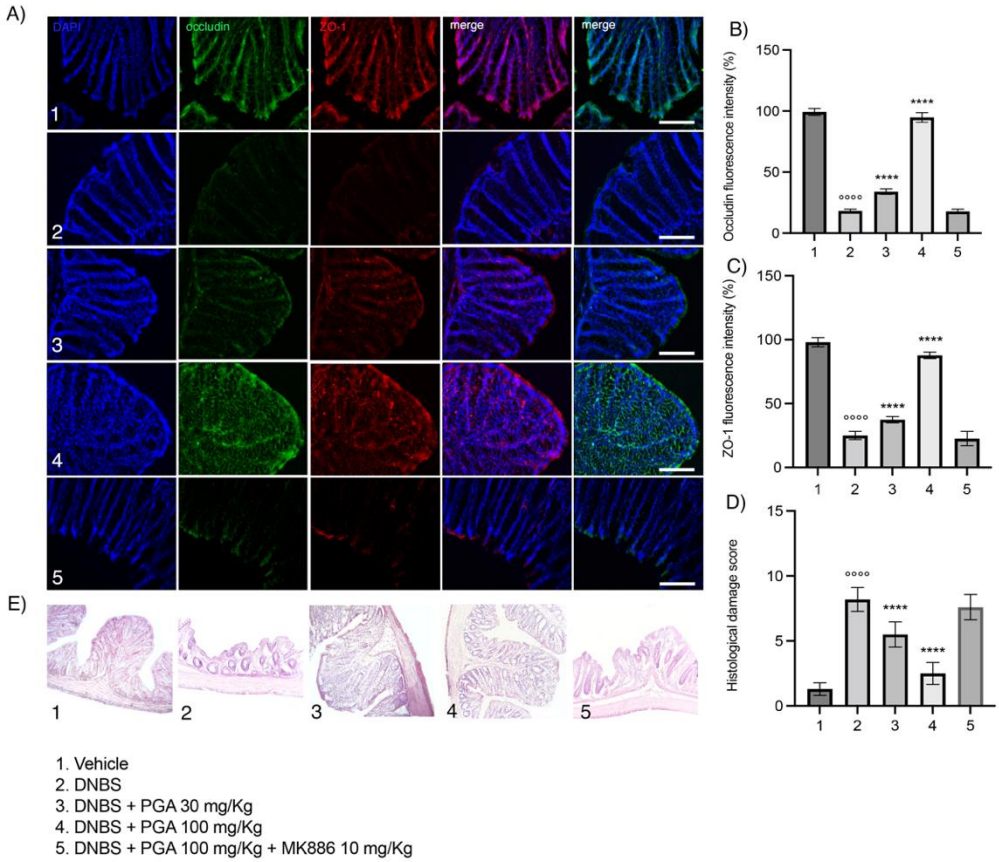

Figure 2. Micronized PGA prevents the loss of tight junction proteins ZO-1 and occludin, and colonic barrier disruption through PPAR-α involvement. (A) Representative images show double-label immunohistochemistry for occludin (green) and ZO-1 (red) in the colon with (B, C) relative quantification. Nuclei were also labeled by DAPI . (E) Representative images of hematoxylin and eosin (H&E)-stained on distal colon sections and (D) relative histological damage score. Results are expressed as the mean ± SD of n=5 experiments. °°°° p< 0.0001 *vs.* vehicle; **** p<0.0001 *vs*. DNBS. Scale bar = 100 µm; magnification 20x.

3.3 Micronized PGA downregulates the TLR-4/NLRP3/iNOS expression and decreases the release of inflammatory mediators in DNBS-treated mice via PPAR-α receptors

Our results show that TLR-4, NLRP3, and iNOS expression was markedly increased within the mucosa following DNBS-induced colitis compared to vehicle (31.38 ± 1.169 RFU, 14.54 ± 1.282 RFU, and 33.93 ± 1.665 RFU for TLR-4, NLRP3 and iNOS, respectively; p<0.0001 for all comparisons; **Fig. 3A-D**). In DNBS mice receiving 30

mg/kg PGA, the expression of TLR-4, NLRP3, and iNOS was significantly reduced (21.08 ± 1.904 RFU, 10.40 ± 1.235 RFU, and 18.26 ± 1.668 RFU for TLR-4, NLRP3 and iNOS, respectively; p<0,0001 for all comparisons; **Fig. 3A-D**) and completely downregulated by PGA 100 mg/kg (14.98 ± 0.712 RFU, 7.54 ± 0.537 RFU, and 12.56 ± 1.105 RFU for TLR-4, NLRP3 and iNOS, respectively; p<0.0001 for all comparisons; **Fig. 3A-D**). According to previous results, 100 mg/kg PGA did not show any effect in DNBS mice co-administered with PPAR-α antagonist MK866 (10mg/kg), supporting that PGA prevents the activation of the TLR4/NLRP3/iNOS pathway through PPAR-α-mediated mechanism. Further, the increased plasma levels of IL-1β and PGE_2 detected in DNBS mice at day 7 after colitis induction (113.1 ± 32.71 pg/ml and 348.5 ± 45.22 pg/ml for IL-1β and PGE_2, respectively; p<0.0001 *vs.* vehicle for both comparisons; **Fig. 3E** and **F**) were significantly and dose-dependently decreased by PGA (62.1 ± 15.09 pg/ml and 36.7 ± 13.12 pg/ml for IL-1β in the lower and higher dose group, respectively; 217.5 ± 61.07 pg/ml and 169.7 ± 37.12 pg/ml for PGE_2 in the lower and higher dose group, respectively; p<0.0001 *vs*. DNBS for all comparisons; **Fig. 3E** and **F**). The anti-inflammatory effect of PGA was significantly inhibited in presence of PPAR-α antagonist MK886 displaying comparable plasma cytokines levels with the DNBS group.

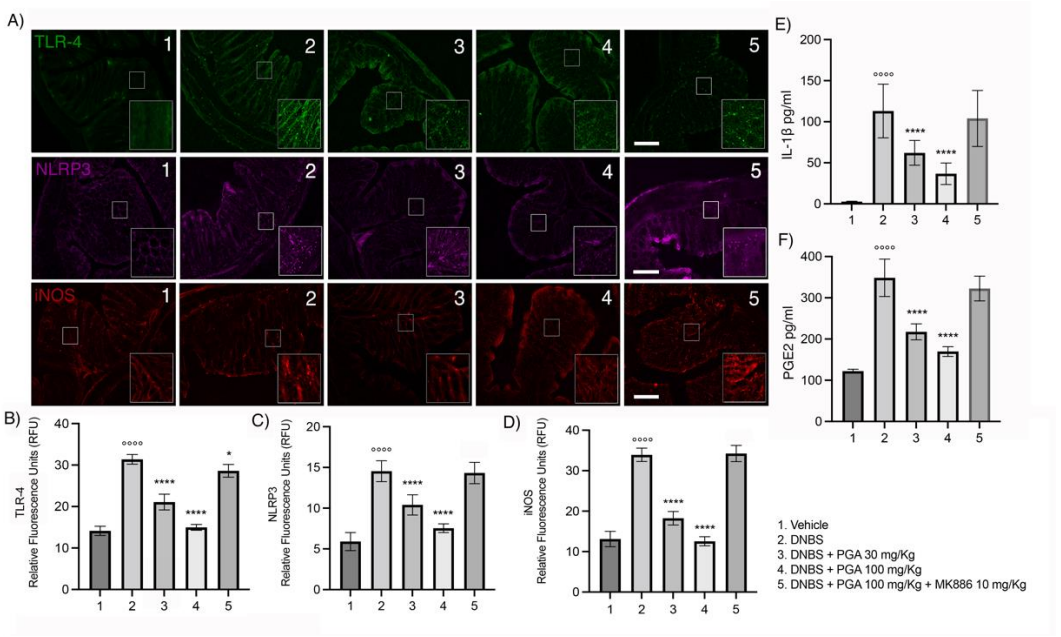

Figure 3. Micronized PGA decreases TLR4/NLRP3/iNOS expression in mice colon and pro-inflammatory cytokines realease in plasma samples throught a selective PPAR-α involvement in

DNBS-treated mice. (A) Immunofluorescence images display TLR-4 (green), NLRP3 (magenta), and iNOS (red) staining and the relative quantification for (B) TLR-4, (C) NLRP3, and (D) iNOS. (E) IL-1β and (F) PGE_2 release in mice plasma. Results are expressed as the mean ± SD of n = 5 experiments. °°°° p<0.0001 *vs.* vehicle; * p<0.05 *vs.* DNBS; **** p<0.0001 *vs.* DNBS. Scale bar = 100 μm; magnification 20x-40x.

4. Discussion

IBD is increasing incidence worldwide and current therapies mainly consist of the chronic administration of immunosuppressive drugs [17]. However, these drugs display a short-term efficacy and they are not suitable as a maintenance therapy due to a variety of systemic adverse reactions [18]. The possibility of exploiting new compounds able to target different steps and pathways of the inflammatory response represents an outstanding challenge for IBD therapy. In the present study, we provided evidence that micronized PGA significantly and dose-dependently counteracts the inflammatory-mediated alteration of the intestinal functions that often persist in the resolution phase of colitis and characterize the remission state of the disease.

Oral administration of micronized PGA improved DAI score and resulted in macroscopic amelioration of intestinal inflammation, as shown by the increased expression of tight junction proteins (ZO-1 and occludin) in the colonic mucosa and lower histological damage score. Similar to the homologous ALIAmide PEA which was successful in the treatment of several colitis models in mice and humans [19, 20, 21, 22, 23], PGA revealed an anti-inflammatory effect through a PPAR-α-dependent mechanism, since in the presence of PPAR-α antagonist MK886, PGA-mediated effects were abolished. We demonstrated that PGA caused a significant decrease of pro-inflammatory mediators, such as iNOS and NLRP3 protein expression in colonic tissues as well as PGE_2 and IL-1β release in plasma.

In agreement with previous studies demonstrating that this ALIAmide negatively regulates TLR-4 signaling enhanced by intestinal inflammation and neuropathic pain [8, 12], our results show that micronized PGA dose-dependently reduced the TLR-4 expression in the colonic mucosa of colitis mice, suggesting that this may contribute to its potent anti-inflammatory activity. The sequel of events triggered by the TLR-4 activation, including NF-kB and NLRP3 activation, and the release fo IL-1β, IL-6, TNF-α, is considered an important event involved in the triggering and the maintenance of a persistent intestinal inflammation during colitis [8, 12] and HIV-1 Tat-induced diahrrea

[24]. In this context, PPAR-α agonists, such as PEA, may mediate TLR-4 down-regulation and efficiently suppress the inflammatory process similar to the evidence observed *in vitro* [13] and in clinical studies [25], in endotoxin induced-uveitis rat model and DSS-induced colitis mice model [19, 26].

In addition to the agonism on PPAR-α, PGA displays structural similarity with the lipopolysaccharide (LPS) component Lipid A, which results in an direct antagonism on TLR-4 [12]. Thus, anti-inflammatory properties of PGA might be related to two distinct mechanisms, although this hypothesis requires further investigations.

Previous studies have shown that PPAR-α activation inhibits immune cell infiltration in colonic mucosa and decreases the expression and release of pro-inflammatory markers typical of IBD, in mice and humans [27, 28]. In line, we have shown that micronized PGA reduces immune cell infiltration within the colonic mucosa and downregulates NLRP3 inflammasome expression via PPAR-α activation. This anti-inflammatory activity probably mediates the ability of PGA to preserve the intestinal epithelial barrier integrity. Actually, NLRP3 plays a key role in exacerbating the mucosal immune response and intestinal epithelial barrier damage [29]. Indeed, NLRP3 overactivation was linked to several inflammatory syndromes, including intestinal inflammation, and the activation of PPAR-α receptors is able to prevent NLRP3 overactivation [27]. Here, we demonstrated that the NLRP3 overexpression is efficiently and dose-dependently counteracted by the oral administration of micronized PGA. This was associated with reduced colitis severity and histological damage of colonic mucosa, supporting that PGA exerts an anti-inflammatory effect by suppressing NLRP3 activity through PPAR-α receptor involvement.

To gain more mechanistic insights, we evaluated the effect of micronized PGA on the expression of TLR-4, which plays an essential role in innate immunity activation by recognizing microbial antigens, such as LPS [30]. The increased translocation of luminal microbe-derived products that follows the epithelial barrier breakdown during intestinal inflammation, leads to higher TLR-4 activation. The downstream sequel events triggered by the TLR-4 activation, including NLRP3 overexpression, iNOS upregulation, and increased release of pro-inflammatory cytokine such as IL-1β and PGE_2 [31, 32], are strictly related to mucosa damage expansion [33], and visceral hypersensitivity associated with the inflammatory process [34, 35]. Oral administration of micronized PGA resulted in the decreased expression of TLR-4 and related downstream pro-inflammatory pathways in DNBS mice, as demonstrated by the parallel downregulation

of iNOS and NLRP3 expression, as well as by the reduced release of IL-1β and PGE_2. This suggests that PGA might act as a safe "multitarget" modulator of intestinal inflammation and prevents the long-term intestinal dyfunction that generally follows the acute phase of colitis.

To note, TLR-4 activation is also associated with visceral hypersensitivity and related behavioral disorders, resulting in episodes of anxiety and recurrent flares of abdominal pain [36, 37, 38]. This latter was also associated with long-term changes in the intestinal microbiota composition, pointing out that compounds able to restore and maintain microbiota homeostasis might provide benefit in IBD patients with recurrent visceral allodynia and hyperalgesia [39]. Interestingly, a bacteria strain deriving from legumes is able to produce PGA (*Rhizobium Leguminosarum*) [40], and successfully colonize the intestinal microenvironment by acting as a xenobiotic metabolizer [38]. This suggests that micronized PGA might have the potential to target distinct pathological aspects of intestinal inflammation by downregulating pro-inflammatory mediators, decreasing the mucosal damage and visceral hypersensitivity, and even restoring the microbiota homeostasis.

Despite further studies being needed to confirm this hypothesis, our results provide the first evidence on the ability of micronized PGA to target colitis through a double mechanism of action: PPAR-α agonism and TLR-4 antagonism [12]. In consideration of the obtained results and the safety profile of micronized PGA, more studies are advised in order to explore the protective effects of micronized PGA in the management of IBD.

Author Contributions: Conceptualization, G.E.; methodology, I.P., L.S. (Luisa Seguella).; software, I.P., L.S. (Luisa Seguella), C.C.; validation, I.P, A.D.L and S.B.F; formal analysis, I.P., A.D.L., C.C., S.R.; investigation, I.P.; resources, S.B.F; data curation, I.P.; writing—original draft preparation, I.P, L.S. (Luisa Seguella) and M.P.; supervision, G.S., G.E., L.S (Luca Steardo); project administration, I.P.; All authors have read and agreed to the published version of the manuscript.

Funding: This research received no external funding

Institutional Review Board Statement: All experimental procedures were approved by Sapienza University's Ethics Committee. Animal care was in compliance with the IASP and European Community (EC L358/1 18/12/86, 30/09/2016) guidelines on the use and protection of animals in experimental research.

Informed Consent Statement: Not applicable.

Data Availability Statement: The data presented in this study are available on request from the corresponding author. The data are not publicly available due to the policy of our research group, we will share data unreservedly on on-line data sharing platform upon request.

Acknowledgments: In Memoriam of Dr. Francesco Della Valle for his profound passion for science and his unparalleled contribution to scientific progress that have given an impulse to pharmaceutical research.

Conflicts of Interest: The authors declare no conflict of interest.

5. References

[1]. Zhang, Y. Z., & Li, Y. Y. (2014). Inflammatory bowel disease: Pathogenesis. World journal of gastroenterology, 20(1), 91–99. Https://doi.org/10.3748/wjg.v20.i1.91.

[2]. Siel, D., Beltrán, C. J., Martínez, E., Pino, M., Vargas, N., Salinas, A., Pérez, O., Pereira, I., & Ramírez-Toloza, G. (2022). Elucidating the Role of Innate and Adaptive Immune Responses in the Pathogenesis of Canine Chronic Inflammatory Enteropathy-A Search for Potential Biomarkers. Animals: An open access journal from MDPI, 12(13), 1645. Https://doi.org/10.3390/ani12131645.

[3]. Kucharzik, T., Koletzko, S., Kannengiesser, K., & Dignass, A. (2020). Ulcerative Colitis-Diagnostic and Therapeutic Algorithms. Deutsches Arzteblatt international, 117(33-34), 564–574. Https://doi.org/10.3238/arztebl.2020.0564.

[4]. Du L, Ha C. Epidemiology and Pathogenesis of Ulcerative Colitis. Gastroenterol Clin North Am. 2020 Dec;49(4):643-654. Doi: 10.1016/j.gtc.2020.07.005. Epub 2020 Sep 25. PMID: 33121686.

[5]. Kobayashi, T., Siegmund, B., Le Berre, C., Wei, S.C., Ferrante M., Shen, B., Bernstein, C.N., Danese, B., Peyrin-Biroulet, L. & Hibi, T. Ulcerative colitis. Nat Rev Dis Primers. 2020 Sep 10;6(1):74. doi: 10.1038/s41572-020-0205-x.

[6]. Gearry, R. B., Barclay, M. L., Burt, M. J., Collett, J. A., & Chapman, B. A. (2004). Thiopurine drug adverse effects in a population of New Zealand patients with inflammatory bowel disease. Pharmacoepidemiology and drug safety, 13(8), 563–567. Https://doi.org/10.1002/pds.926.

[7]. Cordaro, M., Siracusa, R., Impellizzeri, D., D' Amico, R., Peritore, A. F., Crupi, R., Gugliandolo, E., Fusco, R., Di Paola, R., Schievano, C., & Cuzzocrea, S. (2019). Safety and efficacy of a new micronized formulation of the ALIAmide palmitoylglucosamine in preclinical models of inflammation and osteoarthritis pain. Arthritis research & therapy, 21(1), 254. Https://doi.org/10.1186/s13075-019-2048-y.

[8]. Gugliandolo, E., Peritore, A. F., Piras, C., Cuzzocrea, S., & Crupi, R. (2020). Palmitoylethanolamide and Related ALIAmides: Prohomeostatic Lipid Compounds for Animal Health and Wellbeing. Veterinary sciences, 7(2), 78. Https://doi.org/10.3390/vetsci7020078.

[9]. Capasso R, Orlando P, Pagano E, Aveta T, Buono L, Borrelli F, Di Marzo V, Izzo AA.Br J Pharmacol. 2014 Sep;171(17):4026-37. Doi: 10.1111/bph.12759.PMID: 24818658.

[10]. Borrelli F, Romano B, Petrosino S, Pagano E, Capasso R, Coppola D, Battista G, Orlando P, Di Marzo V, Izzo AA.Br J Pharmacol. 2015 Jan;172(1):142-58. Doi: 10.1111/bph.12907.

[11]. Yomogida, S., Kojima, Y., Tsutsumi-Ishii, Y., Hua, J., Sakamoto, K., & Nagaoka, I. (2008). Glucosamine, a naturally occurring amino monosaccharide, suppresses dextran sulfate sodium-induced colitis in rats. International journal of molecular medicine, 22(3), 317–323.

[12]. Iannotta, M., Belardo, C., Trotta, M. C., Iannotti, F. A., Vitale, R. M., Maisto, R., Boccella, S., Infantino, R., Ricciardi, F., Mirto, B. F., Ferraraccio, F., Panarese, I., Amodeo, P., Tunisi, L., Cristino, L., D'Amico, M., Di Marzo, V., Luongo, L., Maione, S., & Guida, F. (2021). N-palmitoyl-D-glucosamine, a Natural Monosaccharide-Based Glycolipid, Inhibits TLR4 and Prevents LPS-Induced Inflammation and Neuropathic Pain in Mice. International journal of molecular sciences, 22(3), 1491. Https://doi.org/10.3390/ijms22031491.

[13]. Del Re, A., Corpetti, C., Pesce, M., Seguella, L., Steardo, L., Palenca, I., Rurgo, S., De Conno, B., Sarnelli, G., & Esposito, G. (2021). Ultramicronized Palmitoylethanolamide Inhibits NLRP3 Inflammasome Expression and Pro-Inflammatory Response Activated by SARS-CoV-2 Spike Protein in Cultured Murine Alveolar Macrophages. Metabolites, 11(9), 592. Https://doi.org/10.3390/metabo11090592.

[14]. Impellizzeri, D., Di Paola, R., Cordaro, M., Gugliandolo, E., Casili, G., Morittu, V. M., Britti, D., Esposito, E., & Cuzzocrea, S. (2016). Adelmidrol, a palmitoylethanolamide analogue, as a new pharmacological treatment for the management of acute and chronic inflammation. Biochemical pharmacology, 119, 27–41. Https://doi.org/10.1016/j.bcp.2016.09.001.

[15]. Clinicopathologic study of dextran sulfate sodium experimental murine colitis. Cooper HS, Murthy SN, Shah RS, Sedergran DJ Lab Invest. 1993 Aug; 69(2):238-49.

[16]. Li R., Kim M.-H., Sandhu A.K., Gao C., Gu L. Muscadine Grape (Vitis rotundifolia) or Wine Phytochemicals Reduce Intestinal Inflammation in Mice with Dextran Sulfate Sodium-Induced Colitis. J. Agric. Food Chem. 2017;65:769–776. Doi: 10.1021/acs.jafc.6b03806.

[17]. Cushing, K., & Higgins, P. (2021). Management of Crohn Disease: A Review. JAMA, 325(1), 69–80. Https://doi.org/10.1001/jama.2020.18936.

[18]. Bruscoli, S., Febo, M., Riccardi, C., & Migliorati, G. (2021). Glucocorticoid Therapy in Inflammatory Bowel Disease: Mechanisms and Clinical Practice. Frontiers in immunology, 12, 691480. Https://doi.org/10.3389/fimmu.2021.691480.

[19]. Wei Shen, Yang Gao, Boyu Lu, Qingjiong Zhang, Yang Hu, Ying Chen, Negatively regulating TLR4/NF-κB signaling via PPARα in endotoxin-induced uveitis, Biochimica et Biophysica Acta (BBA)—Molecular Basis of Disease, Volume 1842, Issue 7, 2014, Pages 1109-1120, ISSN 0925-4439, https://doi.org/10.1016/j.bbadis.2014.03.015.

[20]. Couch, D. G., Cook, H., Ortori, C., Barrett, D., Lund, J. N., & O'Sullivan, S. E. (2019). Palmitoylethanolamide and Cannabidiol Prevent Inflammation-induced Hyperpermeability of the Human Gut In Vitro and In Vivo-A Randomized, Placebo-controlled, Double-blind Controlled Trial. Inflammatory bowel diseases, 25(6), 1006–1018. Https://doi.org/10.1093/ibd/izz017.

[21]. Tartakover Matalon, S., Azar, S., Meiri, D., Hadar, R., Nemirovski, A., Abu Jabal, N., Konikoff, F. M., Drucker, L., Tam, J., & Naftali, T. (2021). Endocannabinoid Levels in Ulcerative Colitis Patients Correlate With Clinical Parameters and Are Affected by Cannabis Consumption. Frontiers in endocrinology, 12, 685289. Https://doi.org/10.3389/fendo.2021.685289.

[22]. Esposito, G., Corpetti, C., Pesce, M., Seguella, L., Annunziata, G., Del Re, A., Vincenzi, M., Lattanzi, R., Lu, J., Sanseverino, W., & Sarnelli, G. (2021). A Palmitoylethanolamide Producing Lactobacillus paracasei Improves Clostridium difficile Toxin A-Induced Colitis. Frontiers in pharmacology, 12, 639728. Https://doi.org/10.3389/fphar.2021.639728.

[23]. Esposito, G., Pesce, M., Seguella, L., Lu, J., Corpetti, C., Del Re, A., De Palma, F., Esposito, G., Sanseverino, W., & Sarnelli, G. (2021). Engineered Lactobacillus paracasei Producing Palmitoylethanolamide (PEA) Prevents Colitis in Mice. International journal of molecular sciences, 22(6), 2945. https://doi.org/10.3390/ijms22062945.

[24]. Sarnelli G, Seguella L, Pesce M, et al. HIV-1 Tat-induced diarrhea is improved by

the PPARalpha agonist, palmitoylethanolamide, by suppressing the activation of enteric glia. J Neuroinflammation. 2018;15(1):94. Published 2018 Mar 24. Doi:10.1186/s12974-018-1126-4.

[25]. Darmani NA, Izzo AA, Degenhardt B, et al. Involvement of the cannabimimetic compound, N-palmitoyl-ethanolamine, in inflammatory and neuropathic conditions: Review of the available pre-clinical data, and first human studies. Neuropharmacology 2005;48:1154–63.

[26]. Grabacka, M., Pierzchalska, M., Płonka, P. M., & Pierzchalski, P. (2021). The Role of PPAR Alpha in the Modulation of Innate Immunity. International journal of molecular sciences, 22(19), 10545. Https://doi.org/10.3390/ijms221910545.

[27]. Dana, N., Vaseghi, G., & Haghjooy Javanmard, S. (2019). Crosstalk between Peroxisome Proliferator-Activated Receptors and Toll-Like Receptors: A Systematic Review. Advanced pharmaceutical bulletin, 9(1), 12–21. Https://doi.org/10.15171/apb.2019.003.

[28]. Takeda, K., & Akira, S. (2004). Microbial recognition by Toll-like receptors. Journal of dermatological science, 34(2), 73–82. Https://doi.org/10.1016/j.jdermsci.2003.10.002.

[29]. Zhen, Y., & Zhang, H. (2019). NLRP3 Inflammasome and Inflammatory Bowel Disease. Frontiers in immunology, 10, 276. https://doi.org/10.3389/fimmu.2019.00276.

[30]. Chen, M. Y., Ye, X. J., He, X. H., & Ouyang, D. Y. (2021). The Signaling Pathways Regulating NLRP3 Inflammasome Activation. Inflammation, 44(4), 1229–1245. Https://doi.org/10.1007/s10753-021-01439-6.

[31]. Zhuang, Y., Zhao, F., Liang, J., Deng, X., Zhang, Y., Ding, G., Zhang, A., Jia, Z., & Huang, S. (2017). Activation of COX-2/mPGES-1/PGE2 Cascade via NLRP3 Inflammasome Contributes to Albumin-Induced Proximal Tubule Cell Injury. Cellular physiology and biochemistry: International journal of experimental cellular physiology, biochemistry, and pharmacology, 42(2), 797–807. Https://doi.org/10.1159/000478070.

[32]. Luo, H., Guo, P., & Zhou, Q. (2012). Role of TLR4/NF-κB in damage to intestinal mucosa barrier function and bacterial translocation in rats exposed to hypoxia. PloS one, 7(10), e46291. Https://doi.org/10.1371/journal.pone.0046291.

[33]. Morales-Soto, W., & Gulbransen, B. D. (2019). Enteric Glia: A New Player in Abdominal Pain. Cellular and molecular gastroenterology and hepatology, 7(2), 433–445. Https://doi.org/10.1016/j.jcmgh.2018.11.005.

[34]. Yuan, B., Tang, W. H., Lu, L. J., Zhou, Y., Zhu, H. Y., Zhou, Y. L., Zhang, H. H., Hu, C. Y., & Xu, G. Y. (2015). TLR4 upregulates CBS expression through NF-κB activation

in a rat model of irritable bowel syndrome with chronic visceral hypersensitivity. World journal of gastroenterology, 21(28), 8615–8628. Https://doi.org/10.3748/wjg.v21.i28.8615.

[35]. Bettoni I, Comelli F, Rossini C, Granucci F, Giagnoni G, Peri F, et al. (2008): Glial TLR4 receptor as new target to treat neuropathic pain: Efficacy of a new receptor antagonist in a model of peripheral nerve injury in mice. Glia 56:1312–1319.

[36]. Hutchinson MR, Zhang Y, Brown K, Coats BD, Shridhar M, Sholar PW, et al. (2008): Non-stereoselective reversal of neuropathic pain by naloxone and naltrexone: Involvement of toll-like receptor 4 (TLR4). Eur J Neurosci 28:20–29.

[37]. Lönnfors S, Vermeire S, Greco M, Hommes D, Bell C, Avedano L. IBD and health-related quality of life—Discovering the true impact. J Crohns Colitis 2014;8:1281–6.

[38]. Cuesta, C. M., Pascual, M., Pérez-Moraga, R., Rodríguez-Navarro, I., García-García, F., Ureña-Peralta, J. R., & Guerri, C. (2021). TLR4 Deficiency Affects the Microbiome and Reduces Intestinal Dysfunctions and Inflammation in Chronic Alcohol-Fed Mice. International journal of molecular sciences, 22(23), 12830. Https://doi.org/10.3390/ijms222312830.

[39]. Philip-Hollingsworth S., Dazzo F., Hollingsworth R. Structural requirements of Rhizobium chitolipooligosaccharides for uptake and bioactivity in legume roots as revealed by synthetic analogs and fluorescent probes. J. Lipid Res. 1997;38:1229–1241. Doi: 10.1016/S0022-2275(20)37204-7.

[40]. Das A., Srinivasan M., Ghosh T.S., Mande S.S. Xenobiotic metabolism and gut microbiomes. PLoS ONE. 2016;11:e0163099. Doi: 10.1371/journal.pone.0163099.

N-palmitoyl-d-glucosamine limits mucosal damage and VEGF-mediated angiogenesis by PPARα-dependent suppression of pAkt/mTOR/HIF1α pathway and increase in PEA levels in AOM/DSS colorectal carcinoma in mice

Irene Palenca, Silvia Basili Franzin, Aurora Zilli, Luisa Seguella, Anna Troiani, Federico Pepi, Martina Vincenzi, Giuseppe Giugliano, Viviana Catapano, Italia Di Filippo, Giovanni Sarnelli, Giuseppe Esposito

Irene Palenca and Silvia Basili Franzin equally contributed to the manuscript

Abstract

Chronic intestinal inflammation and neo-angiogenesis are interconnected in colorectal carcinoma (CRC) pathogenesis. Molecules reducing inflammation and angiogenesis hold promise for CRC prevention and treatment. N-Palmitoyl-d-glucosamine (PGA), a natural glycolipid analog with anti-inflammatory properties, has shown efficacy against acute colitis. Micronized PGA (mPGA) formulations exhibit superior anti-inflammatory activity. This study investigates the *in vivo* anti-angiogenic and protective effects of mPGA in a mouse model of colitis-associated CRC induced by azoxymethane/dextran sodium sulfate (AOM/DSS). CRC was induced in C57BL/6J mice using intraperitoneal azoxymethane followed by three cycles of 2.5% dextran sodium sulfate (DSS) in drinking water. Mice were treated with mPGA (30–150 mg/kg) with or without the PPARα inhibitor MK886 (10 mg/kg). At Day 70 post-azoxymethane injection, mice underwent anesthetized endoscopic colon evaluation. Post-mortem analysis of tumorigenesis and angiogenesis was performed using histological, immunohistochemical, and immunoblotting techniques. mPGA improved disease progression and survival rates in a dose- and PPARα-dependent manner in AOM/DSS-exposed mice. It reduced polyp formation, decreased pro-angiogenic CD31, pro-proliferative Ki67, and pro-inflammatory TLR4 expression levels, and inhibited VEGF and MMP-9 secretion by disrupting the pAkt/mTOR/HIF1α pathway. mPGA increased colon PEA levels, restoring anti-tumoral PPARα and wtp53 protein expression. Given its lack of toxicity, mPGA

shows potential as a nutritional intervention to counteract inflammation-related angiogenesis in CRC.

1. Introduction

Colorectal carcinoma (CRC) ranks third worldwide among the most prevalent and life-threatening malignancies (Sung et al., 2021). Genetic factors, unhealthy dietary habits, and chronic intestinal inflammation significantly contribute to the genesis and advancement of precancerous lesions, thereby facilitating the growth of CRC (Lichtenstern et al., 2020; Mandle et al., 2024). Over the past decade, extensive research has demonstrated that the onset of a chronic inflammatory milieu associated with CRC fosters a supportive environment for hyperproliferation of epithelial cells and promotes angiogenesis, the formation of new blood vessels, which facilitates metastasis in the colon and rectum (Aguilar-Cazares et al., 2019). This process significantly decreases the survival rate of affected patients (Jensen et al., 2006). Chronic inflammation in the colon creates a cancer-growth favorable microenvironment that self-perpetuates by the release of vascular endothelial growth factor (VEGF) and pro-inflammatory cytokines. This ultimately disrupts the normal mucosal histological architecture and leads to uncontrolled hyperproliferation of epithelial cells (Sato et al., 2023). Identifying molecules that target intestinal inflammation and angiogenesis is crucial for the development of preventive and therapeutic strategies that can complement current CRC therapy (Kumar et al., 2023).

In this context, Autacoid Local Injury Antagonist Amides (ALIAmides) are a class of bioactive fatty acid amides that play a pivotal role in locally regulating inflammation and immune responses (Aloe et al., 1993; Chiurchiù et al., 2018). Acting at the Peroxisome Proliferator-Activated Receptors α (PPARα) site (Lo Verme et al., 2005), the ALIAmide palmitoylethanolamide (PEA) interferes with pro-angiogenic VEGF signaling and oncogenic pAkt/mTOR pathway with an excellent safety profile against inflammation, cell proliferation, and angiogenesis (Sarnelli, D'Alessandro, et al., 2016).

Besides PEA, other ALIAmides have been recently investigated (Gugliandolo et al., 2020; Palenca et al., 2022, 2023). Among these, N-palmitoyl-D-glucosamine (PGA) has been identified as a natural derived monosaccharide-based glycolipid resulting from a combination of palmitic acid and glucosamine (Cordaro et al., 2019).

PGA shares anti-inflammatory properties with its endogenous analog PEA and those of glucosamine (Cordaro et al., 2019). Similarly to PEA, micronized formulations of PGA (mPGA) have shown superior activity compared with unprocessed ones (Cordaro et al., 2019). In preclinical *in vivo* models, mPGA has been revealed as a safe anti-inflammatory agent in the treatment of osteoarthritis pain and colon inflammation (Cordaro et al., 2019; Palenca et al., 2022). Such effect has been attributed to PGA-mediated downregulation of the toll-like receptor 4 (TLR4) pathway through PPARα receptor signaling (Iannotta et al., 2021). Despite these observations, no studies have yet investigated the effect of mPGA against chronic inflammation and angiogenesis in colon cancer. To address this gap, our study aims to explore the activity of an orally administered mPGA in a model of chronic inflammation-related CRC in C57BL/6J mice, induced by azoxymethane (AOM) and 2.5% dextran sulfate sodium (DSS) (Dzhalilova et al., 2023). The present study will primarily investigate the dose-dependent effects of mPGA on the following aspects within the AOM/DSS colon cancer mouse model: (i) colorectal polyps' formation and mice survival, (ii) anti-angiogenic effects and changes in epithelial mucosa, (iii) release of pro-angiogenic and inflammatory cytokines, and (iv) activation of the pAkt/mTOR signaling pathway.

2. Materials and Methods

2.1 Animal and experimental design

All *in vivo* experimental protocols were approved by the animal welfare regulation of the University of Naples “Federico II,” Italy, and by the Superior Institute of Health, Italy. Animal studies were carried out in compliance with the ARRIVE (Animal Research: Reporting of In vivo Experiments) guidelines, E.U. Directive 2010/63/EU for animal experiments (date of the approval, 2021). Eight-week-old male C57BL/6J (Charles River, Lecco, Italy) mice were used for all the experiments ($n = 105$). Mice were maintained on a 12 h light/dark cycle in a temperature-controlled environment with access to food and water ad libitum. After mice acclimatization, according to the procedure described by Parang et al. (2016), mice were given an intraperitoneal injection with 10 mg/kg AOM in 0.1 mL phosphate buffer saline (PBS), followed by three cycles of 2.5% DSS in drinking water for 1 week and normal drinking water for 2 weeks (Figure 1a). Mice body weight was recorded weekly, and the overall survival

of the animals at the end of the procedure was also assessed. Concerning the treatment carried out in the experimental plan, an amount of 200 µL of 30, 100, 150 mg/kg mPGA (Epitech Group S.p.A, Saccolongo, Italy), and 150 mg/kg glucosamine was suspended in 1× PBS (Sigma-Aldrich, St. Louis, MO, USA) and carboxymethylcellulose 1:4 (Thermo Fisher Scientific, Waltham, MA, USA); the PPARα antagonist, 10 mg/kg MK886 (Selleck Chemicals, Houston, TX), was dissolved in 1× PBS, according the procedures described by Palenca et al. (2022). Animals were then randomly divided into seven groups ($n = 15$ each), depending upon the experimental protocol described (Figure 1a): (1) vehicle group, receiving 200 µL of 1× PBS plus 1:4 carboxymethylcellulose orally administered 3 days a week; (2) CRC group, receiving 2.5% DSS in the drinking water + single intraperitoneal injection of 10 mg/kg AOM at Day 0; (3) 2.5% DSS + 10 mg/kg AOM + orally administered 30 mg/kg mPGA 3 days a week; (4) 2.5% DSS + 10 mg/kg AOM + 100 mg/kg mPGA 3 days a week; (5) 2.5% DSS + 10 mg/kg AOM + 150 mg/kg mPGA 3 days a week; (6) 2.5% DSS + 10 mg/kg AOM + 150 mg/kg mPGA 3 days a week + intraperitoneal administration of 10 mg/kg PPARα antagonist MK886 at Days 7, 28, and 49; and (7) 2.5% DSS + 10 mg/kg AOM + 150 mg/kg glucosamine sulfate 3 days a week. The dose of glucosamine was chosen in order to administer a higher (i.e., double) dose compared with the amount of glucosamine contained in 150 mg/kg mPGA dose. Starting on Day 7, the animals were monitored to determine the survival curve, concluding the procedures on Day 70 after AOM injection. Before euthanasia, a random subset of $n = 5$ mice from each group underwent endoscopy to identify colon tumor formation. At the end of the experimental protocol, all animals were euthanized via CO_2 hypoxia. Subsequently, colons were isolated, measured for length, and examined macroscopically for polyp formation and enumeration. Colon samples were then processed for further analyses.

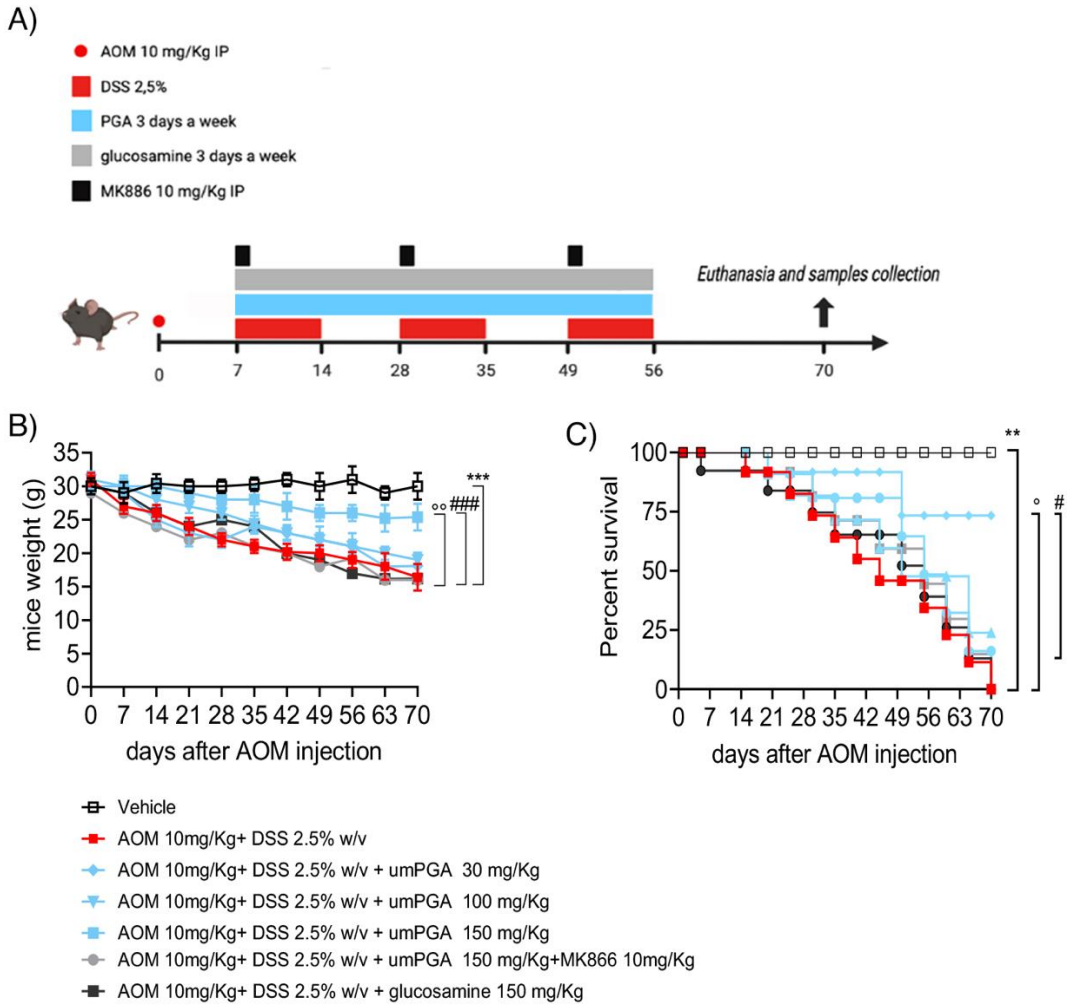

Figure 1. Experimental design and impact of treatments on mice weight loss and survival following AOM/DSS colon cancer induction. Figure shows (a) Schematic overview of the experimental design and treatments in AOM/DSS model of colorectal carcinoma in mice. (b) Time course of body weight changes and (c) log-rank graph showing the survival rate of mice evaluated at Day 70 after AOM injection. The results are expressed as mean ± SD. $^{***}p < 0.001$ vs. vehicle, $^{**}p < 0.01$ vs. vehicle, $^{\circ\circ}p < 0.01$ vs. AOM/DSS group, $^{\circ}p < 0.05$ vs. AOM/DSS group, $^{\#\#\#}p < 0.001$ vs. 150 mg/kg mPGA group, $^{\#}p < 0.05$ vs. 150 mg/kg mPGA group.

2.2 Endoscopic procedures and endoscopic injury score evaluation

For endoscopic procedures, $n = 5$ mice from each experimental group were anesthetized via intraperitoneal injection of 60 mg/kg ketamine and 10 mg/kg xylazine. Before the

procedure, the mice were given a 1× PBS enema to optimize visualization of the colonic mucosa. The experimental endoscopy of the rectum and colon was performed using a bronchoscopy adapted for small rodent use (Karl Storz, Tuttlingen, Germany). Endoscopic frames were captured using a color monitor and digitally recorded on tape (CV-190 PLUS; Olympus, Segrate, Italy). Endoscopic injury scoring was performed according to the method described by Becker et al. (2006).

2.3 Histopathological analyses

Colonic tissues were fixed overnight in ice-cold 4% paraformaldehyde (PFA) (Thermo Fisher Scientific, Waltham, MA, USA) and then transferred to a 1× PBS solution containing 20% sucrose at 4°C for 48 h. Subsequently, the colon specimens were cryo-sectioned into 15 µm slices. Slices underwent staining with hematoxylin and eosin (H&E) (Sigma-Aldrich, St. Louis, MO, USA) to assess histopathological changes, by the methodology described by Li et al. (2017). Criteria included (i) distortion and loss of crypt architecture; (ii) inflammatory cell infiltration; (iii) muscle thickening; (iv) goblet cells depletion; and (v) crypts absence. The analyses were performed using a Nikon Eclipse 80i microscope from Nikon Instruments Europe (Nikon Corporation, Tokyo, Japan), with images captured at 10× magnification using a high-resolution digital camera (Nikon Digital Sight DS-U1). Cumulative damage scores obtained from each experimental group were expressed as average scores.

2.4 Immunofluorescence analysis

Immunofluorescence analyses were performed on 15 µm colonic slices fixed in ice-cold 4% PFA. Tissues were rinsed three times (10 min each) in 1× PBS containing 0.1% Triton X-100 (T-PBS) followed by a 1 h incubation in blocking solution (containing T-PBS, 4% normal donkey serum, and 1% bovine serum albumin) at room temperature (RT). After three washes in T-PBS (10 min each), sections were then stained with anti-Ki67 (1:100 *v/v*; rabbit; Abcam, Cambridge, UK) and anti-CD31 (1:50 *v/v*, mouse; Abcam, Cambridge, UK) overnight at +4°C. Tissues were rinsed three times (10 min each) with T-PBS after removing the primary antibodies, and then, secondary antibodies anti-Rabbit Alexa Fluor 488 (1:400 *v/v*; Jackson Immuno Research, Cambridgeshire, UK) and anti-Mouse Alexa Fluor 564 (1:400 *v/v*; Jackson Immuno Research, Cambridgeshire, UK) were incubated for 2 h at RT. Tissues were rinsed two times (10 min each) in 1× PBS, once in 0.1 M phosphate buffer (10 min), and mounted in DAPI Fluoromount (Southern

Biotech, Birmingham, USA). Sections were analyzed with a Nikon Eclipse 80i microscope, and images were captured by Nikon Digital Sight DS-U1 high-resolution digital camera.

2.5 Protein extraction and western blot analysis

Mice colon specimens were homogenized in ice-cold hypotonic lysis buffer, and the protein concentration was determined using the Bio-Rad protein assay kit (Bio-Rad, Milan, Italy). Subsequently, total protein fractions from the homogenates were utilized for the analysis of various protein expressions. Equivalent amounts of homogenates (50 µg) were subjected to electrophoresis through a polyacrylamide minigel. The proteins were then transferred onto nitrocellulose membranes, which were saturated by incubation with 10% non-fat dry milk in 1× PBS overnight at 4°C. Following saturation, the membranes were incubated according to the experimental protocols with the following primary antibodies: mouse anti-total Akt (1:1000 *v/v*; Cell Signaling Technology, Euroclone, MI, Italy); rabbit monoclonal anti-phospho-Akt (Ser 473) (1:2000 *v/v*; Cell Signaling Technology, Euroclone, MI, Italy); rabbit polyclonal anti-total mTOR (1:1000 *v/v*; Abcam, Cambridge, UK); rabbit polyclonal anti-phospho-mTOR (pSer2448) (1:1000 *v/v*; Cell Signaling Technology, Euroclone, MI, Italy); rabbit polyclonal anti-total p70S6K (1:1000 *v/v*; Cell Signaling Technology, Euroclone, MI, Italy); rabbit polyclonal anti-phospho-p70S6K (Thr421/Ser424, Thr389) (1:1000 *v/v*; Cell Signaling Technology, Euroclone, MI, Italy); rabbit monoclonal anti-VEGF receptor (1:1000 *v/v*; Cell Signaling Technology, Euroclone, MI, Italy); rabbit monoclonal anti-PPARα (1:1000 *v/v*; Abcam, Cambridge, UK); rabbit polyclonal anti TLR4 receptor (Bioss Antibodies, Boston, MA, USA, 1:50 *v/v*), anti-*wt*p53 protein (1:1500 *v/v*; Biocompare, San Francisco, CA, USA) mouse monoclonal anti-HIF1α (1:500 *v/v*; Sigma-Aldrich, MI, Italy); and mouse anti-β-actin (1:2000 *v/v*; Santa Cruz Biotechnology, Santa Cruz, California, USA). Following primary antibody incubation, the membranes were further incubated with specific secondary antibodies conjugated to horseradish peroxidase (HRP) (Dako, Milan, Italy). Immune complexes were visualized using enhanced chemiluminescence detection reagents (Amersham Biosciences, Milan, Italy). Immune complexes were revealed by enhanced chemiluminescence detection reagents, and immunoreactive protein bands were then visualized, scanned, and densitometrically analyzed with ChemiDoc XRS+ apparatus (Bio-Rad Laboratories S.r.l. Segrate, Milano, Italy). The results were

expressed as the % of protein expression and normalized on the expression of the housekeeping protein β-actin for mouse proteins.

2.6 Quantification of PEA in the tissue by HPLC–MS method

The extraction and analysis of PEA level in the tissue were performed according to the protocol outlined by Gachet et al. (2015), with minor adjustments. Initially, colon specimens were firstly lysed using a lysis buffer and subsequently evaporated under a stream of nitrogen. The resulting residues were reconstituted in an extraction solution, followed by ultracentrifugation (14,000 rpm, 4°C, 5 min). The supernatant obtained was then subjected to mass spectrometry analysis. The analyses were conducted using a Jasco Extrema LC-4000 system (Jasco Inc., Easton, MD, USA) coupled with an Advion Expression mass spectrometer (Advion Inc., Ithaca, NY, USA) equipped with an electrospray (ESI) source. Mass spectra were acquired in positive selected ion monitoring (SIM) mode. The capillary voltage was set to +180 V, the spray voltage to 3 kV, the source voltage offset to +20 V, and the capillary temperature to 250°C. Chromatographic separation was carried out using a Kinetex C18 analytical column (150 × 4.6 mm, 3 µm particle size, 100 Å pore size) along with a security guard column, both supplied by Phenomenex (Torrance, CA, USA). The analyses were performed at a flow rate of 0.3 mL/min, employing solvent A (water with 2 mM ammonium acetate) and solvent B (methanol with 2 mM ammonium acetate and 0.1% formic acid). Elution proceeded with a linear gradient: starting at 15% B for 0.5 min, transitioning from 15% to 70% B over 2.5 min, further transitioning from 70% to 99% B over 1.5 min, maintaining 99% B for 4 min, and then returning to 15% B over 3.5 min, with a total run time of 15 min. The injection volume was 10 µL, and the column temperature was maintained at 40°C. For quantitative analysis, standard curves of PEA (Sigma-Aldrich, Milan, Italy) were established across a concentration range of 0.0001–10 ppm, encompassing six concentration levels, with duplicate injections prepared at each level. Data acquisition and processing were conducted using JASCO Chrom NAV (version 2.02.04) and Advion Data Express (4.0.13.8).

2.7 Enzyme-linked immunosorbent assay for VEGF and MMP-9

Enzyme-linked immunosorbent assays (ELISA) for VEGF (Abcam, Cambridge, UK) and MMP-9 (Proteintech, Planegg-Martinsried, Germany) have been carried out on mice homogenized tissue according to the respective manufacturer's protocols. Absorbance

was measured on a microtiter plate reader. VEGF and MMP-9 level were then determined using the standard curve method according to the manufacturer's instructions.

2.8 Hemoglobin content measurement in the colon

Hemoglobin content is an appropriate method for angiogenesis quantification in sampled tissues (Tsuji et al., 1995). Mice colonic specimens were collected and weighed, followed by homogenization in 1× PBS. Subsequently, the homogenates underwent centrifugation at 2500 ***g*** for 20 min at 4°C. The resulting supernatants were subjected to further centrifugation at 5000 ***g*** for 30 min. Hemoglobin concentration in the supernatant was quantified spectrophotometrically at 450 nm using the hemoglobin assay kit (Sigma-Aldrich, MI, Italy). The measured values were then normalized and expressed as mg hemoglobin per gram of wet weight.

2.9 Statistical analysis

The results were expressed as mean ± SD or mean percentage. The effect was calculated as the percentage change between compared treatment groups. Depending upon the experiments, statistical analysis was performed using Log-rank (Mantex-Cox) test for survival rate and parametric one-way analysis of variance (ANOVA) followed by multiple comparisons with Bonferroni's post hoc test. p-values < 0.05 were considered statistically significant. Data were analyzed using Graph-pad Prism 9 and ImageJ 1.53 software.

3. Results

3.1 Dose and PPARα-dependent effect of mPGA on weight loss and survival rate in mice exposed to AOM/DSS

Following AOM administration (Figure 1a), body weight changes were monitored to assess the progression of colon cancer. In addition, before euthanasia endoscopic evaluations of colon were performed, and the general survival rate was recorded.

Compared with the vehicle group, AOM/DSS caused a significant weight loss (Figure 1b, −45.3%, $p < 0.01$ vs. vehicle group) which was dose-dependently (30–150 mg/kg mPGA) reverted by mPGA (Figure 1b, +9.7%, ns; +16%, ns; and +55%, $p < 0.05$, respectively, vs. AOM/DSS group) whereas the co-administration of PPARα antagonist

MK866 significantly reduced the mPGA protective effect on weight loss (Figure 1b, −37%, $p < 0.05$ vs. 150 mg/kg mPGA group). Administration of glucosamine did not result in any significant prevention of weight loss compared with the AOM/DSS group (Figure 1b).

The log-rank percent survival rate at the end of the experimental procedure, 70 days after AOM injection, revealed a significant decrease in mice survival in the AOM/DSS compared with vehicle group (Figure 1c, $p < 0.01$ vs. vehicle group) and mPGA at the highest dosage (150 mg/kg) was able to increase mice survival (Figure 1c, $p < 0.05$ vs. AOM/DSS group); such beneficial effect was significantly reduced in the presence of MK866 (Figure 1c, $p < 0.05$ vs. 150 mg/kg mPGA group), while no significant effect on animal survival was registered following glucosamine alone.

3.2 mPGA dose- and PPARα-dependently reduced endoscopic colon alteration, colon length, and polyps' formation in mice exposed to AOM/DSS

The endoscopic injury score (EIS), used to evaluate the extent of mucosal damage and alterations, was assessed in mice at the end of the experimental procedure, immediately before euthanasia. Following AOM/DSS, a significant increase in the injury score was detected (Figure 2a–c, +618%, $p < 0.001$ vs. vehicle group) and such effect was dose-dependently decreased by 30-150 mg/kg mPGA treatment (Figure 2a–c, −22.5%, $p < 0.05$; −51.6%, $p < 0.01$; and −82.5%, $p < 0.001$, respectively, vs. AOM/DSS group). The protective effect of mPGA was significantly reverted by the co-administration of MK866 (Figure 2a–c, +433%, $p < 0.001$ vs. 150 mg/kg mPGA group). Once again, glucosamine did not cause any significant effect in our experimental conditions (Figure 2a–c, −7.2%, ns vs. AOM/DSS group).

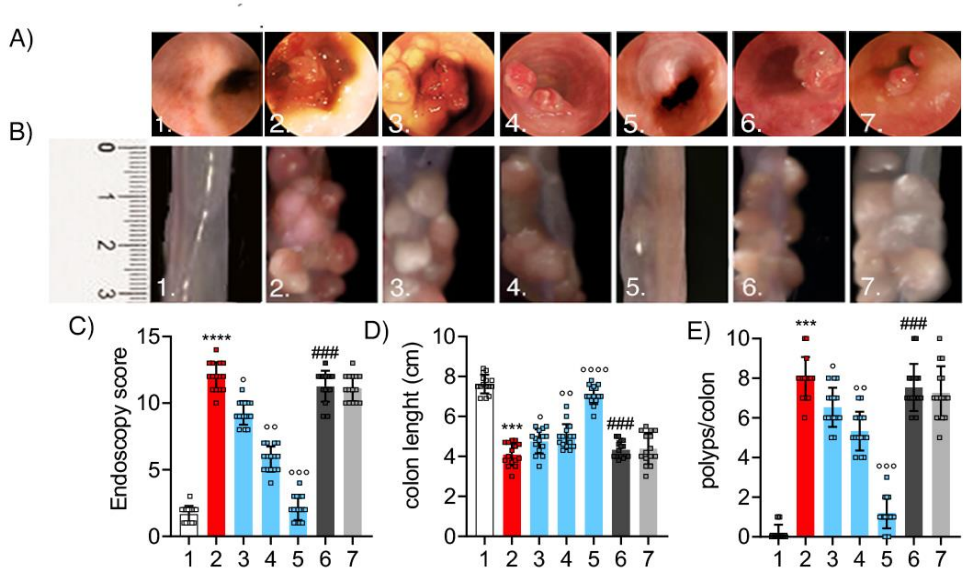

1. Vehicle
2. DSS 2,5% + AOM 10 mg/Kg
3. DSS 2,5% + AOM 10 mg/Kg + PGA 30 mg/Kg
4. DSS 2,5% + AOM 10 mg/Kg + PGA 100 mg/Kg
5. DSS 2,5% + AOM 10 mg/Kg + PGA 150 mg/Kg
6. DSS 2,5% + AOM 10 mg/Kg + PGA 150 mg/Kg + MK886 10 mg/Kg
7. DSS 2,5% + AOM 10 mg/Kg + glucosamine 150 mg/Kg

Figure. 2 Endoscopic and macroscopic evaluation of mPGA on colon polyps' formation and density following AOM/DSS colon cancer induction. Figure shows (a) The endoscopic images of endoluminal polyps in the mouse colon on Day 70 after AOM injection in the different experimental groups; (b) macroscopic image evaluation of polyps in the distal segment mouse colons at Day 70 after AOM injection and relative Centimeter reference scale on the left side; (c) evaluation of tissue damage by relative endoscopic score, (d) colon length, and (e) the number of polyps in the distal segment of the mouse colon. The results are expressed as the mean ± SD of $n = 5$ experiments in triplicate. ****$p < 0.0001$ vs. vehicle, ***$p < 0.001$ vs. vehicle, °°°°$p < 0.0001$ vs. AOM/DSS group, °°°$p < 0.001$ vs. AOM/DSS group, °°$p < 0.01$ vs. AOM/DSS group, °$p < 0.05$ vs. AOM/DSS group, ###$p < 0.001$ vs. 150 mg/kg mPGA group.

AOM/DSS caused a significant reduction in colon length (Figure 2b–d, −46.2%, $p < 0.001$ vs. vehicle group), and such decrease was dose-dependently reverted by 30–150 mg/kg mPGA administration (Figure 2b–d, +15.6, $p < 0.05$; +22%, $p < 0.01$; and +72.5%, $p < 0.001$, respectively, vs. AOM/DSS group). Again, the co-administration of MK866 strongly impaired mPGA effect (Figure 2b,c,

−40%, $p < 0.001$ vs. AOM/DSS group), and no significant effect was observed following glucosamine alone (Figure 2b,c, +6.8%, ns vs. AOM/DSS group). In line with these results, AOM/DSS induced a significant increase in polyp formation in the colon (Figure 2b–e, +3900%, $p < 0.001$ vs. vehicle group) and such effect was dose-dependently reduced by 30–150 mg/kg mPGA administration (Figure 2b–e, −19%, $p < 0.05$; −33.8%, $p < 0.01$ and −85%, $p < 0.001$ vs. AOM/DSS group, respectively). As expected, the protective effect of mPGA on polyp count was inhibited in the presence of MK866 (Figure 2b–e, +525%, $p < 0.001$ vs. 150 mg/kg mPGA group), whereas no significant effect was produced by glucosamine (Figure 2b–e, −10%, ns vs. AOM/DSS group).

3.3 mPGA dose- and PPARα-dependently reduced histological damage score severity, pro-angiogenic CD31 marker, and hyperproliferative Ki67 protein expression in the colon of mice exposed to AOM/DSS

In accordance with endoscopic evaluation, *post-mortem* histological analysis revealed that AOM/DSS induced a significant mucosal damage (Figure 3a–d, +1458%, $p < 0.001$ vs. vehicle group). AOM/DSS also increased the expression of the pro-angiogenic marker CD31 (Figure 3b–e, +190%, $p < 0.001$ vs. vehicle group) and immunofluorescence for the proliferation protein Ki67 in comparison with respective

controls (Figure 3c–f, +335%, $p < 0.001$ vs. vehicle group).

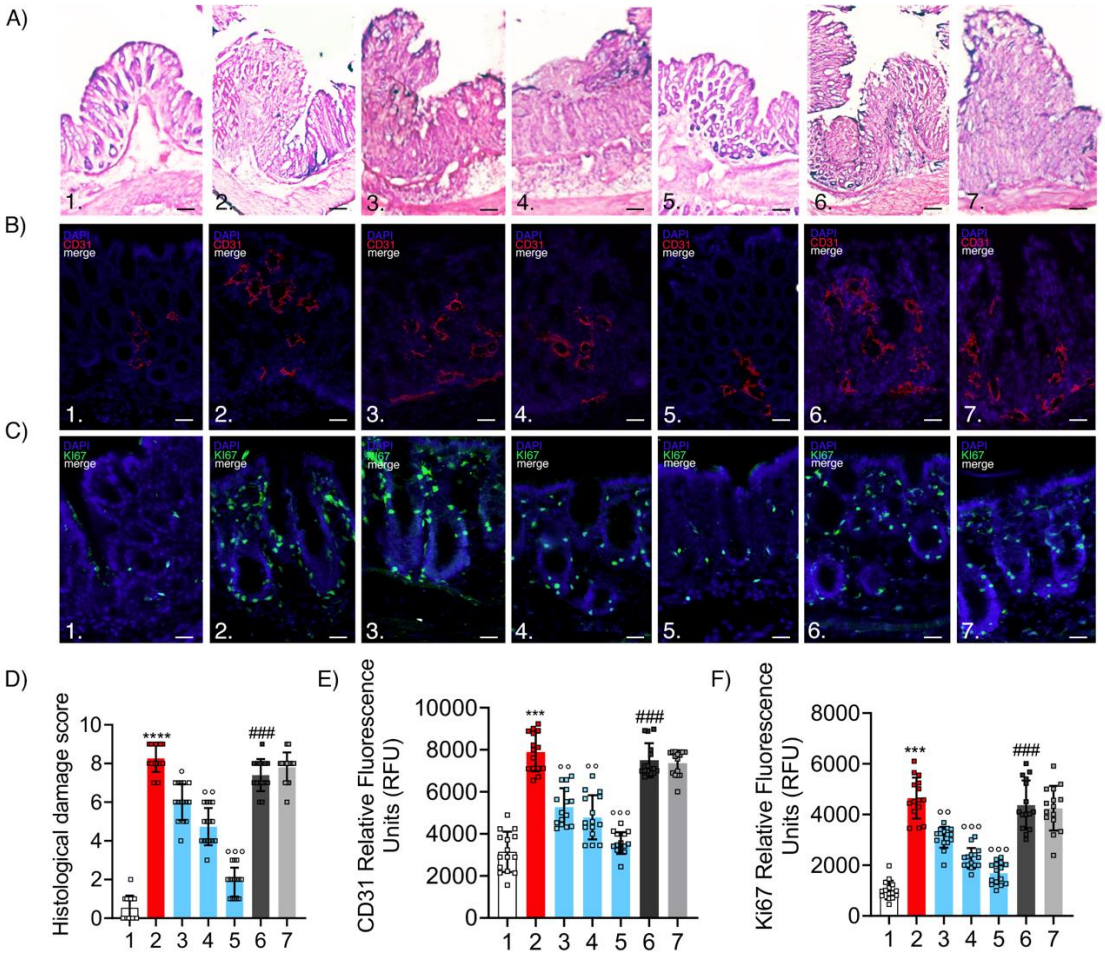

Figure. 3 Effect of mPGA treatments on histological damage and angiogenic/proliferative markers in mucosa following AOM/DSS challenge. (a) Colon tissue morphology and relative (d) histological damage assessment by hematoxylin and eosin staining. The panel shows in (b, c and e, f), respectively, pro-angiogenic CD31 and proliferative Ki67 marker expression by immunofluorescence analysis (b, c) in the colon sections and respective their quantification expressed in terms of relative fluorescence units (RFU) (e, f). The results are expressed as mean ± SD of $n = 5$ experiments in triplicate. ****$p < 0.0001$ vs. vehicle, ***$p < 0.001$ vs. vehicle,

°°°$p < 0.001$ vs. AOM/DSS group, °°$p < 0.01$ vs. AOM/DSS group, °$p < 0.05$ vs. AOM/DSS group, ###$p < 0.001$ vs. 150 mg/kg mPGA group. Magnification 20×; Scale bar: 100 µm.

Administration of 30–150 mg/kg mPGA dose-dependently reduced the histopathological score (Figure 3a–d, −27%, $p < 0.05$; −43%, $p < 0.01$; and −77%, $p < 0.001$, respectively, vs. AOM/DSS group). Such effect was accompanied by dose-dependent inhibition of the expression of CD31 (Figure 3b–e, −33%, $p < 0.05$; −40%, $p < 0.05$; and −55% $p < 0.001$ vs. AOM/DSS group, respectively) and Ki67 (Figure 3c–f, −33%, $p < 0.05$; −51%, $p < 0.001$; and −63%, $p < 0.001$ vs. AOM/DSS group, respectively) in the colon mucosa. In the presence of MK866, the above-described inhibitory effects by 150 mg/kg mPGA were completely lost. Glucosamine alone did not display any significant effect on histological damage score (Figure 3a–d, −5.6%, ns vs. AOM/DSS group), nor on CD31 (Figure 3b–d, −6.7%, ns vs. AOM/DSS group) and Ki67 protein expression (Figure 3c–f, −8.5%, ns vs. AOM/DSS group).

3.4 mPGA dose- and PPARα-dependently reduced hemoglobin content, VEGF, and MMP-9 release in the colon of mice exposed to AOM/DSS

To evaluate colon angiogenesis, we measured the tissue hemoglobin content and the levels of VEGF and MMP-9 proteins. AOM/DSS treatment caused a marked and significant increase in hemoglobin tissue content (Figure 4a, +236%, $p < 0.001$ vs. vehicle group), VEGF (Figure 4b, +290%, $p < 0.001$ vs. vehicle group), and MMP-9 release (Figure 4c, +258%, $p < 0.001$ vs. vehicle group). As expected, 30–150 mg/kg mPGA caused an overall decrease in all the examined parameters, causing a dose-dependent decrease in tissue hemoglobin (Figure 4a, −30%, $p < 0.05$; −40%, $p < 0.01$; and −61%, $p < 0.001$ vs. AOM/DSS group), VEGF (Figure 4b, −37%, $p < 0.01$; −51%, $p < 0.001$; and −62%, $p < 0.001$ vs. AOM/DSS group), and MMP-9 release (Figure 4c, −33%, $p < 0.01$; −52%, $p < 0.001$; and −68%, $p < 0.001$ vs. AOM/DSS group). According to the other experiments, the effect of mPGA was almost completely abolished by MK866 (Figure 4a–c). No significant effects on AOM/DSS-induced angiogenesis were observed following administration of glucosamine alone, neither in terms of hemoglobin variation (Figure 4a, −2.4%, ns vs. AOM/DSS group), VEGF (Figure 4b, −6.7%, ns vs. AOM/DSS group), nor MMP-9 release (Figure 4C, −1.6%, ns vs. AOM/DSS group).

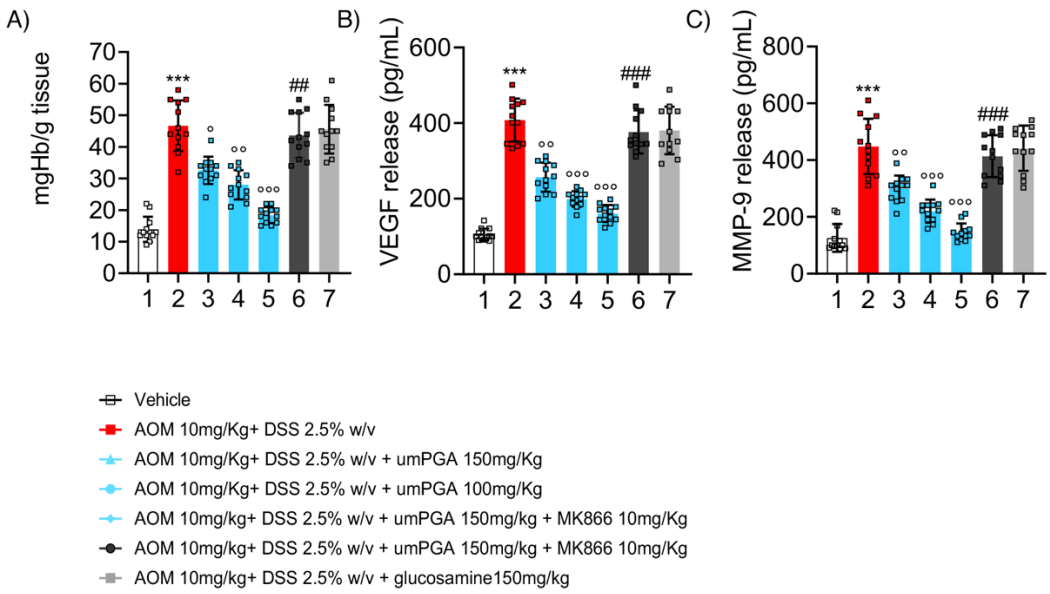

Figure. 4 Effect of mPGA administration on colon hemoglobin content, VEGF, and MMP-9 release in AOM/DSS challenged mice. (a) The hemoglobin content in the colon tissue as indirect marker of neovascularization assessment in the tissue, and the ELISA quantification of specific pro-angiogenic markers (b) VEGF and (c) MMP-9 level in the colon tissues. The results are expressed as the mean ± SD of $n = 5$ experiments in triplicate. $^{***}p < 0.001$ vs. vehicle, $^{°°°}p < 0.001$ vs. AOM/DSS group, $^{°°}p < 0.01$ vs. AOM/DSS group, $^{°}p < 0.05$ vs. AOM/DSS group, $^{###}p < 0.001$ vs. 150 mg/kg mPGA group, $^{##}p < 0.01$ vs. 150 mg/kg mPGA group.

3.5 mPGA dose- and PPARα-dependently reduced pAkt/mTOR/HIF1α signaling induced by AOM/DSS in mice

The molecular pathway involving phosphorylation of Akt and mTOR signaling is crucial to the activation of HIF1α, and this is a key step in colon carcinogenesis (Leiphrakpam & Are, 2024). Immunoblot analysis revealed a significant increase in phosphorylation of Akt (Figure 5a,b, +650%, $p < 0.001$ vs. vehicle group), p70S6K (Figure 5a–c, +1175% $p < 0.001$ vs. vehicle group), HIF1α (Figure 5a–d, +1310%, $p < 0.001$ vs. vehicle group), and mTOR (Figure 5a–e, +697%, $p < 0.001$ vs. vehicle group) following AOM/DSS treatment. Administration of 30–150 mg/kg mPGA resulted in a dose-dependent progressive reduction in the expression of all investigated proteins,

specifically causing a significant reduction in phosphorylation of Akt (Figure 5a,b, −25%, $p < 0.05$; −28%, $p < 0.001$; and −72%, $p < 0.001$ vs. AOM/DSS group), p70S6K (Figure 5a–c, −31%, $p < 0.05$; −67%, $p < 0.001$; and −89%, $p < 0.001$ vs. AOM/DSS group), HIFα (Figure 5a–d, −40%, $p < 0.01$; −58%, $p < 0.001$; and −81%, $p < 0.001$ vs. AOM/DSS group, respectively), and mTOR (Figure 5a–e, −30%, $p < 0.05$; −66%, $p < 0.001$; and −72%, $p < 0.001$ vs. AOM/DSS group). In the presence of MK866, the inhibitory effects of mPGA were significantly reverted in terms of phosphorylation of Akt (Figure 5a,b, +297%, $p < 0.001$ vs. 150 mg/kg mPGA group), p70S6K (Figure 5a–c, +732%, $p < 0.001$ vs. 150 mg/kg mPGA group), HIF1α (Figure 5a–d, +637%, $p < 0.001$ vs. 150 mg/kg mPGA group, respectively), and mTOR (Figure 5a–e, +264%, $p < 0.001$ vs. 150 mg/kg mPGA group) expression. Negligible effects were produced by glucosamine administration in the same experimental conditions, while, on the contrary, no detectable effects on p-Akt, (Figure 5a,b, +8.3%, ns vs. AOM/DSS group), p-70S6K (Figure 5a–c, −13%, ns vs. AOM/DSS group), HIF1α (Figure 5a–d, −6%, ns vs. AOM/DSS group), and p-mTOR (Figure 5a–e, −11%, ns vs. AOM/DSS group) were observed.

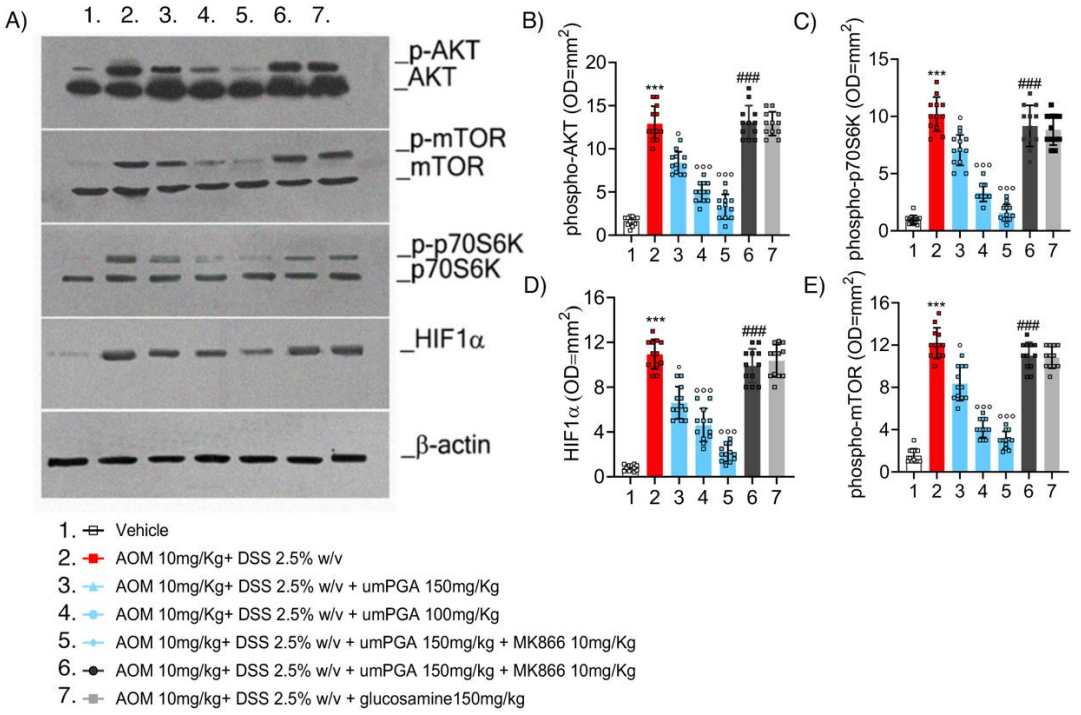

Figure. 5 Effect of mPGA on pAkt/mTOR/HIF1a pathway in AOM/DSS challenged mice. (a) The immunoblot panel expression and respective quantifications of (b) phospho-AKT, (c) mTOR, (d) phosphor-p70S6K, and (e) HIF1α proteins. The results as the mean ± SD of $n = 5$ experiments in triplicate.$^{°°°}p < 0.001$ vs. AOM/DSS group, $^{°}p < 0.05$ vs. AOM/DSS group, $^{###}p < 0.001$ vs. 150 mg/kg mPGA group.

3.6 mPGA increased PEA production in colon tissue in a dose- and PPARα-dependent manner

While no significant variations of endogenous PEA were induced by AOM/DSS treatment (Figure 6a, +6%, ns vs. vehicle group), a significant and dose-dependent upregulation of PEA level was observed following 30–150 mg/kg mPGA administration (Figure 6a, +109%, $p < 0.05$; +151%, $p < 0.01$; and +230%, $p < 0.001$ vs. AOM/DSS group, respectively). Such increase was notably impacted by MK866 administration (Figure 6a, −63%, $p < 0.05$ vs. 150 mg/kg mPGA group), and no effects on PEA level were detected following glucosamine administration (Figure 6a, +15%, ns vs. AOM/DSS group).

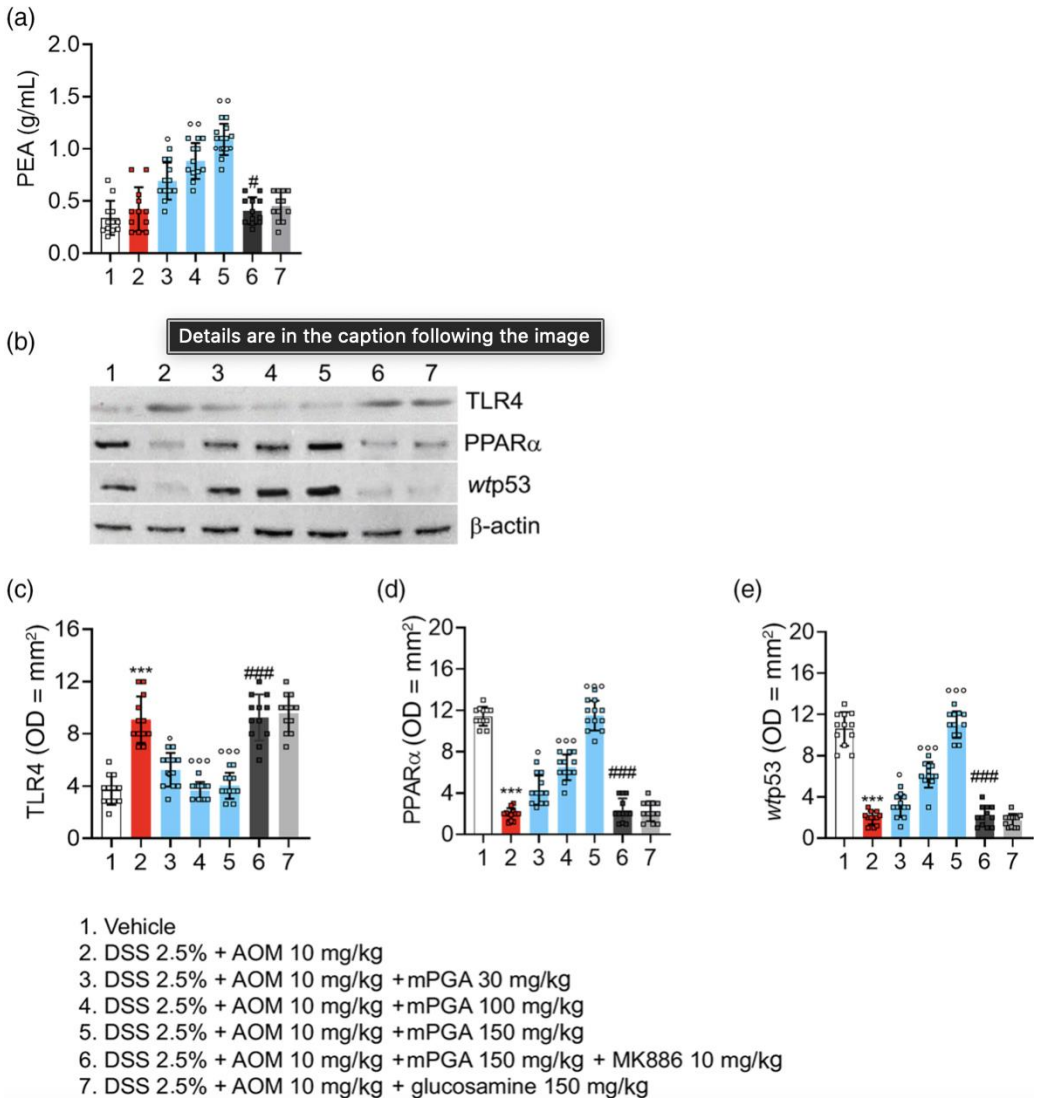

Figure. 6 Effect of mPGA administration on endogenous PEA level, and its modulation on TLR4, PPARα, and *wt*p53 protein expression in AOM/DSS challenged mice. (a) Quantitative HPLC-MS analysis of PEA level and (b) immunoblot panel expression with relative quantification of (c) TLR4, (d) PPARα, and (e) *wt*p53 proteins, respectively, in the mouse colon. The results are expressed as the mean ± SD of $n = 5$ experiments in triplicate. $^{***}p < 0.001$ vs. vehicle, $^{°°°}p < 0.001$ vs. AOM/DSS group, $^{°}p < 0.05$ vs. AOM/DSS group, $^{###}p < 0.001$ vs. 150 mg/kg mPGA group.

Interestingly, a significant increase in TLR4 expression was detected in AOM/DSS group in comparison with vehicle group (Figure 6b,c, +224%, $p < 0.001$ vs. vehicle group). Such increase was counteracted in a dose-dependent manner by 30–

150 mg/kg mPGA treatment (Figure 6b,c, −42%, $p < 0.05$; −58%, $p < 0.001$; and −73.5%, $p < 0.001$, respectively, vs. AOM/DSS group). In the presence of PPARα antagonist MK866, 150 mg/kg mPGA effect was profoundly inhibited (Figure 6b,c, +282%, $p < 0.001$ vs. mPGA 150 mg/kg group) while no significant variation of TLR4 expression was detected in glucosamine alone group (Figure 6b,c, +4.6%, ns vs. AOM/DSS group).

On the contrary, a marked decrease in PPARα expression was observed in AOM/DSS colon tissue (Figure 6b–d, −86%, $p < 0.001$ vs. vehicle group) and this effect was associated to a severe decrease in *wt*p53 expression (Figure 6b–d, −90%, $p < 0.001$ vs. vehicle group). Administration of 30–150 mg/kg mPGA dose-dependently increased both PPARα (Figure 6b–d, +123%, $p < 0.05$; +238%, $p < 0.001$; and +499%, $p < 0.001$ vs. AOM/DSS group) and wtp53 expression (Figure 6b–e, +59%, $p < 0.05$; +210%, $p < 0.001$; and +455%, $p < 0.001$ vs. AOM/DSS group). As expected, such increases were strongly impaired by MK866 administration (Figure 6b–e, −82%, $p < 0.05$; and −78%, $p < 0.05$ vs. 150 mg/kg mPGA group, for PPARα and *wt*p53 expression, respectively), whereas no significant effect was produced neither on PPARα (Figure 6b,c, +14% vs. AOM/DSS group, ns) nor *wt*p53 (Figure 6b–e, +16%, ns vs. AOM/DSS group) expression by glucosamine alone.

4. Discussion

The advancements in early screening and personalized treatments have significantly improved therapy and survival rates for patients with CRC (Koroukian et al., 2023; Zeineddine et al., 2023). Early screening through methods such as colonoscopy allows for the detection of CRC in its initial stages, identifying precancerous growths and enabling timely intervention and treatment (Simon, 2016). In addition to prevention, healthy lifestyle, and proper diet, reducing the chronic pro-inflammatory conditions in the colon may be beneficial (Janakiram & Rao, 2014).

Introducing molecules that favorably affect chronic mucosal inflammation and reduce mucosal hyperproliferation is crucial for promptly halting the molecular pathways driving cancer growth and progression (Singh et al., 2019). Developing new tools with a safe profile and high tolerability, which can act on multiple levels to inhibit the transition from chronic inflammation to angiogenesis and cancer, is

essential. These advancements pave the way for personalized therapies and enhance the effectiveness of current drugs available against CRC.

Natural functional lipids such as PEA have demonstrated significant anti-inflammatory properties. These benefits have been observed in both the field of rheumatology (Schweiger et al., 2019) and in controlling experimental acute colitis in mice (Borrelli et al., 2015). Our study has revealed that mPGA exhibits marked and dose-dependent protection against mucosal damage and angiogenesis, thus limiting carcinogenesis and rectal colon polyps' formation in a murine colon cancer model induced by chronic inflammation from AOM/DSS. Notably, mPGA demonstrated a significant and dose-dependent reduction in both the number and size of tumoral neoformations, accompanied by a noteworthy decrease in mucosal damage as evidenced by both *in vivo* endoscopic and post-mortem macroscopic evaluations, alongside a significant improvement in mice survival rates. The mPGA reported LD50 of >2000 mg/kg further indicates an excellent safety profile (Cordaro et al., 2019). Our findings highlight that mPGA maintains a normal histological architecture in colon mucosal samples. Additionally, mPGA is capable of exerting a significant management over colon epithelial angiogenesis and proliferation, respectively, causing a marked reduction in the number of new CD31-positive vessels and Ki67-positive proliferating cells in the gut mucosa. The reduction in VEGF and MMP-9 levels in the colon mucosa induced by mPGA further strengthens the anti-angiogenetic effect of the tested compound. Interestingly, colon mast cells, a source of both MMP-9 and VEGF (Liu et al., 2023), are suggested to play key roles in CRC progression (Acikalin et al., 2005; Yu et al., 2018). Although our present study did not directly address the issue, it can be speculated that the inhibitory effect of mPGA on VEGF and MMP-9 levels might depend, at least in part, on the down-modulation of colon mast cells. Indeed, mPGA was shown to decrease *in vivo* mast cell hyperplasia (Cordaro et al., 2019). The data further reveal that in our experimental conditions mPGA effect is independent from the glucosamine (monosaccharide portion of PGA), since glucosamine alone showed no beneficial effect in any of the studied parameters. In line with previous findings (Palenca et al., 2022), the effects of mPGA are mediated through agonism at the PPARα receptors. This is underscored by the nearly complete abolition of mPEA protective effects in our carcinogenesis model upon co-administration of MK866. As known, at molecular sight, the activation of the Akt/mTOR axis has been specifically linked to

neovascularization in the development of CRC (Sarnelli, Gigli, et al., 2016). This pathway triggers the overexpression of HIF1α, interacting with reactive oxygen species (ROS) to induce the release of VEGF, thus promoting neo-angiogenesis (Sarnelli, D'Alessandro, et al., 2016). In line with these findings and similarly to the previously documented anti-angiogenic effects of PEA in models of chronic colon inflammation (Sarnelli, D'Alessandro, et al., 2016), the results reported here demonstrate that mPGA significantly inhibits the Akt/mTOR pathway, crucial in the pro-angiogenic mechanisms associated with CRC carcinogenesis. Specifically, mPGA exhibits significant and dose-dependent inhibition of AOM/DSS-induced Akt, mTOR, and p7065 phosphorylation, leading to downstream suppression of HIF1α expression, VEGF release, and hemoglobin content (an indirect marker of neovascularization). In this context, the effects of mPGA were also found to be PPARα-dependent and independent of the monosaccharide component. No effects were detected in the presence of the MK866, and glucosamine alone failed to elicit any significant impact on Akt/mTOR signaling induced by AOM/DSS. Of particular interest, in situ evaluation of endogenous PEA level in the mice colon revealed a moderate decrease following AOM/DSS treatment. Surprisingly, the administration of mPGA reversed this effect, leading to a progressive and dose-dependent increase in PEA accumulation in the colon. This effect was not influenced by the monosaccharide component of PGA and was strictly dependent on PPARα activation. These findings suggest a genuine synergistic enhancement of endogenous PEA effect potentiation induced by mPGA. It is worth noting that disruption of PPARα expression in the intestine exacerbates AOM/DSS-induced colon carcinogenesis, resulting in larger tumor size, increased tumor multiplicity and malignancy, and enhanced neo-angiogenesis (Luo et al., 2019). The clear inverse correlation between PPARα levels and poor prognosis in CRC is evident, as low levels of PPARα are associated with a reduction in pro-apoptotic mechanisms that control tumor proliferation (Kaipainen et al., 2007). Our data demonstrate that oral supplementation of mPGA, likely through increased colon PEA production, leads to a progressive restoration of PPARα levels. Consistent with findings from previous studies on acute colitis models (Palenca et al., 2023), our research in the AOM/DSS model demonstrates that mPGA significantly reduces TLR4 expression. This aligns with the well-established notion that TLR4 upregulation in colon cancer serves as a predictive marker for carcinogenesis promotion (Fukata et al., 2007; Hu et al., 2021).

Consequently, we can infer that the pleiotropic effects mediated by mPGA, including the upregulation of PPARα, the reduction in TLR4, and the enhancement of *wt*p53 expression, collectively exert a potent influence on intestinal neoplastic proliferation. These findings underscore a novel mechanism by which natural ALIAmides such as mPGA exert colon-protective and anti-angiogenic effects in CRC. While further studies are warranted to define any potential direct antineoplastic activity of mPGA in colon carcinoma cell lines, additional investigations will aim to evaluate its possible, yet undefined, antiproliferative effect in genetic models of colon cancer. These experimental advancements will shed light on whether mPGA, beyond its anti-inflammatory and colon-protective effects, can indeed exert cancer prevention properties.

Author Contributions

Irene Palenca: Conceptualization; data curation; formal analysis; methodology; project administration; software; validation; writing – original draft; writing – review and editing. **Silvia Basili Franzin:** Conceptualization; data curation; formal analysis; methodology; writing – original draft; writing – review and editing. **Aurora Zilli:** Formal analysis; methodology; validation. **Luisa Seguella:**Methodology; validation. **Anna Troiani:** Formal analysis; methodology. **Federico Pepi:** Formal analysis; methodology. **Martina Vincenzi:** Data curation. **Giuseppe Giugliano:** Formal analysis. **Viviana Catapano:** Formal analysis; methodology; validation. **Italia Di Filippo:** Data curation. **Giovanni Sarnelli:** Supervision. **Giuseppe Esposito:** Conceptualization; data curation; supervision; writing – original draft; writing – review and editing.

Acknowledgment

Open access publishing facilitated by Universita degli Studi di Roma La Sapienza, as part of the Wiley - CRUI-CARE agreement.

Conflict of Interest Statement

The authors declare that the research was conducted in the absence of any conflict of interest.

5. References

1. Zhang, Y.-Z.; Li, Y.-Y. Inflammatory bowel disease: Pathogenesis. *World J. Gastroenterol.* **2014**, *20*, 91–99. [CrossRef] [PubMed]
2. Siel, D.; Beltrán, C.J.; Martínez, E.; Pino, M.; Vargas, N.; Salinas, A.; Pérez, O.; Pereira, I.; Ramírez-Toloza, G. Elucidating the Role of Innate and Adaptive Immune Responses in the Pathogenesis of Canine Chronic Inflammatory Enteropathy—A Search for

Potential Biomarkers. *Animals* **2022**, *12*, 1645. [CrossRef] [PubMed]

3. Kucharzik, T.; Koletzko, S.; Kannengießer, K.; Dignaß, A. Ulcerative Colitis—Diagnostic and Therapeutic Algorithms.

Dtsch. Ärzteblatt Int. **2020**, *117*, 564–574. [CrossRef] [PubMed]

4. Du, L.; Ha, C. Epidemiology and Pathogenesis of Ulcerative Colitis. *Gastroenterol. Clin. N. Am.* **2020**, *49*, 643–654. [CrossRef]
5. Gearry, R.B.; Barclay, M.L.; Burt, M.J.; Collett, J.A.; Chapman, B.A. Thiopurine drug adverse effects in a population of New

Zealand patients with inflammatory bowel disease. *Pharmacoepidemiol. Drug Saf.* **2004**, *13*, 563–567. [CrossRef] [PubMed]

6. Kobayashi, T.; Siegmund, B.; Le Berre, C.; Wei, S.C.; Ferrante, M.; Shen, B.; Bernstein, C.N.; Danese, S.; Peyrin-Biroulet, L.; Hibi, T.

Ulcerative colitis. *Nat. Rev. Dis. Prim.* **2020**, *6*, 1–20. [CrossRef] [PubMed]

7. Cordaro, M.; Siracusa, R.; Impellizzeri, D.; D'Amico, R.; Peritore, A.F.; Crupi, R.; Gugliandolo, E.; Fusco, R.; Di Paola, R.;

Schievano, C.; et al. Safety and efficacy of a new micronized formulation of the ALIAmide palmitoylglucosamine in preclinical

models of inflammation and osteoarthritis pain. *Arthritis Res. Ther.* **2019**, *21*, 254. [CrossRef]

8. Gugliandolo, E.; Peritore, A.F.; Piras, C.; Cuzzocrea, S.; Crupi, R. Palmitoylethanolamide and Related ALIAmides: Prohomeostatic

Lipid Compounds for Animal Health and Wellbeing. *Veter.-Sci.* **2020**, *7*, 78. [CrossRef]

9. Capasso, R.; Orlando, P.; Pagano, E.; Aveta, T.; Buono, L.; Borrelli, F.; Di Marzo, V.; Izzo, A.A. Palmitoylethanolamide normalizes

intestinal motility in a model of post-inflammatory accelerated transit: Involvement of CB1 receptors and TRPV1 channels.

J. Cereb. Blood Flow Metab. **2014**, *171*, 4026–4037. [CrossRef]

10. Borrelli, F.; Romano, B.; Petrosino, S.; Pagano, E.; Capasso, R.; Coppola, D.; Battista, G.; Orlando, P.; Di Marzo, V.; Izzo, A.A.
Palmitoylethanolamide, a naturally occurring lipid, is an orally effective intestinal anti-inflammatory agent. *Br. J. Pharmacol.* **2014**,
172, 142–158. [CrossRef]
11. Yomogida, S.; Kojima, Y.; Tsutsumi-Ishii, Y.; Hua, J.; Sakamoto, K.; Nagaoka, I. Glucosamine, a naturally oc-curring amino
monosaccharide, suppresses dextran sulfate sodium-induced colitis in rats. *Int. J. Mol. Med.* **2008**, *22*, 317–323. [PubMed]
12. Bak, Y.-K.; Lampe, J.W.; Sung, M.-K. Effects of dietary supplementation of glucosamine sulfate on intestinal inflammation in a
mouse model of experimental colitis. *J. Gastroenterol. Hepatol.* **2014**, *29*, 957–963. [CrossRef]
13. Navarro, S.L.; Levy, L.; Curtis, K.R.; Lampe, J.W.; Hullar, M.A.J. Modulation of Gut Microbiota by Glucosamine and Chondroitin
in a Randomized, Double-Blind Pilot Trial in Humans. *Microorganisms* **2019**, *7*, 610. [CrossRef] [PubMed]
14. Iannotta, M.; Belardo, C.; Trotta, M.C.; Iannotti, F.A.; Vitale, R.M.; Maisto, R.; Boccella, S.; Infantino, R.; Ricciardi, F.; Mirto, B.F.; et al. N-palmitoyl-D-glucosamine, a Natural Monosaccharide-Based Glycolipid, Inhibits TLR4 and Prevents LPS-Induced
Inflammation and Neuropathic Pain in Mice. *Int. J. Mol. Sci.* **2021**, *22*, 1491. [CrossRef] [PubMed]
15. Del Re, A.; Corpetti, C.; Pesce, M.; Seguella, L.; Steardo, L.; Palenca, I.; Rurgo, S.; De Conno, B.; Sarnelli, G.; Esposito, G. Ultramicronized Palmitoylethanolamide Inhibits NLRP3 Inflammasome Expression and Pro-Inflammatory Response Activated
by SARS-CoV-2 Spike Protein in Cultured Murine Alveolar Macrophages. *Metabolites* **2021**, *11*, 592. [CrossRef] [PubMed]
16. Impellizzeri, D.; Di Paola, R.; Cordaro, M.; Gugliandolo, E.; Casili, G.; Morittu, V.M.; Britti, D.; Esposito, E.; Cuzzocrea, S. Adelmidrol, a palmitoylethanolamide analogue, as a new pharmacological treatment for the management of acute and chronic
inflammation. *Biochem. Pharmacol.* **2016**, *119*, 27–41. [CrossRef]

17. Cooper, H.S.; Murthy, S.N.; Shah, R.S.; Sedergran, D.J. Clinicopathologic study of dextran sulfate sodium experimental murine
colitis. Laboratory investigation. *J. Tech. Methods Pathol.* **1993**, *69*, 238–249.
18. Li, R.; Kim, M.-H.; Sandhu, A.K.; Gao, C.; Gu, L. Muscadine Grape (*Vitis rotundifolia*) or Wine Phytochemicals Reduce Intestinal
Inflammation in Mice with Dextran Sulfate Sodium-Induced Colitis. *J. Agric. Food Chem.* **2017**, *65*, 769–776. [CrossRef]
19. Cushing, K.; Higgins, P.D.R. Management of Crohn Disease. *JAMA* **2021**, *325*, 69–80. [CrossRef]
20. Bruscoli, S.; Febo, M.; Riccardi, C.; Migliorati, G. Glucocorticoid Therapy in Inflammatory Bowel Disease: Mechanisms and
Clinical Practice. *Front. Immunol.* **2021**, *12*. [CrossRef]
21. Shen, W.; Gao, Y.; Lu, B.; Zhang, Q.; Hu, Y.; Chen, Y. Negatively regulating TLR4/NF-κB signaling via PPARα in endotoxin-
induced uveitis. *Biochim. Et Biophys. Acta (BBA)—Mol. Basis Dis.* **2014**, *1842*, 1109–1120. [CrossRef] [PubMed]
22. Couch, D.G.; Cook, H.; Ortori, C.; Barrett, D.; Lund, J.N.; O'Sullivan, S.E. Palmitoylethanolamide and Cannabidiol Prevent Inflammation-induced Hyperpermeability of the Human Gut In Vitro and In Vivo—A Randomized, Placebo-controlled, Double-
blind Controlled Trial. *Inflamm. Bowel Dis.* **2019**, *25*, 1006–1018. [CrossRef] [PubMed]
23. Matalon, S.T.; Azar, S.; Meiri, D.; Hadar, R.; Nemirovski, A.; Abu Jabal, N.; Konikoff, F.M.; Drucker, L.; Tam, J.; Naftali,
T. Endocannabinoid Levels in Ulcerative Colitis Patients Correlate with Clinical Parameters and Are Affected by Cannabis
Consumption. *Front. Endocrinol.* **2021**, *12*. [CrossRef]
24. Esposito, G.; Corpetti, C.; Pesce, M.; Seguella, L.; Annunziata, G.; Del Re, A.; Vincenzi, M.; Lattanzi, R.; Lu, J.; Sanseverino, W.; et al. A
Palmitoylethanolamide Producing Lactobacillus paracasei Improves Clostridium difficile Toxin A-Induced Colitis. *Front. Pharmacol.*
2021, *12*. [CrossRef] [PubMed]
25. Esposito, G.; Pesce, M.; Seguella, L.; Lu, J.; Corpetti, C.; Del Re, A.; De Palma, F.; Esposito, G.; Sanseverino, W.; Sarnelli, G.

Engineered *Lactobacillus paracasei* Producing Palmitoylethanolamide (PEA) Prevents Colitis in Mice. *Int. J. Mol. Sci.* **2021**, *22*, 2945. [CrossRef]
Biomolecules **2022**, *12*, 1163 12 of 13

26. Goodman, M.J.; Kent, P.W.; Truelove, S.C. Glucosamine synthetase activity of the colonic mucosa in ulcerative colitis and Crohn's disease. *Gut* **1977**, *18*, 219–228. [CrossRef]
27. Goodman, M.J.; Kent, P.W.; Truelove, S.C. Glucosamine synthetase activity of the colonic mucosa in membranous colitis. *Gut* **1977**, *18*, 229–231. [CrossRef]
28. Salvatore, S.; Heuschkel, R.; Tomlin, S.; Davies, S.E.; Edwards, S.; Walker-Smith, J.A.; French, I.; Murch, S.H. A pilot study of N-acetyl glucosamine, a nutritional substrate for glycosaminoglycan synthesis, in paediatric chronic inflammatory bowel disease. *Aliment. Pharmacol. Ther.* **2000**, *14*, 1567–1579. [CrossRef]
29. Kantor, E.D.; Zhang, X.; Wu, K.; Signorello, L.B.; Chan, A.T.; Fuchs, C.S.; Giovannucci, E.L. Use of glucosamine and chondroitin supplements in relation to risk of colorectal cancer: Results from the Nurses' Health Study and Health Professionals follow-up study. *Int. J. Cancer* **2016**, *139*, 1949–1957. [CrossRef]
30. Kantor, E.D.; Newton, C.C.; Giovannucci, E.L.; McCullough, M.L.; Campbell, P.T.; Jacobs, E.J. Glucosamine use and risk of colorectal cancer: Results from the Cancer Prevention Study II Nutrition Cohort. *Cancer Causes Control* **2018**, *29*, 389–397. [CrossRef]
31. Lee, D.H.; Cao, C.; Zong, X.; Zhang, X.; O'Connell, K.; Song, M.; Wu, K.; Du, M.; Cao, Y.; Giovannucci, E.L.; et al. Glucosamine and Chondroitin Supplements and Risk of Colorectal Adenoma and Serrated Polyp. *Cancer Epidemiol. Biomark. Prev.* **2020**, *29*, 2693–2701. [CrossRef] [PubMed]
32. Navarro, S.L.; White, E.; Kantor, E.; Zhang, Y.; Rho, J.; Song, X.; Milne, G.; Lampe, P.D.; Lampe, J.W. Randomized Trial of Glucosamine and Chondroitin Supplementation on Inflammation and Oxidative Stress Biomarkers and Plasma Proteomics Profiles in Healthy Humans. *PLoS ONE* **2015**, *10*, e0117534. [CrossRef] [PubMed]
33. Sarnelli, G.; Seguella, L.; Pesce, M.; Lu, J.; Gigli, S.; Bruzzese, E.; Lattanzi, R.; D'Alessandro, A.; Cuomo, R.; Steardo, L.; et al. HIV-1 Tat-induced diarrhea is improved by the PPARalpha agonist, palmitoylethanolamide, by suppressing the activation of enteric glia. *J. Neuroinflamm.* **2018**, *15*, 94. [CrossRef]

34. Darmani, N.A.; Izzo, A.A.; Degenhardt, B.; Valenti, M.; Scaglione, G.; Capasso, R.; Sorrentini, I.; Di Marzo, V. Involvement of the cannabimimetic compound, N-palmitoyl-ethanolamine, in inflammatory and neuropathic conditions: Review of the available pre-clinical data, and first human studies. *Neuropharmacology* **2005**, *48*, 1154–1163. [CrossRef] [PubMed]
35. Grabacka, M.; Pierzchalska, M.; Płonka, P.M.; Pierzchalski, P. The Role of PPAR Alpha in the Modulation of Innate Immunity. *Int. J. Mol. Sci.* **2021**, *22*, 10545. [CrossRef] [PubMed]
36. Dana, N.; Vaseghi, G.; Haghjooy-Javanmard, S. Crosstalk between Peroxisome Proliferator-Activated Receptors andToll-Like Receptors: A Systematic Review. *Adv. Pharm. Bull.* **2019**, *9*, 12–21. [CrossRef]
37. Takeda, K.; Akira, S. Microbial recognition by Toll-like receptors. *J. Dermatol. Sci.* **2004**, *34*, 73–82. [CrossRef]
38. Zhen, Y.; Zhang, H. NLRP3 Inflammasome and Inflammatory Bowel Disease. *Front. Immunol.* **2019**, *10*, 276. [CrossRef]
39. Chen, M.-Y.; Ye, X.-J.; He, X.-H.; Ouyang, D.-Y. The Signaling Pathways Regulating NLRP3 Inflammasome Activation. *Inflammation*

2021, *44*, 1229–1245. [CrossRef]

40. Zhuang, Y.; Zhao, F.; Liang, J.; Deng, X.; Zhang, Y.; Ding, G.; Zhang, A.; Jia, Z.; Huang, S. Activation of COX-2/mPGES-1/PGE2

Cascade via NLRP3 Inflammasome Contributes to Albumin-Induced Proximal Tubule Cell Injury. *Cell. Physiol. Biochem.* **2017**, *42*,

797–807. [CrossRef]

41. Luo, H.; Guo, P.; Zhou, Q. Role of TLR4/NF-κB in Damage to Intestinal Mucosa Barrier Function and Bacterial Translocation in

Rats Exposed to Hypoxia. *PLoS ONE* **2012**, *7*, e46291. [CrossRef] [PubMed]

42. Morales-Soto, W.; Gulbransen, B.D. Enteric Glia: A New Player in Abdominal Pain. *Cell. Mol. Gastroenterol. Hepatol.* **2019**, *7*,

433–445. [CrossRef] [PubMed]

43. Yuan, B.; Tang, W.-H.; Lu, L.-J.; Zhou, Y.; Zhu, H.-Y.; Zhou, Y.-L.; Zhang, H.-H.; Hu, C.-Y.; Xu, G.-Y. TLR4 upregulates

CBS expression through NF-κB activation in a rat model of irritable bowel syndrome with chronic visceral hypersensitivity.

World J. Gastroenterol. **2015**, *21*, 8615–8628. [CrossRef]

44. Bettoni, I.; Comelli, F.; Rossini, C.; Granucci, F.; Giagnoni, G.; Peri, F.; Costa, B. Glial TLR4 receptor as new target to treat
neuropathic pain: Efficacy of a new receptor antagonist in a model of peripheral nerve injury in mice. *Glia* **2008**, *56*, 1312–1319.
[CrossRef]
45. Hutchinson, M.R.; Zhang, Y.; Brown, K.; Coats, B.D.; Shridhar, M.; Sholar, P.W.; Patel, S.J.; Crysdale, N.Y.; Harrison, J.A.; Maier,
S.F. Non-stereoselective reversal of neuropathic pain by naloxone and naltrexone: Involvement of toll-like receptor 4 (TLR4).
Eur. J. Neurosci. **2008**, *28*, 20–29. [CrossRef] [PubMed]
46. Lönnfors, S.; Vermeire, S.; Greco, M.; Hommes, D.; Bell, C.; Avedano, L. IBD and health-related quality of life—Discovering the
true impact. *J. Crohn's Colitis* **2014**, *8*, 1281–1286. [CrossRef] [PubMed]
47. Cuesta, C.M.; Pascual, M.; Pérez-Moraga, R.; Rodríguez-Navarro, I.; García-García, F.; Ureña-Peralta, J.R.; Guerri, C. TLR4
Deficiency Affects the Microbiome and Reduces Intestinal Dysfunctions and Inflammation in Chronic Alcohol-Fed Mice.
Int. J. Mol. Sci. **2021**, *22*, 12830. [CrossRef] [PubMed]
48. Philip-Hollingsworth, S.; Dazzo, F.B.; I Hollingsworth, R. Structural requirements of Rhizobium chitolipooligosaccharides for
uptake and bioactivity in legume roots as revealed by synthetic analogs and fluorescent probes. *J. Lipid Res.* **1997**, *38*, 1229–1241.
[CrossRef]
49. Das, A.; Srinivasan, M.; Ghosh, T.S.; Mande, S.S. Xenobiotic metabolism and gut microbiomes. *PLoS ONE* **2016**, *11*. [CrossRef]
Biomolecules **2022**, *12*, 1163 13 of 13

50. Matuszyk, A.; Ceranowicz, D.; Warzecha, Z.; Ceranowicz, P.; Fyderek, K.; Gała ̨zka, K.; Cieszkowski, J.; Bonior, J.; Jaworek, J.; Pihut, M.; et al. The Influence of Ghrelin on the Development of Dextran Sodium Sul-fate-Induced Colitis in Rats. *BioMed Res. Int.* **2015**, *2015*, 718314. [CrossRef]
51. Dembin´ski, A.; Warzecha, Z.; Ceranowicz, P.; Dembin´ski, M.; Cieszkowski, J.; Gosiewski, T.; Bulanda, M.; Kus´nierz-Cabala, B.; Gała ̨zka, K.; Konturek, P.C. Synergic Interaction of Rifaximin and Mutaflor (*Escherichia coli* Nissle 1917) in

the Treatment of Acetic Acid-Induced Colitis in Rats. *Gastroenterol. Res. Pract.* **2016**, *2016*, 3126280. [CrossRef] [PubMed]

52. Matuszyk,A.;Ceranowicz,P.;Warzecha,Z.;Cieszkowski,J.;Gała ̨zka,K.;Bonior,J.; Jaworek,J.;Konturek,P.C.;Gil,K.;Dembin´ski, A. Pretreatment with obestatin inhibits the development of acetic acid-induced colitis in rats. *Arch. Med. Sci.* **2018**, *14*, 920–929. [CrossRef] [PubMed]

Intrarectal Administration of Adelmidrol plus Hyaluronic Acid Gel Ameliorates Experimental Colitis in Mice and Inhibits Pro-Inflammatory Response in *Ex Vivo* Cultured Biopsies Derived from Ulcerative Colitis-Affected Patients

Irene Palenca , Luisa Seguella , Aurora Zilli , Silvia Basili Franzin , Alessandro Del Re , Federico Pepi , Anna Troiani , Marcella Pesce , Sara Rurgo , Fatima Domenica Elisa De Palma , Gaetano Luglio , Francesca Paola Tropeano , Giovanni Sarnelli and Giuseppe Esposito

Abstract: Improving clinical outcomes and delaying disease recrudescence in Ulcerative Colitis (UC) patients is crucial for clinicians. In addition to traditional and new pharmacological therapies that utilize biological drugs, the development of medical devices that can ameliorate UC and facilitate the remission phase should not be overlooked. Drug-based therapy requires time to be personalized and to evaluate the benefit/risk ratio. However, the increasing number of diagnosed UC cases worldwide necessitates the exploration of new strategies to enhance clinical outcomes. By incorporating medical devices alongside pharmacological treatments, clinicians can provide additional support to UC patients, potentially improving their condition and slowing down the recurrence of symptoms. Chemically identified as an azelaic acid derivative and palmitoylethanolamide (PEA) analog, adelmidrol is a potent anti-inflammatory and antioxidant compound. In this study, we aimed to evaluate the effect of an intrarectal administration of 2% adelmidrol (Ade) and 0.1% hyaluronic acid (HA) gel formulation in both the acute and resolution phase of a mouse model of colitis induced via DNBS enema. We also investigated its activity in cultured human colon biopsies isolated from UC patients in the remission phase at follow-up when exposed in vitro to a cytomix challenge. Simultaneously, with its capacity to effectively alleviate chronic painful inflammatory cystitis when administered intravesically to urological patients such as Vessilen, the intrarectal administration of Ade/HA gel has shown remarkable potential in improving the course of colitis. This treatment approach has demonstrated a reduction in the histological damage score and an increase in the

expression of ZO-1 and occludin tight junctions in both *in vivo* studies and human specimens. By acting independently on endogenous PEA levels and without any noticeable systemic absorption, the effectiveness of Ade/HA gel is reliant on a local antioxidant mechanism that functions as a “barrier effect” in the inflamed gut. Building on the findings of this preliminary study, we are confident that the Ade/HA gel medical device holds promise as a valuable adjunct in supporting traditional anti-UC therapies.

Keywords: experimental mouse colitis; DNBS; intrarectal adelmidrol/hyaluronic acid gel administration; medical device; human biopsies

1. Introduction

Inflammatory bowel diseases (IBDs) are chronic and multifactorial illnesses characterized by remission periods and recurrent flares in which diarrhea, visceral pain, rectal bleeding/bloody stools, and weight loss are the main clinical symptoms [1]. Ulcerative Colitis (UC) and Chron’s disease (CD) are the most common forms of IBDs, and despite their uncertain etiology [2,3], according to Global Disease Burden (GBD) IBD Collaborators, UC affects millions of people worldwide (2020), and current treatments have varying levels of efficacy and adverse reactions with a refined evaluation by the clinician and patients about the best combination of the risk/benefit ratio [4]. Despite being commonly prescribed for a UC treatment, traditional long-term therapies like corticosteroids, immunosuppressants, and biologic agents can cause substantial and unpredictable side effects, negatively impacting the stability of patients [5]. It is, thus, pivotal to identify and pharmacologically characterize new drugs and/or medical devices to amplify the current tools against UC. Adelmidrol (N,N’-bis(2-hydroxyethyl-nonanediamide) is a synthetic compound with anti-inflammatory, analgesic, and antioxidant properties deriving from azelaic acid and plays interesting roles in modulating the immune response and reducing oxidative stress [6]. Oral adelmidrol administration in mice revealed powerful anti-inflammatory effects, and it has been demonstrated to reduce oxidative stress, increasing the integrity of the intestinal mucosal barrier during experimental colitis damage [7]. Many of the beneficial effects displayed by adelmidrol are linked to its intrinsic capability to increase the level of the endogenous palmitoylethanolamide (PEA) via the so-called “entourage effect” [8]. Furthermore, we recently showed that adelmidrol can effectively enhance the therapeutic approach based on PEA in various intestinal disorders. It achieves this by increasing the production and availability of PEA through its selective targeting of

peroxisome proliferator-activated receptors- γ (PPAR- γ) [9]. To maximize adelmidrol's beneficial effects, adelmidrol has been co-administered with hyaluronic acid (HA), a glycosaminoglycan of the extracellular matrix, [10] and such an association has demonstrated promising benefits in controlling the inflammatory processes characteristic of pathological conditions, such as osteoarthritis [11] and spinal cord injury [12]. However, there is currently a lack of evidence regarding the potential therapeutic effect of adelmidrol/HA association in intrarectal medical device systems during colitis. Nevertheless, pharmacologically associated adelmidrol (Ade)/HA restored the urothelium tissue's integrity in interstitial cystitis/painful bladder syndrome (IC/PBS) via topic intravesical administration. In this way, such a sterile medical device can topically reduce inflammation in the urothelium, displaying a synergistic anti-inflammatory effect in the bladder [13]. Based on this background, the aims of the present study were to (i) investigate the mechanical effect of the association of Ade/HA administered via an intrarectal route in a mouse model of DNBS-induced colitis, testing the effect of HA 0,1% and adelmidrol 2% gel formulation on the amelioration of colon inflammation during both the acute (3rd day) and late (7th day) resolution of colitis. (ii) In this context, we evaluated the inhibitory effect of HA on the absorption of adelmidrol, addressing its function through a mechanical action in situ that promotes intestinal homeostasis and exhibits inhibitory effects against the degradation of HA by hyaluronidase-1 (HYAL-1). (iii) From a translational perspective, to confirm the protective effect of Ade/HA gel, we also assessed its protective effect in human biopsies isolated from patients diagnosed with UC in the remission phase. The biopsies were treated with cytomix (lipo-polisaccharide (LPS), interferon-γ (IFN-γ), and tumor necrosis factor-α (TNF-α)) in vitro to re-activate the inflammatory process. The results of the study demonstrated the protective action of the Ade/HA formulation, leading to a reduction in colon inflammation and a potential decrease in mucosal damage and permeability. Overall, this study suggests that the mechanical action of the Ade/HA gel formulation makes it a promising medical device for the prevention of mucosal damage and related inflammatory complications for the treatment of colitis.

2. Results

2.1. The Endoscopic Evaluation, Colon Length Measurement, Spleen Weight and DAI Score Showed That Ade/HA Intrarectal Administration Ameliorated both the Acute and Post-Remission Phase of DNBS-Induced Colitis

The endoscopic evaluation of mouse rectal mucosa (rectoscopy) revealed that the administration of DNBS caused a significant increase in colitis features measured as the injury score on the third day after DNBS stimulus (+392% *** $p < 0.001$ vs. *vehicle*) [Figure 1]. Such increased damage was slightly reduced in the resolving phase of DNBS-induced colitis on the seventh day, but it remained significantly higher in comparison to the corresponding vehicle (+185% *** $p < 0.001$ vs. *vehicle*) [Figure 1]. Every 72 h, the intrarectal administration of Ade/Ha gel markedly impacted the colitis' course since it resulted in a significant reduction in injury score values both on the 3rd day (−75% °°° $p < 0.001$ vs. *DNBS*) and on the 7th day (−55% °°° $p < 0.001$ vs. *DNBS*) [Figure 1]. Conversely, no relevant impact on mouse mucosa protection was observed following HA gel treatment alone. In fact, in the same experimental conditions, histological damage scores were not affected significantly on the 3rd (−4.6% vs. *DNBS*) or 7th day (−10% vs. *DNBS*) [Figure 1]. Our data show that DNBS treatment caused a marked and significant decrease in the colon length with respect to the vehicle group, and colon shortening was particularly evident on the 3rd day (−70% ** $p< 0.01$ vs. *vehicle*) and was still observable on the 7th day (−50% ** $p < 0.01$ vs. *vehicle*) [Figure 1]. In parallel to the endoscopic evaluation, Ade/HA resulted in a marked rescue of colon length in the two time points on the 3rd (+169% °°°$p < 0.001$ vs. *DNBS*) and 7th day (+100% °°° $p < 0.001$ vs. *DNBS*), whereas no significant effect was detected following HA treatment alone in both the acute (+9.4% vs. *DNBS*) and remission phase (+10% vs. *DNBS*) of the colitis [Figure 1]. As expected, the DNBS challenge caused significant spleen weight in both the acute (+ 63% *** $p < 0.001$ vs. *vehicle*) and remission phase (+25% ** $p < 0.01$ vs. *vehicle*); these data were accompanied by a marked increase in the DAI score on the 3rd day (+305% *** $p < 0.001$ vs. *vehicle*) and 7th day (+166% ** $p < 0.01$ vs. *vehicle*). The intrarectal administration of Ade/HA gel every 72 h resulted in a significant improvement in all the parameters. It reduced spleen weight on the 3rd day (−34% ° $p < 0.05$ vs. *DNBS*) and 7th day (−42% °°° $p < 0.001$ vs. *DNBS*) and attenuated the DAI score on the 3rd (−64% °°° $p < 0.001$) and 7th days (−77% °°° $p < 0.001$) vs. *DNBS.* No significant spleen weight reduction was observed following the HA treatment on the 3rd (−10% vs. *DNBS*) and 7th days (−3% vs. *DNBS*); the DAI score for the same intervals was (+2% vs. *DNBS*) and (−2.4% vs. *DNBS)*, respectively [Figure 1].

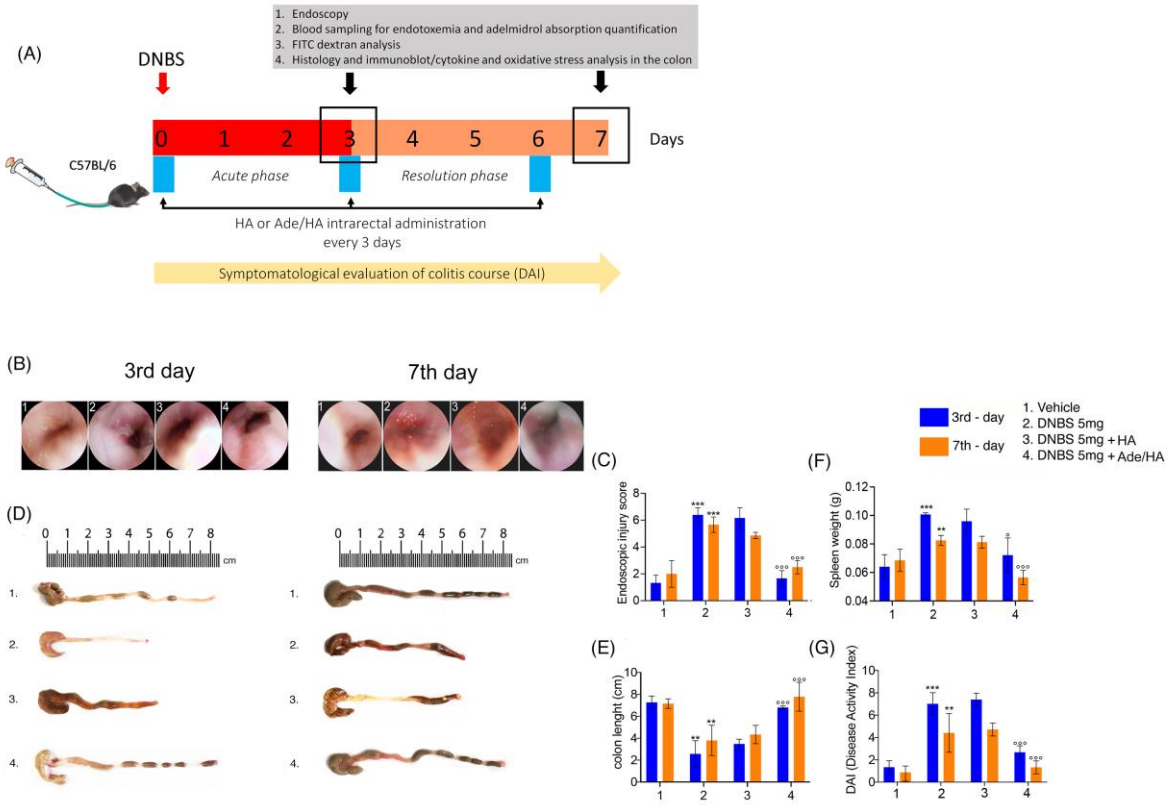

Figure 1. Experimental design and the ameliorative effect of intrarectal Ade/HA gel administration on DNBS-induced colitis in mice. Synoptic frame showing (**A**) the experimental plan of colitis induction and relative treatments in mice and relative time points for the DAI course, treatments, blood collection, and endoscopic procedures, and the post-mortem processing of the samples. The figure shows the endoscopic (**B**) images of the mice colon on the 3rd and 7th days after DNBS enema and (**C**) the respective endoscopic injury score evaluation; (**D**,**E**) representative post-mortem colon length examination and quantification. (**F**) Spleen weight quantification in mice on the 3rd and 7th day after DNBS enema and (**G**) DAI course in the experimental intervals. Results are expressed as the mean ± SD of n = 5 experiments *** $p < 0.001$ vs. *vehicle;* ** $p < 0.01$ vs. *vehicle;* °°° $p < 0.001$ vs. *DNBS*; ° $p < 0.001$ vs. *DNBS*.

2.2. Intrarectal Ade/HA Administration Reduced ZO-1 and Occludin Loss Induced by DNBS in both Acute and Remission Phase of Colitis

After the DNBS challenge, significant mucosal damage was observed at both time points according to the macroscopic evaluation carried out before. The histological damage score was significantly increased in the DNBS vs. the vehicle group on the 3rd day

(+800% *** $p < 0.001$ vs. *vehicle*) and was still evident on the 7th day (+567% *** $p < 0.001$ vs. *vehicle*). A significant increase in the infiltration of macrophages labeled with MAC387 was evident in the DNBS vs. vehicle group on the 3rd (+378% **** $p < 0.0001$ vs. *vehicle*) and 7th days (+398% ****$p < 0.0001$ vs. *vehicle*). In parallel to this, the absorption of FITC dextran dye was markedly increased across the colitis mucosa on the 3rd (+700% *** $p < 0.001$ vs. *vehicle*) and 7th days (+760% *** $p < 0.001$ vs. *vehicle*) following the DNBS challenge, confirming the overall damage of the mouse mucosa revealed by histological analysis [Figure 2]. No significant protective effect was observed by HA administration in the same experimental conditions. Conversely, there was a significant and consistent reduction in both mucosal damage and FITC-dextran permeability following the intrarectal administration of Ade/HA. This effect was evident for a significant reduction in the histological damage score of DNBS-induced tissue injury on the 3rd day (compared to *DNBS*, −53% °°° $p < 0.001$) and 7th day (compared to *DNBS*, −80% °°° $p < 0.001$). Furthermore, a significant reduction in MAC387-positive cell counts in the mucosa on the 3rd day (−75%°°°° $p < 0.0001$ vs. *DNBS*) and 7th day (−79%°°°° $p < 0.0001$ vs. *DNBS*) was detected. Moreover, Ade/HA treatment led to a significant decrease in the transmucosal passage of FITC dye on the 3rd day (compared to DNBS, −63% °°° $p < 0.001$) and 7th day (compared to DNBS, −78% °°° $p < 0.001$) [Figure 2]. Immunofluorescence and immunoblot analysis confirmed that the DNBS challenge resulted in a significant reduction in ZO-1 and occludin expression, indicating a severe disruption of the gut barrier integrity in colitis. Specifically, on day 3 post-DNBS challenge, we identified a significant decrease in ZO-1 (−69% *** $p < 0.001$ vs. *vehicle*) and occludin (65% *** $p < 0.001$ vs. *vehicle*). This effect persisted to a lesser but still significant extent during the resolution phase of colitis on day 7 post-DNBS challenge, with reductions in ZO-1 (77% *** $p < 0.001$ vs. *vehicle*) and occludin (75% *** $p < 0.001$ vs. *vehicle*). Immunoblot analysis confirmed these findings, showing significant reductions in ZO-1 and occludin expression compared to the DNBS challenge, both in the acute phase (−70%**** $p < 0.0001$ and −80% **** $p < 0.0001$ vs. *respective vehicle groups* for ZO-1) and resolution phase of colitis (−75%**** $p < 0.0001$ and −70%**** $p < 0.0001$ vs. *respective vehicle groups* for occludin). HA alone did not restore the expression of tight junctions in time point intervals via the immunofluorescence of ZO-1 on the 3rd or 7th day after the DNBS challenge (+0.5% vs. *DNBS* and +1% vs. *DNBS*, respectively). In parallel to this, no HA effect was detected for occludin both on the 3rd and 7th day after the DNBS challenge (+1% and +2% vs. *DNBS*, respectively). Such

data matched with immunoblot analysis showing that HA alone did not impact both ZO-1 expression on the 3rd (+2% vs. *DNBS*) and 7th days after the DNBS challenge (+2.2% vs. *DNBS*), and nor did it result in the ability to modify occludin expression in the same interval range (+1% vs. *DNBS* at 3rd day and +2% vs. *DNBS* at 7th day after DNBS challenge, respectively). Immunofluorescence analysis demonstrated that Ade/HA gel intrarectal administration significantly preserved the mucosal barrier by improving both ZO-1 and occludin expression on the 3rd (+190% °°° $p < 0.001$ for ZO-1 and +115% °°° $p < 0.001$ for occludin vs. *respective DNBS groups*) and 7th day (+290% °°° $p < 0.001$ for ZO-1 °°° $p < 0.001$ and +105% °°$p < 0.01$ for occludin vs. *respective DNBS groups*). According to these data, immunoblot analysis confirmed that Ade/HA gel caused the significant restoration of both ZO-1 and occludin expression on the 3rd (+180% °°°° $p < 0.0001$ for ZO-1 and +135% °°°° $p < 0.0001$ for occludin vs. *respective DNBS groups*) and 7th day (+100% for ZO-1 °°°° $p < 0.0001$ and +105% °°°° $p < 0.0001$ for occludin vs. *respective DNBS groups*) [Figure 2].

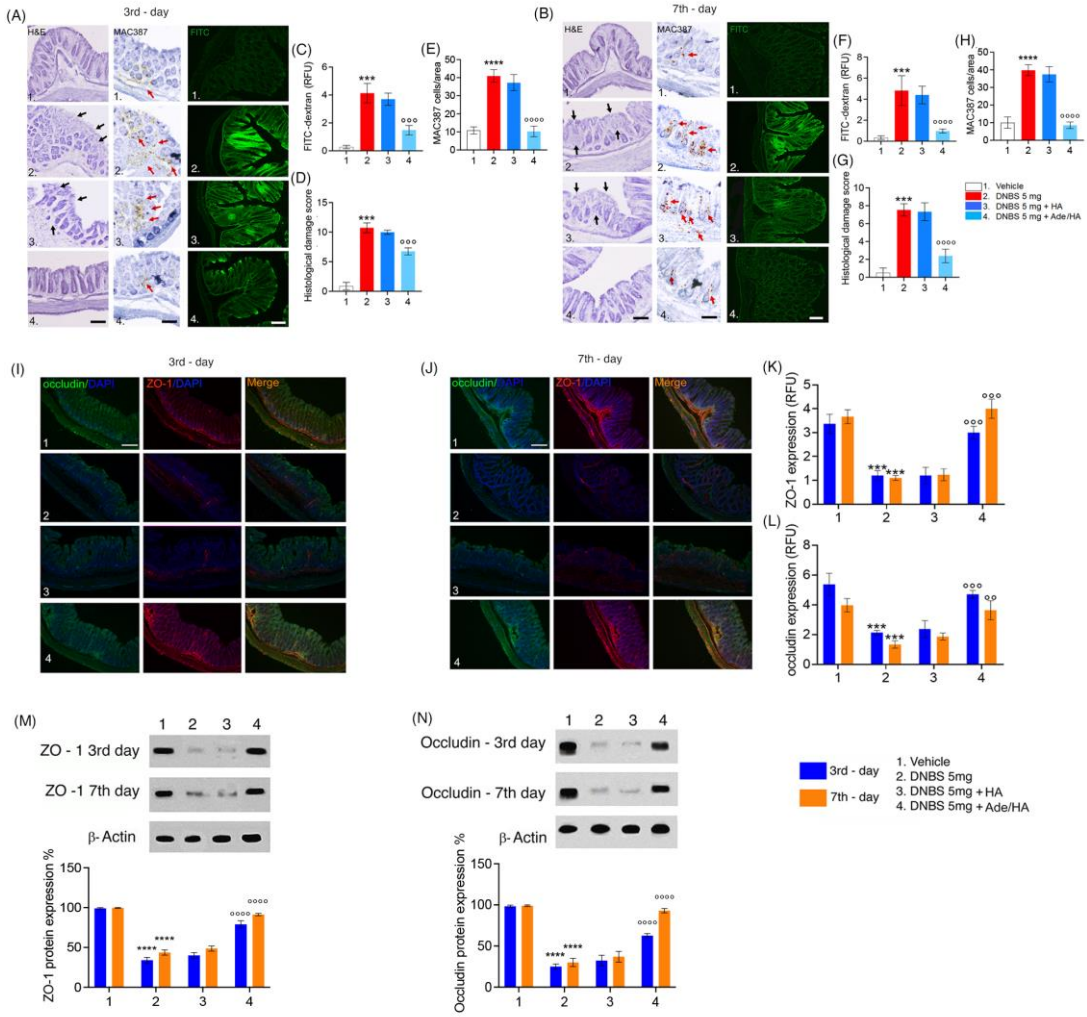

Figure 2. Intrarectal Ade/Ha gel administration ameliorates DNBS-induced histological damage and improves mucosal integrity by rescuing ZO-1 and occludin expression in mice. Synoptic frame showing the protective effect of Ade/Ha on mice mucosa in the acute and resolution phase of colitis induced by DNBS enema. The figure at the top shows the histological evaluation using hematoxylin–eosin staining and colon permeability via FITC-dextran immunofluorescence analysis carried out on the mice colon on the 3rd (**A**) and 7th day (**B**), respectively, after DNBS enema in the presence of different treatments. Respective quantification of both FITC-dextran relative fluorescence units (RFU), the histological damage score, and immunohistochemical expression of MAC387-positive cell on the 3rd (**C**–**E**) and 7th day (**F**–**H**). Magnification 20×; Scale bar 100 µm. The middle panel shows the immunofluorescence analysis of occludin and ZO-1 and their merged expression, respectively, on the 3rd and 7th day after DNBS enema (**I**–**J**) and

respective quantification by RFU (KL)—Magnification 20×; Scale bar 100 µm. In the lower panel, the figure shows the immunoblot expression and respective quantifications of ZO-1 (**M**) and Occludin (**N**), respectively, on the 3rd and 7th day after the DNBS enema. Results are expressed as the mean ± SD of $n = 5$ experiments **** $p < 0.0001$ vs. vehicle; *** $p < 0.001$ vs. vehicle; °°°° $p < 0.0001$ vs. DNBS; °°° $p < 0.001$ vs. DNBS; °° $p < 0.01$ vs. DNBS. Black arrows indicate areas of crypt loss and inflammation. Red arrows indicate a positive cluster of resident macrophages expressing the MAC387 protein.

2.3. Intrarectal Ade/HA Administration Reduced DNBS-Induced Proinflammatory Response, Oxidative Stress and Endotoxemia without Affecting Endogenous PEA Level and in Absence of Systemic Adelmidrol Absorption

Consistent with the expectations, the DNBS challenge elicited a pronounced pro-inflammatory response and oxidative stress in the mouse colon, as evidenced by significant increases in IL-1β (+138% *** $p < 0.001$ vs. *vehicle*), IL-6 (+1005% **** $p < 0.0001$ vs. *vehicle*) and TNF-α (+766% **** $p < 0.0001$ vs. *vehicle*), neutrophil infiltration indicated by up-regulation of MPO (+540% *** $p < 0.001$ vs. *vehicle*) and the oxidative stress induction manifested by a substantial rise in the lipid peroxidation marker malondyaldheide (MDA) (+158% *** $p < 0.001$ vs. *vehicle*) during the acute phase of colitis [Figure 3]. Moreover, the previously mentioned disruption of gut mucosal integrity was accompanied by a significant increase in endotoxemia during the acute phase of colitis (+218% *** $p < 0.001$ vs. *vehicle*) [Figure 3]. Even during the resolution phase of colitis, although to a slightly lesser extent, all the pro-inflammatory parameters remained markedly increased compared to the respective vehicle group. Notably, there was a significant up-regulation of IL-1β (+131% *** $p < 0.001$ vs. *vehicle*), IL-6 (+632% **** $p < 0.0001$ vs. *vehicle*) and TNF-α (+861% **** $p < 0.0001$ vs. *vehicle*), MPO (+177% *** $p < 0.001$ vs. *vehicle*), MDA accumulation (+90% *** $p < 0.001$ vs. *vehicle*) and LPS detection (+110% *** $p < 0.001$ vs. *vehicle*) in the serum [Figure 3]. According to the previously obtained data, no significant effect of HA alone was detected at both time points, clearly showing no significant improvement in all pro-inflammatory, oxidative, and endotoxemia parameters in comparison to the DNBS groups. Conversely, the intrarectal administration of Ade/HA was able to produce a significant reduction in IL-1β (−48% °°° $p < 0.001$ vs. *DNBS*), IL-6 (−87% °°°° $p < 0.0001$ vs. *DNBS*), TNF-α (−74% °°°° $p < 0.0001$ vs. *DNBS*), MPO (−58% °°° $p < 0.001$ vs. *DNBS*), MDA production (−55% °°° $p < 0.001$ vs. DNBS) and endotoxemia (−66% °°° $p < 0.001$ vs. *DNBS*) in the acute phase of colitis, and such an effect was still preserved in the resolution phase of the

experimental colitis, whereas a marked inhibition of IL-1β (−51% °°° $p < 0.001$ vs. *DNBS*), IL-6 (−80%°°°° $p < 0.0001$ vs. *DNBS*), TNF-α (−86% °°°° $p < 0.0001$ vs. *DNBS*), MPO (−52% °°° $p < 0.001$ vs. *DNBS*), MDA production (−44% °°° $p < 0.001$ vs. *DNBS*) and endotoxemia (−45% °°° $p < 0.001$ vs. *DNBS*) was reported [Figure 3]. Moreover, the DNBS challenge caused a massive increase in HYAL-1 expression on the 3rd day (152% *** $p < 0.001$ vs. DNBS group), and such an effect was still preserved on the 7th day after colitis induction (+172% *** $p < 0.001$ vs. *DNBS group*). In full agreement with the previous results, HA alone did not show any significant effect on HYAL-1 expression in the tissue both in the acute (−5% vs. *DNBS group*) and resolution phase (−4% vs. *DNBS group*) of colitis. On the contrary, Ade/HA administration resulted in a significant HYAL-1 reduction on the 3rd (−58% °°° $p < 0.001$ vs. *DNBS group*) and 7th (−60% °°° $p < 0.001$ vs. *DNBS group*) day after the DNBS challenge. Our data revealed that after the DNBS challenge, endogenous PEA levels were elevated on the 3rd day following colitis induction (+91% *** $p < 0.001$ vs. *vehicle*), but neither HA administration (+9% vs. *DNBS*) nor, more interestingly, Ade/HA administration (+8% vs. *DNBS*) significantly altered PEA accumulation during the acute phase of colitis. Interestingly, the DNBS-induced increase in PEA levels was no longer present on the 7th day of colitis (+2% vs. *vehicle*), and, once again, neither HA (−0.6% vs. *DNBS*) nor Ade/HA (−1% vs. *DNBS*) administration had a significant effect on PEA levels. This suggests that the protective effects of the intrarectal administration of the Ade/HA gel were independent of any potentiation of endogenous PEA effects [Figure 3]. Furthermore, our results demonstrate that the intracolonic administration of adelmidrol plus HA gel did not result in the detectable systemic absorption of this molecule (Table 1).

Table 1. Quantification of adelmidrol.

Time (Hours after Intrarectal Administration)	Level of Quantification (LOQ) [ng/mL] in the Plasma
0	<71.4
72	<71.4
168	<71.4

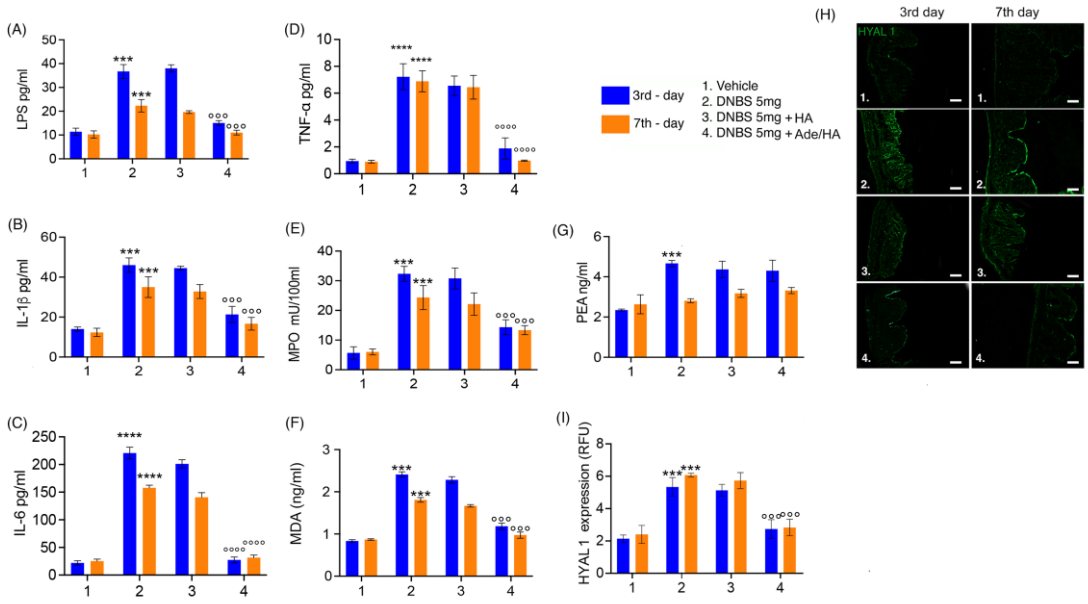

Figure 3. Ade/Ha intrarectal administration reduces endotoxemia and oxidative stress without interfering with the PEA level and inhibiting HYAL-1 expression in the mice colon during DNBS-induced colitis. The figure shows the effect of the intrarectal administration of Ade/HA on endotoxemia (**A**) and IL-1*β* release (**B**) in the plasma affected by colitis on the 3rd and 7th day after DNBS challenge; the Figure also shows (**C**) IL-6 release, (**D**) TNF-α release, (**E**) MPO, (**F**) MDA, (**G**) and the quantification of PEA. On the right panel, (**H**) the immunofluorescence analysis of HYAL1 expression on the 3rd and 7th day after the DNBS challenge in the presence of different treatments and (**I**) the relative quantification expressed as RFU are presented. Magnification: 10X; scale bar: Results are expressed as the mean ± SD of *n* = 5 experiments **** $p < 0.0001$ vs. vehicle; *** $p < 0.001$ vs. vehicle °°°° $p < 0.0001$ vs. DNBS; °°°° $p < 0.0001$ vs. DNBS; °°° $p < 0.001$ vs. DNBS.

2.4. Ade/HA Inhibited Cytomix-Induced Pro-Inflammatory Response in Cultured Human UC-Deriving Biopsies without Interfering with in Ex-Vivo PEA Production

When biopsies deriving from patients with UC in the remission phase underwent a challenge with cytomix (TNF-α, INF-γ, LPS) for 24h, a consistent pro-inflammatory response was stimulated in vitro and a significant increase in the histological damage score was observed *ex vivo* (+471% *** $p < 0.001$ vs. *control*), including a significant increase in MAC387-positive cell infiltration (+328% **** $p < 0.0001$ vs. *control*) as well as a marked decrease in both ZO-1 (−87% *** $p < 0.001$ vs. *control*) and occludin (−77%

*** $p < 0.001$ vs. *control*) expression observed via immunofluorescence [Figure 4]. Such data were confirmed using immunoblot analysis (−85% **** $p < 0.0001$ vs. *control* for ZO-1 and −88% **** $p < 0.0001$ vs. *control* for occludin, respectively) [Figure 4]. In the same experimental conditions, the cytomix stimulation caused a consistent increase in HYAL-1 expression in cultured biopsies (+266% **** $p < 0.001$ vs. *control*). Accordingly, to *in vivo*-obtained data, the cytomix challenge also resulted in a parallel increase in tissue IL-1β (+116% *** $p < 0.001$ vs. *control*), IL-6 (+1425%**** $p < 0.0001$ vs. *control*), TNF-α (+951% **** $p < 0.0001$ vs. *control*), MPO (+200% **** $p < 0.0001$ vs. *control*), and oxidative stress via MDA accumulation (+400% *** $p < 0.001$ vs. *control*) in cultured bioptic samples [Figure 4]. Treatment with HA alone did not lead to a detectable reduction in any of the observed parameters. This was evident from the lack of significant effects on histological damage, occluding, ZO-1, and HYAL-1 expression , as well as the absence of a reduction in IL-1β, MPO and MDA accumulation in the biopsy's milieu[Figure 4].

As expected, Ade/HA gel markedly reduced the pro-inflammatory response evoked by cytomix incubation *ex vivo*, and a significant reduction in the histological damage score (−60% °° $p < 0.01$ vs. *cytomix group*), MAC387-positive cell count (−72% °°°° $p < 0.0001$ vs. *cytomix group),* as well as a consistent rescue of both ZO-1 (+350% °°° $p < 0.001$ vs. *cytomix group*) and occludin (+300% °°° $p < 0.001$ vs. *cytomix group*) via immunofluorescence analysis, was in agreement with immunoblot analysis whereas both ZO-1 (+305% °°°° $p < 0.0001$ vs. *cytomix group*) and occludin (+290% °°°° $p < 0.0001$ vs. *cytomix group*) were markedly rescued by Ade/HA treatment [Figure 4]. Ade/HA incubation caused a marked decrease in cytomix-induced HYAL-1 up-regulation (−70% °° $p < 0.01$ vs. *cytomix group*), and, at the same time it accounted for an IL-1β (−55% °°° $p < 0.001$ vs. *cytomix group*), IL-6 (−90%°°°° $p < 0.0001$ vs. *cytomix group*), TNF-α (−84%°°°° $p < 0.0001$ vs. *cytomix group*), MPO (−70% °° $p < 0.01$ vs. *cytomix group*) and MDA accumulation decrease (−60% °°° $p < 0.001$ vs. *cytomix group*) in comparison with the cytomix group [Figure 4]. Consistent with our *in vivo* findings, the inflammatory response induced by cytomix incubation in the bioptic samples led to a significant increase in PEA release (+118% *** $p < 0.001$ vs. *control group*). Importantly, none of the treatments had an impact on PEA levels in the *ex vivo* setting. Our results clearly demonstrate that Ade/HA did not alter PEA levels *ex vivo*, further supporting the conclusion that PEA was not involved in mediating the effects of Ade/HA under our experimental conditions [Figure 4].

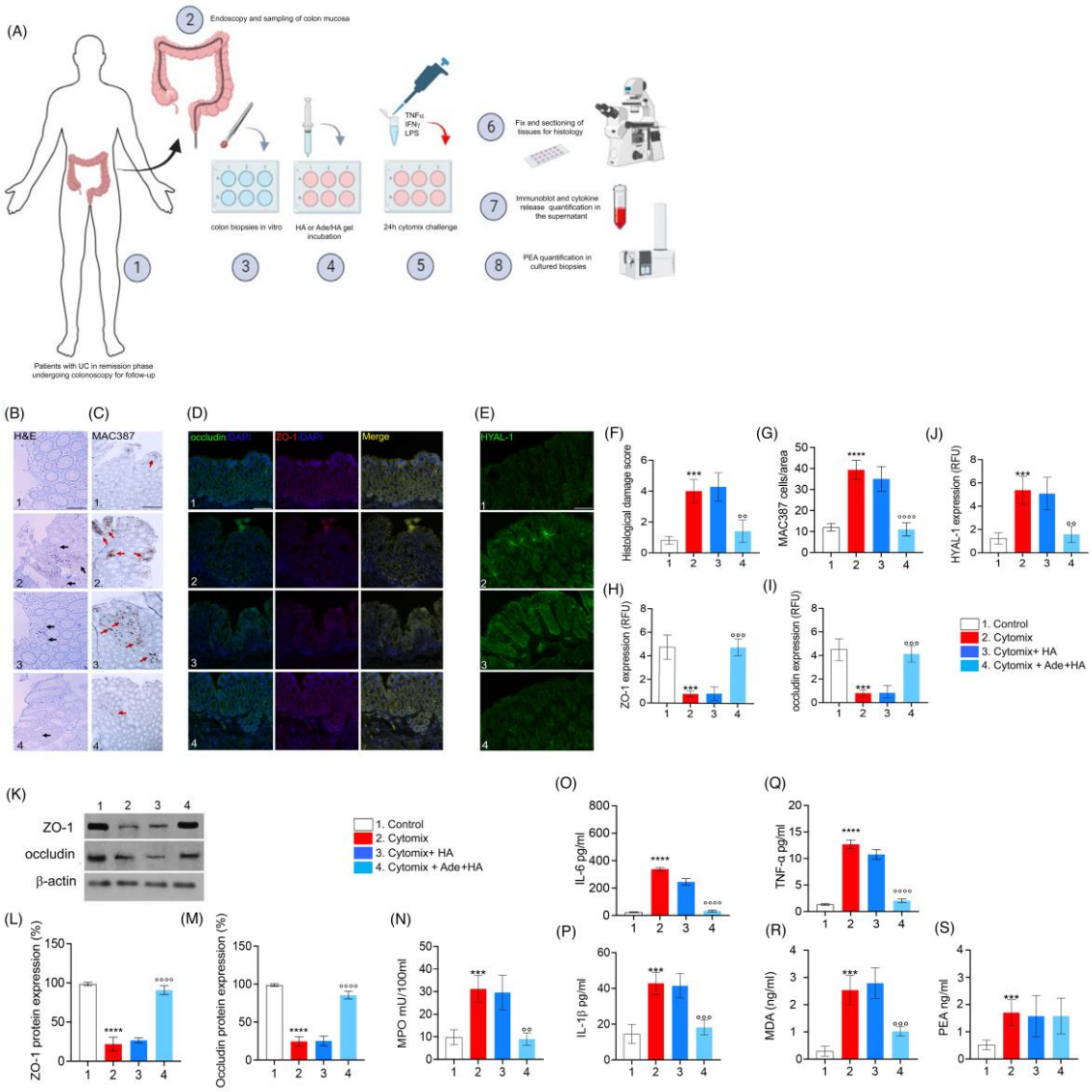

Figure 4. The in vitro incubation of Ade/HA gel ameliorates the pro-inflammatory status in remission phase-isolated UC biopsies stimulated with cytomix without affecting PEA release. The synoptic frame is shown at the top (**A**) with the experimental plan and procedures for *ex vivo* experiments in human biopsies isolated by UC patients in the remission phase having undergone follow-up colonoscopy in vitro-challenged with cytomix. In the middle part of the figure panel, we show, from left to the right, the protective effect of Ade/HA on histological damage via hematoxylin/eosin analysis (**B**), the immunohistochemical expression of MAC387 positive cells (**C**), the rescue of occludin and ZO-1, (**D**) the inhibition of HYAL-1 immunofluorescence analysis (**E**) and the respective quantification of the histological damage score, cell count and RFU (**F**–**J**)

in human colon biopsies exposed to the cytomix challenge for 24 in vitro after their isolation. Magnification 20×; Scale bar: 100 µm. In the lower panel, the figure shows the effect of Ade/Ha on ZO-1 and occludin expression via immunoblot analysis (**K**) and its relative quantification (**L**,**M**); in the same experimental conditions, the effect of Ade/Ha and other treatments were evaluated on (**N**) MPO, (**O**) IL-6, (**P**) IL-1*β*, (**Q**) TNF-α, (**R**) MDA and (**S**) PEA quantification in cultured biopsies. Results are expressed as the mean ± SD of $n = 5$ experiments *** $p < 0.001$ *vs. Control*; **** $p < 0.0001$ *vs. Control*; °° $p < 0.01$ *vs. Cytomix* °°° $p < 0.001$ *vs. Cytomix*. °°°° $p < 0.0001$ *vs. Cytomix*. Black arrows indicate areas of crypt loss and inflammation. Red arrows indicate a positive cluster of resident macrophages expressing the MAC387 protein.

3. Discussion

One of the key challenges faced by gastroenterologists and pharmacologists currently is the quest for novel therapeutic approaches that can manage IBDs while ensuring optimal patient compliance and acceptability and considering the risk/benefit ratio [4]. It is, therefore, mandatory to investigate new therapeutic strategies that can complement existing therapies and enhance treatment outcomes over time [14]. In this regard, adelmidrol, as an analog of PEA, has garnered significant attention due to its anti-inflammatory and antioxidant properties [15,16] across various experimental conditions. In recent years, adelmidrol's oral administration has demonstrated efficacy in the management of experimental colitis induced by DNBS in mice via inhibiting the translocation of Nuclear Factor kappa-B (NF-κB) and promoting a reduction in Intercellular Adhesion Molecule 1 (ICAM1) expression through its specific interaction with PPAR-γ receptors [7]. Although pre-clinical evidence for adelmidrol administration in mice has shown promising results, translating these findings into effective treatments for human IBDs poses a considerable challenge. The process of testing new anti-colitis drugs in humans is inherently complex and laborious. Nevertheless, with the rising global incidence of IBDs, there is an urgent demand for innovative therapeutic approaches [17]. In this regard, the use of a medical device incorporating adelmidrol and leveraging its protective potential during colitis could present a significant therapeutic approach for the treatment of UC in humans. By leveraging the benefits of adelmidrol in a localized and targeted manner, medical devices can provide a more focused and efficient delivery of the therapeutic compound. This potential medical device could be beneficial in combination with other pharmacological therapies used in the treatment of UC to improve therapy adherence, potentially lowering the dosage of the co-administered drug and thereby reducing potential systemic side effects. Furthermore, the well-known safety

profile of adelmidrol and HA makes them suitable candidates for medical device applications. This formulation, with a non-pharmacological physical mechanism of action, combined with their favorable safety profiles, highlights the potential of these molecules as medical devices for the prevention and treatment of UC flareups.

In addition to its established oral anti-inflammatory properties, our research has demonstrated that the intrarectal application of Ade/HA gel leads to a significant reduction in symptom severity and colonic tissue damage in a mouse model of DNBS-induced colitis. This highlights the potential of Ade/HA gel as a promising therapeutic approach in the treatment of colitis. Our data suggest that the protective effect of such an intrarectal application increases over time. We observed that the treatment's efficacy began during the acute phase of colitis induction on the 3rd day and reached its peak on the 7th day after the DNBS enema challenge. The Ade/HA association caused a significant improvement in colonic mucosal condition mouse colitis, exerting a topic "barrier effect" on the colon due to its capability to promote a marked inhibition of colitis-induced gut hyper-permeability, preventing a leaky gut syndrome. Our findings revealed that the Ade/HA intrarectal administration caused a significant reduction in the DNBS-induced leaky gut effect in mice, as evidenced by the prevention of FITC-dextran mucosal infiltration and a subsequent reduction in the endotoxemia level. Additionally, this treatment rescued the expression of important proteins involved in maintaining the intestinal barrier's integrity, such as ZO-1 and occludin [18], which were negatively affected by the DNBS challenge. Such effects were, thus, accompanied by a significant increase in MAC387-positive cells, as well as a marked up-regulation of pro-inflammatory cytokines, such as IL-1β, IL-6, TNF-α, the lipid peroxidation product MDA, and a reduction in MPO levels in the inflamed colon, indicating the effectiveness of the topical administration of Ade/HA gel in reducing the extent of mucosal pro-inflammatory cells' infiltration during colitis. In the same experimental conditions, Ade/HA gel promoted a significant antioxidant effect, reducing the amount of MDA generated by the DNBS challenge in the mouse mucosa, thus providing a synergistic effect on barrier integrity maintenance. Our data, in agreement with the formerly described antioxidant effects of adelmidrol in other inflammatory conditions [6], led us to identify such beneficial activity as the protective mechanism at the basis of the topical effect of Ade/HA gel in our experimental conditions. This is highlighted by the observation that no detectable systemic absorbance of Adelmidrol via the intrarectal administration of the Ade/HA formulation, and notably, no adelmidrol-mediated "entourage effect" on the endogenous

PEA level's up-regulation in the colon was detectable. Although recent studies have demonstrated the possible protective and anti-inflammatory role of HA during colitis [19], in our experimental conditions, this was not evident, and HA alone did not show any significant amelioration for the severity of colitis *in vivo* and in *ex vivo* experiments. Moreover, it has recently been demonstrated that intrarectal HA's co-administration with Acetylsalicilic acid (ASA) is a very interesting approach to improving the course of colitis [20]. However, it is important to note that the studies mentioned have employed significantly higher dosages and more frequent administration compared to our experimental plan. Additionally, it is crucial to acknowledge that other studies have demonstrated the anti-IBD effects of chemically modified forms of HA, which differ from the naïve HA used in our study [21]. Furthermore, our findings revealed that that intrarectal administration of Ade/HA gel effectively reduces the expression of HYAL-1, an enzyme responsible for HA degradation, especially in the colon [22]. These results suggest the potentially synergistic effect of adelmidrol, functioning as an antioxidant agent while simultaneously inhibiting the degradation of HA in situ. By slowing down the degradation of HA, adelmidrol allows for the increased duration of the protective physical barrier that is achieved with this formulation. Mucosal biopsies deriving from patients affected by UC and challenged with cytomix were used to test Ade/HA efficacy, resulting in significant inhibition of mucosal inflammatory infiltration, with the consequent increase in the *ex vivo* expression of occludin and ZO-1. Consistently with the data obtained in murine colitis, Ade/HA determined a significant decrease in the release of IL-1β, TNF-α, IL-6, MPO, and MDA accumulation in cytomix-stimulated tissues, and these effects were accompanied by a significant reduction in the expression of HYAL-1. Also, in this case, no significant variation in terms of PEA release by Ade/HA gel treatment was observed *in vitro*; this confirmed the "virtually" independent PEA release via Ade/HA as having an "entourage" effect capable of the observed anti-inflammatory activity in human biopsies. Although the topical application of 5-ASA is commonly used for treating distal colitis, several studies have demonstrated that the effectiveness of *in vitro* 5-ASA is directly linked to its dose and tissue concentration, which, in turn, drive clinical response [23]. In this context, our data highlight, for the first time, that the intrarectal instillation of Ade/HA gel has the potential to be a new therapeutic tool against experimental colitis. This is attributed to the "mechanic" and antioxidant protective barrier effect of Ade/HA gel on the gut mucosa, introducing such a formulation as an innovative approach helpful for its clinical and fast translation. Given, in fact, the observed lack of absorption of adelmidrol

in our study due to its topical effect, we are led to consider Ade/HA gel a medical device rather than a traditional drug. This classification is like its application in controlling bladder inflammation as Vessilen® [13]. In conclusion, despite the undeniable successes of biological drugs in the treatment of IBDs that are increasingly performing, the potential utilization of medical devices that provide a local supportive effect to conventional UC therapies should be taken into account in optimizing therapeutic treatments. Additional clinical studies are necessary to evaluate the true efficacy of Ade/HA gel as a medical device, exploring the mechanisms underlying the here-observed “barrier” effect, and determine the optimal dosage and formulation for humans in the consideration of leaky gut as a pivotal factor in UC, the implementation of this formulation alongside traditional pharmacological therapies presents a promising avenue for improved patient care and the management of this disease.

4. Materials and Methods

4.1. Animals and Experimental Design

Eight-week-old female C57BL/8J mice (Charles River, Lecco, Italy) (*n* = 64) were used for all the experiments. The procedures included in the experimental plan were approved by Sapienza University’s Ethics Committee. Animal care followed the (International Association for the Study of Pain) IASP and European Community (EC L358/1 18/12/86) guidelines on the use and protection of animals in experimental research. Colitis was induced via a single intracolonic administration of 5 mg of DNBS (Sigma Aldrich, St. Louis, MO, USA) dissolved in 100 µL of 50% ethanol (EtOH) (Sigma Aldrich, St. Louis, MO, USA) and saline (Thermo Fisher Scientific, Waltham, MA, USA) [24], whereas the vehicle group received a single intracolonic administration of saline and EtOH at 100 µL. EtOH was used as a means to effectively break the intestinal barrier and enable the interaction of DNBS with colon tissue proteins, thereby triggering the host’s innate and adaptive immune responses. Overnight-fasted mice were treated with DNBS on day 0 through a flexible catheter (Hugo-Sachs Elektronik, March, Germany) rapidly inserted approximately 3 cm from the anus without anesthesia. A total of 100 µL of the DNBS solution was introduced slowly into the colon–rectal tract and the animals were kept slightly reclined throughout the procedure. Therefore, the mice were returned to their cages and placed overnight on a heating pad to facilitate recovery. The progression of experimental colitis, and the efficacy of treatments was assessed both on the acute (3rd) day and in the remission phase (7th day) post DNBS enema. Mice were randomly divided

into the following groups (*n* = 16 each): *(i)* vehicle (receiving 100 µL sterile saline); *(ii)* DNBS (colitis group, receiving 100 µL of DNBS at 5 mg in EtOH 50% sterile saline); *(iii)* HA (100 µL of 0.1% sodium hyaluronate saline every 72 h starting on day 0 until day 7; *(iv)* Adelmidrol/HA gel (100 µL HA 0.1% plus 2% adelmidrol) every 72 h starting on day 0 until day 7.

4.2. Patients and Tissue Culture Treatments

Recto-sigmoid mucosal biopsies were obtained from patients with a diagnosis of distal UC. Patients were considered in clinical and biochemical remission and underwent colonoscopy for screening (*n* = 8, median age: 32 years range 25–40; 4 female). Patients were asked to stop any pharmacological treatment during the 2 weeks preceding the endoscopy; exclusion criteria were *(i)* a history of cancer; *(ii)* the use of an immunosuppressant, anti-platelet, or anti-coagulant drugs; (iii) significant uncontrolled comorbidity. Patients gave their written informed consent, and the protocol was approved by the Ethics Committee of the Federico II University of Naples.

Four mucosal biopsies obtained from the recto-sigmoid region were used. In brief, specimens were immediately placed in 24-well plates and cultured in Dulbecco-Modified Eagle's Medium (DMEM) (Sigma, Milan, Italy) supplemented with 5% fetal bovine serum, 2 mmol/l of glutamine, 100 U/l of penicillin, and 100 µg/mL of streptomycin (Biowhittaker, Milan, Italy) at 37 °C in 5% CO_2/95% air for 24 h, as previously described [25, 26, 27]. To mimic active inflammation, we used a protocol previously reported by our group [28], comprising the incubation of isolated biopsies in a pro-inflammatory Cytomix constituted by LPS (10 µg/mL), plus IFN-γ (300 U/mL) and TNF-α (100 U/mL) (all from Sigma, Milan, Italy), in the presence or absence of 0.1% of HA or 2% Adelmidrol plus 0.1% HA gel, (Ade/HA) (both from Epitech group, Saccolongo-Padua, Italy) for another 24 h before being addressed to a histological, immunofluorescence and immunoblot or cytokine assay as indicated in the experiment [Figure 4A] and as described subsequently.

4.3. Endoscopic Procedures in Mouse and Endoscopic Damage Score Evaluation

For endoscopic procedures, *n* = 4 mice from each experimental group on both the 3rd and 7th day after the DNBS stimulus underwent anesthesia via the intraperitoneal injection of ketamine at 100 mg/mL and xylazine at 20 mg/mL [29]. The experimental endoscopy of the rectum and colon was performed using a bronchoscopy adapted for small rodent use (Karl Storz, Tuttlingen, Germany). The animals were fasted 24 h before endoscopy and underwent PBS 1X enema to favor the adequate visualization of the

colonic mucosa. The endoscopic frames were acquired by a color monitor and digitally recorded on a tape (CV-190 PLUS, Olympus, Segrate, Italy). The endoscopic injury score was determined according to the method described [29].

4.4. Colon Length, Spleen Weight and Disease Activity Index (DAI)

Depending upon the experimental design, a group of *n* = 8 mice derived from each experimental group were euthanized on days 3 and 7 after DNBS-induced colitis. Spleen weight and colon length were measured, and colonic tissues were removed to perform macroscopic, histochemical, and biochemical analyses, as described in the experimental protocol (Figure 1A). The DAI scale was used to evaluate colitis induction and progression. The DAI score was determined by two independent observers blinded to the treatments and according to the criteria proposed by Cooper et al. (1993) [30] changes in body weight (0 = none; 1 = 1 to 5%; 2 = 5 to 10%; 3 = 10 to 20%; 4 = >20%); stool consistency (0 = normal; 2 = loose; 4 = diarrhea) and rectal bleeding (0 = normal; 2 = occult bleeding; 4 = gross bleeding) were scored. The DAI score was recorded on days 3 and 7, and the results were expressed as cumulative average scores in each experimental group.

4.5. Histopathological Analysis of the Mouse and Human Ex Vivo Cultured Colonic Biopsies

After sacrifice, mouse distal colons were collected on the 3rd and 7th day after the DNBS challenge. Similarly, bioptic samples were cultured *ex vivo* and exposed to the cytomix challenge for 24 h. The samples were then fixed in 4% paraformaldehyde (PFA), sliced into 15 µm sections, and stained with hematoxylin and eosin (H&E) for a macroscopic and histopathological assessment. Histological damage was evaluated using the complex scoring system proposed by Li et al. (2017) [31] and based on the following parameters: *(i)* the distortion and loss of crypt architecture; *(ii)* the infiltration of the inflammatory; *(iii)* muscle thickening; *(iv)* goblet cell depletion; and *(v)* crypt absence. The slides were analyzed using a Nikon Eclipse 80i microscope (Nikon Corporation, Tokyo, Japan), and images were captured at 10× magnification using a high-resolution digital camera (Nikon Digital Sight DS-U1). The cumulative histological damage scores were expressed as average scores in each experimental group.

4.6. Macrophage Infiltration Immunohistochemical Assay

Tissue samples were fixed in 4% PFA, embedded in paraffin, and sectioned into 15 µm slices for subsequent immunohistochemical processing. The slices underwent heat-mediated antigen retrieval using a sodium citrate buffer, followed by incubation with anti-MAC387 (Abcam, Cambridge, UK) at room temperature (RT), as described by Thoree et al. [32], and were then subjected to detection using the horseradish peroxidase (HRP)-conjugated compact polymer system. 3,30-diaminobenzidine (DAB) was employed as chromogen. Subsequently, the slices were counterstained with hematoxylin and examined using a microscope (Optika XDS-3L4 Ponteranica, Bergamo Italy). Images were captured at 20× magnification using a high-resolution digital camera. The quantitative analysis was performed by blinded assessors, with the results expressed as the median number of MAC387-positive cells per unit area and determined using ImageJ 1.53 software (National Institutes of Health).

4.7. In Vivo Assay of the Intestinal Permeability

Before being euthanized, a group of n = 3 mice for each treatment on the 3rd and 7th day following DNBS enema were weighed and gavaged with 1% body weight (volume to mass) of fluorescein isothiocyanate-dextran (FITC-Dextran, 4 kDa, Sigma) and were euthanized 5 h after administration. Colon samples were fixed in PFA 4% (Thermo Fisher Scientific, Waltham, MA, USA) and cryo-sectioned in 15 µm slices. These sections were analyzed with a microscope Nikon Eclipse 80i, and images were captured at 10× magnification by a high-resolution digital camera (Nikon Digital Sight DS-U1). The results were expressed as relative fluorescence units (RFU) and as arbitrary units.

4.8. Zonula Occludens (ZO-1) and Occludin Immunofluorescence

On day 3rd and 7th day after DNBS, enema mice were sacrificed, and the distal colon was isolated, fixed, and sectioned into 25 µm slices. In a similar way, *ex vivo* cultured human biopsies were sectioned in 15 µm slices. Both mouse and human sections were blocked with bovine serum albumin and subsequently stained with the rabbit anti-ZO-1 antibody (1:100 dilution *v*/*v*; Proteintech, Manchester, UK), rabbit anti-occludin antibody (1:100 dilution *v*/*v*; Novus Biologicals, Abingdon, UK) or mouse anti-HYAL1 antibody (1:150 dilution *v*/*v*; Santa Cruz Biotechnology, CA, USA). The slices were then washed with PBS 1X and incubated in the dark with the fluorescein isothiocyanate-conjugated anti-rabbit (Abcam, Cambridge, UK). The nuclei were stained by Hoechst. Sections were analyzed with a microscope (Nikon Eclipse 80i), and images were captured by a high-resolution digital camera (Nikon Digital Sight DS-U1).

4.9. Protein Extraction and ZO-1 and Occludin Immunoblot Analysis

Colonic tissue isolated on the 3rd and 7th day after colitis induction or bioptic samples were processed for Western blot analysis. Briefly, the samples were homogenized in an ice-cold hypotonic lysis buffer with (10 mM of 4-(2-hydroxyethyl)-1-piperazineethanesulfonic acid (HEPES), 1.5 mM of $MgCl_2$, 10 mM of KCl, 0.5 mM of phenyl-methyl-sulphonylfluoride, 1.5 mg/mL of the soybean trypsin inhibitor, 7 mg/mL of pepstatin A, 5 mg/mL of leupeptin, 0.1 mM of benzamidine and 0.5 mM of dithiothreitol (DTT)). The resulting cytosolic extracts were mixed with a non-reducing gel loading buffer (50 mM Tris (hydroxymethyl) aminomethane (Tris), 10% sodium-dodecylsulfate (SDS), 10% glycerol, 2 mg bromophenol/mL) at a 1:1 ratio, and then boiled for 3 min followed by centrifugation at 10,000× *g* for 10 min. The protein concentration was determined using the Bradford assay, and equivalent amounts (50 µg) of each homogenate underwent electrophoresis through a polyacrylamide mini gel. Proteins were transferred to nitrocellulose membranes that were saturated via incubation with 10% non-fat dry milk in PBS 1X overnight at 4 °C before incubating with rabbit polyclonal anti-ZO-1, rabbit monoclonal anti-occludin (Abcam, Cambridge, UK) or mouse monoclonal anti-β-actin (Santa Cruz Biotechnology, CA, USA) for 2 h at room temperature (RT). Membranes were then incubated with the specific secondary antibodies conjugated to horseradish peroxidase (HRP) (Dako, Milan, Italy). Immune complexes were revealed by enhanced chemiluminescence detection reagents, and immunoreactive protein bands were then visualized, scanned, and densitometrically analyzed with ChemiDoc XRS+ apparatus (Bio-Rad Laboratories S.r.l. Segrate, Milano, Italy). The results were expressed as the % of protein expression and normalized on the expression of the housekeeping protein β-actin for mouse proteins.

4.10. Plasma Collection and Adelmidrol Quantification in the Blood

Mouse blood samples were obtained via a cardiac puncture during anesthesia for the endoscopic procedure. Blood samples were, thus, collected in 5% EDTA vials immediately prior to sacrifice to determine the adelmidrol level in the blood following its intrarectal administration. The adelmidrol level was measured according to the procedure described by D'Amico et al. (2020) [33], using LC-MS/MS (Agilent Technologies G6470A) as a function of time. Briefly, an amount of 100µL of the plasma samples was diluted in 900µL of acetonitrile, and the relative absorption rate of Adelmidrol in the plasma was quantified using a stock solution of adelmidrol in methanol.

The five-point calibration curve was prepared by dilution in acetonitrile from the stock solution as previously described [31].

*4.11. ELISA Quantification of LPS (endotoxemia), IL-1*β, IL-6, and TNF-α *in the Mouse Plasma and Human Bioptic Samples*

Enzyme-linked immunosorbent assay (ELISA) kits were used to quantify both LPS (Chondrex Inc., Woodinville, WA, USA), IL-1*β, IL-6, and TNF-α* (Thermo Fisher Scientific, MA, USA) in the plasma of collected mice blood samples and homogenized human bioptic samples according to the relative manufacturer's instructions.

4.12. Myeloperoxidase Activity

Myeloperoxidase (MPO) activity was evaluated in colonic tissues to determine the extent of neutrophil infiltration and activation, as previously described [34]. After removal, mouse colonic tissues or human-cultured bioptic samples were rinsed in a cold saline solution, then homogenized in a solution containing 0.5% hexadecyltrimethylammonium bromide (Sigma-Aldrich) dissolved in 10 mM of a potassium phosphate buffer and centrifuged for 30 min at 20,000× *g* at 37 °C. An aliquot of the supernatant was mixed with a solution of tetramethylbenzidine (1.6 mM; Sigma-Aldrich) and 0.1 mM of hydrogen peroxide (Sigma-Aldrich). The absorbance was then spectrophotometrically measured at 650 nm. MPO activity was determined as the amount of the enzyme degrading 1 mmol/min of peroxide at 37 °C and was expressed in milliunits per 100 mL of the homogenized sample.

4.13. Lipid Peroxidation Assay

Malonyl dialdehyde (MDA) was measured via the thiobarbituric acid colorimetric assay according to the method described by Esposito et al. (2012) [35] in isolated colonic tissues on the 3rd and 7th day after DNBS challenge and in *ex vivo* human-cultured biopsies. Briefly, 1 mL of 10% (*w*/*v*) trichloroacetic acid was added to 450 µL of the tissue lysate. After centrifugation, 1.3 mL 0.5% (*w*/*v*) of thiobarbituric acid was added, and the mixture was heated at 80 °C for 20 min. After cooling, MDA formation was recorded (absorbance 530 nm and absorbance 550 nm) in a Perkin Elmer (Waltham, MA, USA) spectrofluorimeter, and the results were presented as ng MDA/mL.

4.14. PEA Level Quantification

The extraction and analysis of PEA levels were performed according to [36], with slight modifications. Mouse colonic tissues or human-cultured bioptic samples were firstly lysed and then evaporated under a nitrogen stream. Residues were suspended in an extraction solution, ultracentrifuged (14,000 rpm, 4 °C, 5 min), and the supernatant was injected for mass spectrometry analysis. Analyses were run on a Jasco Extrema LC-4000 system (Jasco Inc., Easton, MD, USA) coupled to an Advion Expression mass spectrometer (Advion Inc., Ithaca, NY, USA) and equipped with an electrospray (ESI) source. Mass spectra were recorded in the positive SIM mode. The capillary voltage was set at +180 V, the spray voltage was set at 3 kV, the source voltage offset was set at +20 V, and the capillary temperature was set at 250 °C. The chromatographic separation was performed on the analytical column Kinetex C18 (150 × 4.6 mm, id. 3 µm, 100 Å) and a security guard column, both supplied by Phenomenex (Torrance, CA, USA). The analyses were performed at a flow rate of 0.3 mL/min, with solvent A (water containing 2 mM ammonium acetate) and solvent B (methanol containing 2 mM ammonium acetate and 0.1% formic acid). Elution was performed according to the following linear gradient: 15% B for 0.5 min, 15–70% B from 0.5 to 2.5 min, 7–99% B from 2.5 to 4.0 min, and held at 99% B from 4.0 to 8.0 min. From 8 to 11.50 min, the column was equilibrated to 15% B and conditioned from 11.5 to 15.0 at 15% B. The injection volume was 10 µL, and the column temperature was fixed at 40 °C. For quantitative analysis, standard curves of PEA (Sigma-Aldrich, Milan, Italy) were prepared over a concentration range of 0.0001–10 ppm with six different concentration levels, and duplicate injections were prepared at each level. All data were collected and processed using JASCO Chrom NAV (version 2.02.04) and Advion Data Express (4.0.13.8).

4.15. Statistical Analysis

The results were expressed as the mean percentage. Statistical analysis was performed using parametric one-way analysis of variance (ANOVA), and multiple comparisons were performed using Bonferroni's post hoc test. p-values < 0.05 were considered statistically significant. Data were analyzed using Graphpad Prism 9 and ImageJ 1.53 software.

Author Contributions: Conceptualization, G.E. and G.S.; methodology, I.P., S.B.F., A.Z., F.P., A.D.R., M.P., and A.T.; software, I.P.; validation, I.P., L.S., and A.Z.; formal analysis, I.P., A.Z., S.B.F., A.D.R., S.R., F.D.E.D.P., G.L., and F.P.T.; investigation, G.L., F.P.T., M.P., and S.R.; data curation, I.P., L.S., and G.E.; writing—original draft preparation, I.P. and G.E.; writing—review and

editing, I.P., G.E., and L.S.; supervision, G.E. and G.S.; project administration, I.P. All authors have read and agreed to the published version of the manuscript.

Funding: This research received no external funding.

Institutional Review Board Statement: All experimental procedures were approved by Federico II University's Ethics Committee (protocol No. 340/21). Animal care was in compliance with Sapienza University's ethics committee, IASP and the European Community (EC L358/1 18/12/86, 30 September 2016) guidelines on the use and protection of animals in experimental research.

Informed Consent Statement: Informed consent was obtained from all subjects involved in this study.

Data Availability Statement: The data presented in this study are available on request from the corresponding author.

Conflicts of Interest: The authors declare no conflicts of interest.

References

1. Gecse, K.B.; Vermeire, S. Differential diagnosis of inflammatory bowel disease: Imitations and complications. *Lancet Gastroenterol. Hepatol.* **2018**, *3*, 644–653. https://doi.org/10.1016/S2468-1253(18)30159-6.
2. Ananthakrishnan, A.N.; Bernstein, C.N.; Iliopoulos, D.; Macpherson, A.; Neurath, M.F.; Ali, R.A.R.; Vavricka, S.R.; Fiocchi, C. Environmental triggers in IBD: A review of progress and evidence. *Nat. Rev. Gastroenterol. Hepatol.* **2018**, *15*, 39–49. https://doi.org/10.1038/nrgastro.2017.136.
3. Zhang, Y.Z.; Li, Y.Y. Inflammatory bowel disease: Pathogenesis. *World J. Gastroenterol.* **2014**, *20*, 91–99. https://doi.org/10.3748/wjg.v20.i1.91.
4. De Felice, K.M. Patients Perception of Risks and Benefits of Biologic Therapy. *Inflamm. Bowel Dis.* **2020**, *26*, 147–149. https://doi.org/10.1093/ibd/izz122.
5. Siegel, C.A. Review article: Explaining risks of inflammatory bowel disease therapy to patients. *Aliment. Pharmacol. Ther.* **2011**, *33*, 23–32. https://doi.org/10.1111/j.1365-2036.2010.04489.x.
6. Fusco, R.; Cordaro, M.; Genovese, T.; Impellizzeri, D.; Siracusa, R.; Gugliandolo, E.; Peritore, A.F.; D'Amico, R.; Crupi, R.; Cuzzocrea, S.; et al. Adelmidrol: A New Promising Antioxidant and Anti-Inflammatory Therapeutic Tool in Pulmonary Fibrosis. *Antioxidants* **2020**, *9*, 601. https://doi.org/10.3390/antiox9070601.
7. Cordaro, M.; Impellizzeri, D.; Gugliandolo, E.; Siracusa, R.; Crupi, R.; Esposito, E.; Cuzzocrea, S. Adelmidrol, a Palmitoylethanolamide Analogue, as a New Pharmacological Treatment for the Management of Inflammatory Bowel Disease. *Mol. Pharmacol.* **2016**, *90*, 549–561. https://doi.org/10.1124/mol.116.105668.

8. Petrosino, S.; Puigdemont, A.; Della Valle, M.F.; Fusco, M.; Verde, R.; Allarà, M.; Aveta, T.; Orlando, P.; Di Marzo, V. Adelmidrol increases the endogenous concentrations of palmitoylethanolamide in canine keratinocytes and down-regulates an inflammatory reaction in an in vitro model of contact allergic dermatitis. *Vet. J.* **2016**, *207*, 85–91. https://doi.org/10.1016/j.tvjl.2015.10.060.
9. Del Re, A.; Palenca, I.; Seguella, L.; Pesce, M.; Corpetti, C.; Steardo, L.; Rurgo, S.; Sarnelli, G.; Esposito, G. Oral Adelmidrol Administration Up-Regulates Palmitoylethanolamide Production in Mice Colon and Duodenum through a PPAR-γ Independent Action. *Metabolites* **2022**, *12*, 457. https://doi.org/10.3390/metabo12050457.
10. Volpi, N.; Schiller, J.; Stern, R.; Soltés, L. Role, metabolism, chemical modifications and applications of hyaluronan. *Curr. Med. Chem.* **2009**, *16*, 1718–1745. https://doi.org/10.2174/092986709788186138.
11. Di Paola, R.; Fusco, R.; Impellizzeri, D.; Cordaro, M.; Britti, D.; Morittu, V.M.; Evangelista, M.; Cuzzocrea, S. Adelmidrol, in combination with hyaluronic acid, displays increased anti-inflammatory and analgesic effects against monosodium iodoacetate-induced osteoarthritis in rats. *Arthritis Res. Ther.* **2016**, *18*, 291. https://doi.org/10.1186/s13075-016-1189-5.
12. Campolo, M.; Siracusa, R.; Cordaro, M.; Filippone, A.; Gugliandolo, E.; Peritore, A.F.; Impellizzeri, D.; Crupi, R.; Paterniti, I.; Cuzzocrea, S. The association of adelmidrol with sodium hyaluronate displays beneficial properties against bladder changes following spinal cord injury in mice. *PLoS ONE.* **2019**, *14*, e0208730.
13. Ostardo, E.; Impellizzeri, D.; Cervigni, M.; Porru, D.; Sommariva, M.; Cordaro, M.; Siracusa, R.; Fusco, R.; Gugliandolo, E.; Crupi, R.; et al. Adelmidrol + sodium hyaluronate in IC/BPS or conditions associated to chronic urothelial inflammation. A translational study. *Pharmacol. Res.* **2018**, *134*, 16–30. https://doi.org/10.1016/j.phrs.2018.05.013.
14. Fiocchi, C.; Iliopoulos, D. Numbers Do Not Lie: The Dire Need for New Directions in IBD. *J. Crohns Colitis.* **2022**, *16*, 1649–1650. https://doi.org/10.1093/ecco-jcc/jjac102.
15. De Filippis, D.; D'Amico, A.; Cinelli, M.P.; Esposito, G.; Di Marzo, V.; Iuvone, T. Adelmidrol, a palmitoylethanolamide analogue, reduces chronic inflammation in a carrageenin-granuloma model in rats. *J. Cell Mol. Med.* **2009**, *13*, 1086–1095. https://doi.org/10.1111/j.1582-4934.2008.00353.x.
16. Impellizzeri, D.; Di Paola, R.; Cordaro, M.; Gugliandolo, E.; Casili, G.; Morittu, V.M.; Britti, D.; Esposito, E.; Cuzzocrea, S. Adelmidrol, a palmitoylethanolamide analogue, as a new pharmacological treatment for the management of acute and chronic inflammation. *Biochem. Pharmacol.* **2016**, *119*, 27–41. https://doi.org/10.1016/j.bcp.2016.09.001.
17. Mak, W.Y.; Zhao, M.; Ng, S.C.; Burisch, J. The epidemiology of inflammatory bowel disease: East meets west. *J. Gastroenterol. Hepatol.* **2020**, *35*, 380–389. https://doi.org/10.1111/jgh.14872.

18. Casili, G.; Cordaro, M.; Impellizzeri, D.; Bruschetta, G.; Paterniti, I.; Cuzzocrea, S.; Esposito, E. Dimethyl Fumarate Reduces Inflammatory Responses in Experimental Colitis. *J. Crohns Colitis.* **2016**, *10*, 472–483. https://doi.org/10.1093/ecco-jcc/jjv231.
19. Liu, W.; Liu, Y.Y.; Zhang, M.Q.; Qin, M.Z.; Yang, Y.Y.; Liu, B.W.; Zhang, D.J.; Jiang, C.H.; Yin, Z.Q.; Lu, M.; et al. A comparative study of the ameliorative effects of hyaluronic acid oligosaccharides and hyaluronic acid on DSS-induced colitis in mice and research on relevant mechanisms. *Food Funct.* **2023**, *14*, 6482–6495. https://doi.org/10.1039/d2fo03644d.
20. Jhundoo, H.D.; Siefen, T.; Liang, A.; Schmidt, C.; Lokhnauth, J.; Moulari, B.; Béduneau, A.; Pellequer, Y.; Larsen, C.C.; Lamprecht, A. Hyaluronic Acid Increases Anti-Inflammatory Efficacy of Rectal 5-Amino Salicylic Acid Administration in a Murine Colitis Model. *Biomol. Ther.* **2021**, *29*, 536–544. https://doi.org/10.4062/biomolther.2020.227.
21. Hlaing, S.P.; Cao, J.; Lee, J.; Kim, J.; Saparbayeva, A.; Kwak, D.; Kim, H.; Hwang, S.; Yun, H.; Moon, H.R.; et al. Hyaluronic Acid-Conjugated PLGA Nanoparticles Alleviate Ulcerative Colitis via CD44-Mediated Dual Targeting to Inflamed Colitis Tissue and Macrophages. *Pharmaceutics* **2022**, *14*, 2118. https://doi.org/10.3390/pharmaceutics14102118.
22. Weber, G.C.; Buhren, B.A.; Schrumpf, H.; Wohlrab, J.; Gerber, P.A. Clinical Applications of Hyaluronidase. *Adv. Exp. Med. Biol.* **2019**, *1148*, 255–277. https://doi.org/10.1007/978-981-13-7709-9_12.
23. Naganuma, M.; Iwao, Y.; Ogata, H.; Inoue, N.; Funakoshi, S.; Yamamoto, S.; Nakamura, Y.; Ishii, H.; Hibi, T. Measurement of colonic mucosal concentrations of 5-aminosalicylic acid is useful for estimating its therapeutic efficacy in distal ulcerative colitis: Comparison of orally administered mesalamine and sulfasalazine. *Inflamm. Bowel Dis.* **2001**, *7*, 221–225. https://doi.org/10.1097/00054725-200108000-00007.
24. Wirtz, S.; Neufert, C.; Weigmann, B.; Neurath, M.F. Chemically induced mouse models of intestinal inflammation. *Nat.Protoc.* **2007**, *2*, 541–546. https://doi.org/10.1038/nprot.2007.41.
25. Seguella L, Rinaldi F, Marianecci C, Capuano R, Pesce M, Annunziata G, Casano F, Bassotti G, Sidoni A, Milone M, Aprea G, de Palma GD, Carafa M, Pesce M, Esposito G, Sarnelli G. Pentamidine niosomes thwart S100B effects in human colon carcinoma biopsies favouring wtp53 rescue. J Cell Mol Med. 2020 Mar;24(5):3053-3063. doi: 10.1111/jcmm.14943. Epub 2020 Feb 5. PMID: 32022398; PMCID: PMC7077541.
26. De Palma GD, Colavita I, Zambrano G, Giglio MC, Maione F, Luglio G, Sarnelli G, Rispo A, Schettino P, D'Armiento FP, De Palma FDE, D'Argenio V, Salvatore F. Detection of colonic dysplasia in patients with ulcerative colitis using a targeted fluorescent peptide and confocal laser endomicroscopy: A pilot study. PLoS One. 2017 Jun 30;12(6):e0180509. doi: 10.1371/journal.pone.0180509. PMID: 28666016; PMCID: PMC5493408.
27. Coeffier M, Miralles-Barrachina O, Le Pessot F et al. Influence of glutamine on cytokine production by human gut in vitro. Cytokine 2001; 13: 148– 54.

28. Cirillo C, Sarnelli G, Esposito G, Grosso M, Petruzzelli R, Izzo P, Calì G, D'Armiento FP, Rocco A, Nardone G, Iuvone T, Steardo L, Cuomo R. Increased mucosal nitric oxide production in ulcerative colitis is mediated in part by the enteroglial-derived S100B protein. Neurogastroenterol Motil. 2009 Nov;21(11):1209-e112. doi: 10.1111/j.1365-2982.2009.01346.x. Epub 2009 Jun 24. PMID: 19558426.
29. Becker, C.; Fantini, M.C.; Neurath, M.F. High resolution colonoscopy in live mice. *Nat. Protoc.* **2006**, *1*, 2900–2904.
30. Cooper, H.S.; Murthy, S.N.; Shah, R.S.; Sedergran, D.J. Clinicopathologic study of dextran sulfate sodium experimental murine colitis. *Lab. Investig.* **1993**, *69*, 238–249.
31. Li, R.; Kim, M.-H.; Sandhu, A.K.; Gao, C.; Gu, L. Muscadine Grape (*Vitis rotundifolia*) or Wine Phytochemicals Reduce Intestinal Inflammation in Mice with Dextran Sulfate Sodium-Induced Colitis. *J. Agric. Food Chem.* **2017**, *65*, 769–776. https://doi.org/10.1021/acs.jafc.6b03806.
32. Thoree, V.; Skepper, J.; Deere, H.; Pele, L.C.; Thompson, R.P.H.; Powell, J.J. Phenotype of exogenous microparticle-containing pigment cells of the human Peyer's patch in inflamed and normal ileum. *Inflamm. Res.* **2008**, *57*, 374–378. https://doi.org/10.1007/s00011-007-7216-x.
33. D'Amico, R.; Siracusa, R.; Fusco, R.; Cordaro, M.; Genovese, T.; Peritore, A.F.; Gugliandolo, E.; Crupi, R.; Impellizzeri, D.; Cuzzocrea, S.; et al. Protective effects of Colomast®, A New Formulation of Adelmidrol and Sodium Hyaluronate, in A Mouse Model of Acute Restraint Stress. *Int. J. Mol. Sci.* **2020**, *21*, 8136. https://doi.org/10.3390/ijms21218136.
34. Cassini-Vieira, P.; Moreira, C.F.; da Silva, M.F.; da Silva Barcelos, L. Estimation of Wound Tissue Neutrophil and Macrophage Accumulation by Measuring Myeloperoxidase (MPO) and N-Acetyl-β-D-glucosaminidase (NAG) Activities. *Bio-Protoc.* **2015**, *5*, e1662. https://doi.org/10.21769/BioProtoc.1662.
35. Esposito, G.; Capoccia, E.; Sarnelli, G.; Scuderi, C.; Cirillo, C.; Cuomo, R.; Steardo, L. The antiprotozoal drug pentamidine ameliorates experimentally induced acute colitis in mice. *J. Neuroinflammation* **2012**, *9*, 277. https://doi.org/10.1186/1742-2094-9-277.
36. Gachet, M.S.; Rhyn, P.; Bosch, O.G.; Quednow, B.B.; Gertsch, J. A quantitiative LC-MS/MS method for the measurement of arachidonic acid, prostanoids, endocannabinoids, N-acylethanolamines and steroids in human plasma. *J. Chromatogr. B* **2015**, *976–977*, 6–18. https://doi.org/10.1016/j.jchromb.2014.11.001.

Background (II)

1. COVID-19 pandemic

1.1 Epidemiology of COVID-19

The COVID-19 pandemic, caused by the SARS-CoV-2 virus, has dramatically impacted global health, economies, and social structures since its emergence in late 2019. This highly contagious respiratory illness spread rapidly, leading the World Health Organization (WHO) to declare it a global pandemic in March 2020. Understanding the epidemiology of COVID-19 — including patterns of transmission, incidence, and prevalence — has been crucial in guiding public health interventions and policy-making. Epidemiological studies have revealed that COVID-19 spreads primarily through respiratory droplets and aerosols, with transmission dynamics influenced by factors such as population density, social behaviors, and health system responses. Risk factors associated with severe COVID-19 outcomes include advanced age, gender, pre-existing health conditions (e.g., cardiovascular disease, diabetes, chronic respiratory diseases), and certain demographic factors (Didac et al., 2020; Mueller et al., 2020)(Chakravarty et al., 2020). Socioeconomic status, racial and ethnic backgrounds, and occupational exposure also play significant roles, as these factors often influence access to healthcare and likelihood of exposure (Pan et al., 2020; Ravi, 2020).

1.2 Etiopathogenesis of COVID-19

Severe acute respiratory syndrome coronavirus 2 (SARS-CoV-2) was first identified as the causative agent of COVID-19 in Wuhan in 2019 (Huang et al., 2020; Zhu et al., 2020). In the early stages, the similarities between SARS-CoV, Middle East respiratory syndrome coronavirus (MERS-CoV), and SARS-CoV-2 helped researchers trace its zoonotic origins (Rabaan et al., 2020). Although various hypotheses have been proposed, including the lab escape scenario, evidence points to bats as the primary source of SARS-CoV-2, while the intermediate host remains unidentified (Schindell et al., 2022). Structurally, SARS-CoV-2 features a crown-like outer envelope and a positive-stranded RNA genome that encodes several structural proteins, including spike (S), membrane (M), envelope (E), nucleocapsid

(N), and hemagglutinin-esterase (HE) proteins, along with sixteen non-structural proteins and six accessory proteins. The entry of SARS-CoV-2 into host cells is facilitated by the transmembrane S glycoprotein, whose heterodimers extend from the viral surface, creating the characteristic crown-like appearance of coronaviruses (Beniac et al., 2006; Delmas and Laude, 1990). Differences in the S proteins may account for the rapid transmission of SARS-CoV-2 compared to SARS-CoV (Rabaan et al., 2020). The S protein is often cleaved by a furin-like host protease into two subunits: S1, which binds to the host cell's ACE2 receptor, and S2, which contains the fusion machinery (Walls et al., 2020). The S1/ACE2 binding exposes an internal site on S2, which is subsequently cleaved by transmembrane protease serine 2 (TMPRSS2) in the endosomal compartment, releasing the fusion peptide and initiating the formation of the fusion pore (Jackson et al., 2022). Variations in the S glycoprotein are responsible for the emergence of different viral variants (Ong et al., 2022). Infection typically occurs in the epithelium of the upper respiratory tract, as respiratory droplets are the primary mode of transmission, leading to either symptomatic or asymptomatic COVID-19 cases. About 80% of cases, categorized as mild to moderate, present with a range of symptoms such as fever, headache, anosmia, shortness of breath, fatigue, and mild cough, which may develop after an incubation period of 4-10 days (He et al., 2020; Long et al., 2022). The remaining 20% of patients may experience severe disease, as the infection disrupts gas exchange in the alveolar epithelial cells, resulting in hypoxemia, edema, and fibrosis (Mason, 2020). When the infection reaches the lower respiratory tract, it can lead to pneumonia, which may result in severe complications, including respiratory failure (Huang et al., 2020; Lentz et al., 2020). Furthermore, SARS-CoV-2 has been detected in various tissues where ACE2 and TMPRSS2 are abundant, contributing to the occurrence of multiple extrapulmonary symptoms (Bilinska et al., 2020; Khreefa et al., 2023). These tissues, acting as viral reservoirs, may also facilitate viral transmission. Indeed, viral particles have been found not only in respiratory droplets but also in aerosols, blood, ocular secretions, urine, and stool (Long et al., 2022).

1.3 Acute respiratory distress syndrome (ARDS)

Acute respiratory distress syndrome (ARDS) induced by COVID-19 represents one of the most severe complications of SARS-CoV-2 infection, characterized by intense inflammation and profound respiratory failure. In COVID-19-associated ARDS, the inflammatory response is a central pathological feature, driven by an exaggerated immune response known as a "cytokine storm." This condition results from the overproduction of pro-inflammatory cytokines, such as IL-6, IL-1β, and TNF-α, which amplify inflammation in lung tissues and lead to widespread alveolar damage. The inflammatory pathways activated in COVID-19 ARDS involve both innate and adaptive immune components, including the NF-κB pathway, and activation of inflammasomes. These pathways work together to recruit immune cells like neutrophils and macrophages to the lung, further propagating inflammation and exacerbating tissue damage. Understanding the mechanisms of these inflammatory pathways is crucial for developing targeted treatments, as they offer potential therapeutic avenues to mitigate severe respiratory complications in COVID-19 patients, reduce mortality, and improve patient outcomes.

1.4 Current COVID-19 Treatments and Their Limitations

The COVID-19 pandemic has prompted a rapid evolution of therapeutic strategies aimed at managing the disease and improving patient outcomes. Current treatments primarily include antiviral medications, monoclonal antibodies, and supportive therapies, which together address various aspects of the illness. Antiviral agents like remdesivir have been shown to reduce viral replication and shorten recovery times for hospitalized patients. Monoclonal antibodies are utilized to target the virus early in infection, helping to prevent severe disease progression. Additionally, corticosteroids, particularly dexamethasone, have become essential in treating severe cases by dampening the inflammatory response associated with COVID-19. Despite these advancements, significant limitations persist in the treatment landscape. The effectiveness of antiviral medications can vary based on the timing of administration and the presence of variants with resistance. Monoclonal antibodies, while effective, may lose efficacy against certain variants, limiting their applicability in a constantly evolving viral environment.

Furthermore, the use of corticosteroids is primarily beneficial in patients with severe disease, and their role in mild to moderate cases remains unclear. Moreover, access to these therapies can be limited by logistical challenges, regulatory barriers, and disparities in healthcare systems. As the pandemic evolves, ongoing research is crucial to identify new treatment modalities, optimize existing therapies, and address the limitations inherent in current approaches. This dynamic and challenging landscape underscores the need for continued vigilance and innovation in the fight against COVID-19.

1.5 Potential of Aliamides in the Treatment of COVID-19-Related Acute Lung Injury

In the search for effective treatments for ARDS, ALIAmides have garnered attention due to their unique properties and mechanisms of action. Preclinical studies have indicated that aliamides can exert anti-inflammatory effects by influencing the pathways involved in cytokine release and immune cell activation, potentially mitigating the hyperinflammation associated with COVID-19. One of the most promising aspects of ALIAmides is their ability to selectively target pathways involved in the immune response without broadly suppressing it, thereby preserving the body's ability to fight the virus. This targeted approach could be particularly beneficial in COVID-19 patients, where a balanced immune response is crucial to avoid worsening the condition. Furthermore, the safety profile of ALIAmides appears favorable, with limited side effects reported in preliminary studies. This makes them suitable candidates for adjunctive therapy alongside existing treatments for COVID-19 and ARDS, such as corticosteroids and antiviral medications.

Aims (ii)

The primary aims of this study was to investigate the therapeutic potential of the pNAPE-LP in mitigating lung inflammation triggered by the SARS-CoV-2 Spike Protein (SP). Specifically, the study seeks to elucidate the efficacy of intranasal administration of pNAPE-LP/palmitate in a murine model, focusing on its ability to colonize pulmonary tissues and facilitate the localized release of the anti-inflammatory compound palmitoylethanolamide (PEA). The study intended to assess the impact of pNAPE-LP on innate immune responses and histological lung damage following SP challenge. Key

objectives include the evaluation of cellular infiltration, morphological integrity of alveoli, and the modulation of pro-inflammatory mediators, including cytokines and myeloperoxidase activity. Additionally, the investigation aims to determine the role of pNAPE-LP in downregulating ACE-2 expression in lung tissues, which may contribute to the attenuation of infection severity. By addressing these aims, the study aims to contribute valuable insights into a potential adjunctive therapeutic strategy for managing acute respiratory distress syndrome associated with SARS-CoV-2, while advancing the understanding of probiotic-engineered therapies in inflammatory lung conditions.

Intranasal delivery of PEA-producing *Lactobacillus paracasei F19* alleviates SARS- CoV-2 spike protein-induced lung injury in mice

Alessandro Del Re, Silvia Basili Franzin, Jie Lu, Irene Palenca, Aurora Zilli, Federico Pepi, Anna Troiani, Luisa Seguella, Marcella Pesce, Giovanni Esposito, Giovanni Sarnelli and Giuseppe Esposito

Abstract

Background SARS-CoV-2 belongs to the *coronaviridae* family and infects human cells by directly interacting with the angiotensin-converting enzyme-2 (ACE-2) through the viral Spike Protein (SP). While vaccines are crucial, much attention has been directed towards managing the symptoms of acute respiratory distress syndrome. Our present study highlights the potential in counteracting lung inflammation triggered by SARS-CoV-2 SP of the intranasal administration of the engineered probiotic *Lactobacillus paracasei F19* expressing the enzyme NAPE-PLD (pNAPE-LP) able to in situ release palmitoylethanolamide (PEA) under a super-low boost of palmitate.

Methods C57BL/6J mice undergo prophylactic treatment with intranasal pNAPE-LP/palmitate for 7 days before a 7 days challenge with intranasal SARS-CoV-2 SP. Then the capability of pNAPE-LP of colonizing the lungs and actively release PEA in situ have been determined by immunofluorescence, western blot and HPLC-MS. Moreover, the innate immune system downregulation and the histological damage rescue exerted by pNAPE-LP have been tested by immunofluorescence, hematoxylin and eosin staining, western blot analysis and ELISA test for the release of the pro- inflammatory mediators.

Results pNAPE-LP effectively colonizes mice lungs and releases the anti-inflammatory compound PEA. Moreover, pNAPE-LP exhibits a protective effect on alveolar morphology, innate immune cells infiltration and in the reduction of neutrophil count, effectively reducing lung injury induced by SARS-CoV-2 SP. This is achieved by mitigating TLR4- mediated NLRP3 activation and the downstream pro-inflammatory products such as ILs, TNFα, C-reactive protein and the myeloperoxidase activity. Interestingly we observed a global reduction ACE2 expression in the lungs.

Conclusion pNAPE-LP actively protect from severe inflammatory-related symptoms in SP-challenged mice. Also, it can downregulate the expression of ACE-2 receptors at the lung site potentially preventing the spreading of the infection.

Keywords Engineered probiotic, Palmitoylethanolamide, SARS-CoV-2, Spike protein, ARDS, NLRP3

1. Background

Over the past two decades, there has been a concerning surge in the emergence of novel viral diseases [1] and lastly the world has been grappling with the SARS-CoV-2 pandemic, resulting in nearly 7 million deaths to date [2]. SARS-CoV-2 is classified within the *coronaviridae* fam- ily and engages human cells through a direct interaction with the angiotensin-converting enzyme-2 (ACE-2) via the viral Spike Protein (SP). This infection precipitates a range of symptoms, notably including acute respiratory distress syndrome (ARDS) and multiorgan failure in the worst-case scenario [3]. Despite the conclusion of the crisis and the gradual global reversion to a state of normalcy, numerous schol- arly investigations are underscored by the prospect that COVID-19 possesses the capacity to transmute its epi- demiological characteristics from a pandemic manifesta- tion into an endemic counterpart [4], thereby undergoing a change into a seasonal infection. Moreover, taking into account the the impending threat of future pandem- ics [5], coupled with the fact that recent viral diseases predominantly propagate via airborne transmission, an imperative and pressing demand arises for efficacious preventative interventions. While vaccines were effectively preventing the worst clinical outcomes of the COVID-19 [6], the possible emergence of new variants of concern as well as the pos- sibility of new airborne outbreaks, much attention has been directed towards managing ARDS. This condition occurs when macrophages and mast cells fail to regulate the innate immune response [7, 8], leading to an exces- sive release of pro-inflammatory mediators furtherly amplified by the activation of the Nod-like receptor fam- ily pyrin domain containing 3 (NLRP3) inflammasome [9–12]. It appears that the SP of SARS-CoV-2 triggers this hyper-inflammatory response by interacting with the Toll-like receptor 4 (TLR4) and triggering a sort of bacte- rial-like response in the innate immune system [13–15]. Extensive research has demonstrated the direct asso- ciation between these components, which plays a pivotal role in ARDS development and various short-term and long-term manifestations of COVID-19 [16, 17]. Further- more, TLR4-related

pathways may enhance viral infec- tivity by indirectly upregulating the ACE-2 receptor in different cell subtypes during inflammatory conditions [18–20]. Recent scientific studies have shed light on autacoid local injury amides (ALIAmides), a class of naturally occurring molecules synthesized by the N-acyl phospha- tidylethanolamine-specific phospholipase D (NAPE PLD) in response to specific demands. ALIAmides are promis- ing valuable tool in the clinical management of COVID- 19 and other viral diseases by acting on peroxisome proliferator-activated receptors (PPARs) and reducing the inflammatory response [21–23]. They achieve this by downregulating the expression of several pro-inflam- matory mediators and cytokines, including interleukin (IL)-6 and IL-1β. Additionally, ALIAmides can decrease the expression of TLR4 and NLRP3, both of which are involved in the development of ARDS [24–26]. Our research group recently demonstrated that pal- mitoylethanolamide (PEA), a specific type of ALIAmide, can effectively reduce in vitro the expression of ACE-2 in alveolar macrophages activated by the SP of SARS-CoV-2 (see Fig. 1 for a summary of our previous findings) [18]. Notably, clinical trials have shown the clinical efficacy and safety of PEA in treating other viral lung diseases such as influenza and the common cold [27]. Currently, PEA is the subject of two clinical trials in Italy and the United States, assessing its effectiveness in managing COVID-19-related symptoms [28, 29]. However, the clinical utility of PEA is limited by its low solubility and the consequent need of using high doses to attain and maintain the therapeutic effect, under- scoring the importance of localizing the release of PEA to enhance regional absorption [30]. To enhance its local bioavailability, our laboratory developed a modi- fied strain of *Lactobacillus paracasei subsp. paracasei F19* carrying a plasmid that expresses the NAPE-PLD enzyme (pNAPE-LP). By releasing PEA under a super- low boost of palmitate, this probiotic system has already demonstrated effectiveness in reducing inflammation in the gut across various colitis models. In these previ- ous investigation we observed an *optimum* of PEA pro- duction at the palmitate concentration of 0.003 μM [31, 32]. Moreover, considering the established connection between lung microbiota disruption and ARDS, pNAPE- LP holds promise as a prophylactic agent against ARDS by mitigating inflammatory responses also by restoring lung microbiota [33, 34]. Finally, its local action makes it a compelling candidate for intranasal delivery. Therefore, the objective of this study is to investigate the prophylac- tic anti-inflammatory effect of intranasal administration of the pNAPE-LP system combined with palmitate in a SARS-CoV-2 SP-induced lung injury model. Initially, we confirmed the ability of pNAPE-LP to colonize the lungs and release PEA in situ.

Subsequently, through histo- logical, immunofluorescence, Western blot, and ELISA analyses, we assessed the ability of our probiotic system to preserve alveolar architecture integrity and reduce the increase of pro-inflammatory markers (NLRP3, TLR4, etc.).

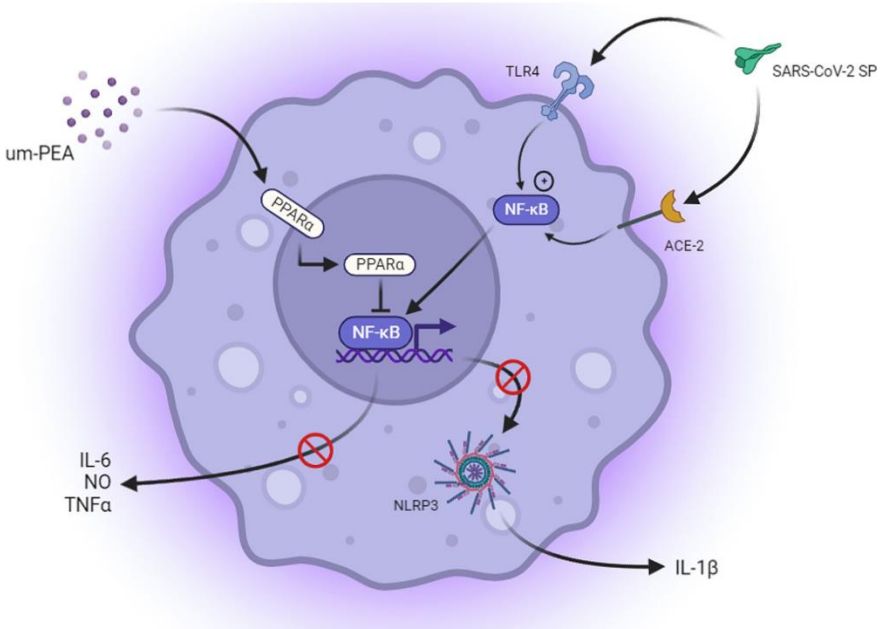

Fig. 1 Summary of previous findings. Effect of ultramicronized(um)-PEA on SP-challenged murine alveolar macrophages. Anti-inflammatory effect of um-PEA in SARS-CoV-2 spike protein challenged murine alveolar macrophages depends upon PPARα-mediated control of NF-κB and NLRP3 inflamma- some signaling pathways. Schematic representation of SARS-CoV-2 spike protein-induced inflammasome activation and relative proposed anti-inflam- matory mechanism of um-PEA in mice alveolar macrophages. Spike protein interacts at TLR4 and ACE-2 receptor sites, activating phosphorylation of p38MAPK and consequent NF-κB activation. This is accompanied by cytokine release (IL-6 and TNF-α) and inflammasome pathway activation, featured by NLRP3 and Caspase-1/IL-1β upregulation. Um-PEA acting at PPAR-α receptor site inhibits NF-κB transcription and NLRP-3 inflammasome signaling leading to a significant anti-inflammatory effect in spike protein-challenged alveolar macrophages

2. Materials and methods

2.1 Generation of genetically modified strains of Lactobacillus paracasei subsp. paracasei

The pTRKH3-slpGFP vector obtained from Add- gene (Watertown, MA, USA) underwent several modifications. Firstly, the GFP sequence was eliminated at SalI/PstI restriction sites, followed by the insertion of T7 transcriptional terminators at BamHI/EcoRV sites, and finally, linker sequences containing BsaI-BsaI were added at PstI/XmaI restriction sites. Then, using the In- Fusion method (Clontech, Mountain View, CA, USA), the cDNA of human NAPE-PLD was inserted into the BsaI sites. Electroporation was used to transfect the resulting pTRKH3-slp-NAPE-PLD construct and the parental plasmid (which does not express the NAPE-PLD gene and is used as a negative control) into *Lactobacil- lus paracasei subsp. paracasei F19* strain (Arla Foods, Hoersholm, Denmark). Positive clones were obtained by erythromycin (5 μg/mL) selection. The parental plasmid (pLP) and NAPE-PLD-expressing bacteria (pNAPE-LP) were then anaerobically amplified in Man, Rogosa and Sharpe (MRS)-broth (Conda, Torrejón de Ardoz Madrid, Spain) and isolated in MRS agar (Conda, Torrejón de Ardoz Madrid, Spain) supplemented with erythromycin 5 μg/mL (Sigma-Aldrich, Milan, Italy) under anaerobic conditions at 37 °C for 72 h. Finally, the viability of the bacteria was determined by manually counting colonies, and the colony forming units (CFU)/mL were obtained by correcting the number of colonies for the dilution factor.

2.2 Animals and experimental plan

Eight-week-old male C57BL/6J mice (Charles River, Lecco, Italy) were used for the experiments. Sapienza University's Ethics Committee approved all experimen- tal procedures. Animal care was in compliance with the IASP and European Community (EC L358/1 18/12/86) guidelines on the use and protection of animals in experimental research. The Experimental plans last for 14 days in total (from day − 7 to day 7, see Fig. 2).

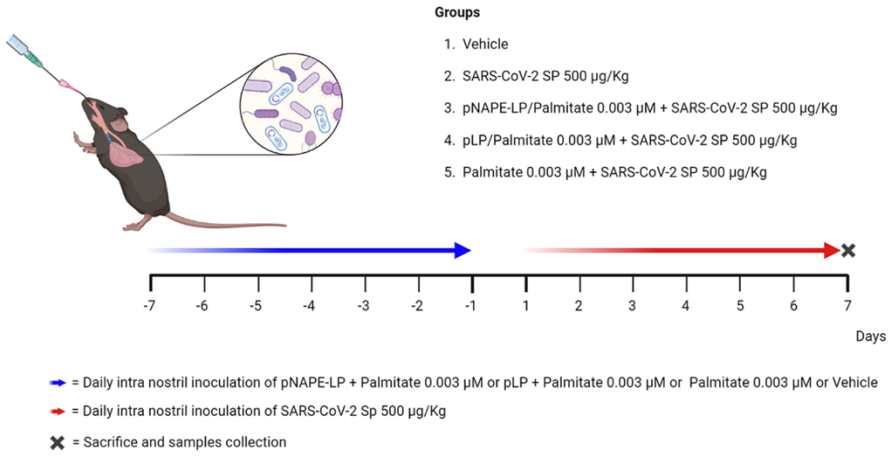

Fig. 2 Experimental plan

For the intranasal administration the animals were lightly anesthetized by inhaled isoflurane (Abbott Labo- ratories, Montreal, PQ, Canada), and 2 or 4 volumes (25 µl each) of bacterial suspensions, SP solution, Pal- mitate solution or vehicle were intranasally delivered dropwise to the nares using a pipetman (model P20 or P200, Gilson) while the mouse was in a supine position. In details, the animals were randomly divided into 5 groups *n*=8 each and undergo treatments as follow: (1) Vehicle, daily intranasal administration of sterile saline solution along the entire experimental plan; (2) SARS- CoV-2 SP 500 µg/Kg, daily intranasal administration of sterile saline solution from day −7 to -1 and daily intra- nasal administration of SP 500 µg/Kg from day 1 to day 7; (3) pNAPE-LP/Palmitate 0.003 µM, daily intranasal administration of 109 CFU of pNAPE-LP+Palmitate 0.003 µM from day −7 to day −1 and daily intranasal administration of SP 500 µg/Kg from day 1 to day 7; (4) pLP/Palmitate 0.003 µM, daily intranasal administration of 109 CFU of pLP+Palmitate 0.003 µM from day −7 to day −1 and daily intranasal administration of SP 500 µg/ Kg from day 1 to day 7; (5) Palmitate 0.003 µM, daily intranasal administration of Palmitate 0.003 µM from day −7 to day −1 and daily intranasal administration of SP 500 µg/Kg from day 1 to day 7. All the solutions for the intranasal inoculation have been prepared in sterile saline as described in the Supplementary Table 1. Rectal temperature was measured daily for the entire duration of the experiment. To obtain the rectal temperature, the mice were hand-restrained and placed on a horizontal surface. The tail was then lifted, and the probe (covered with

Vaseline) was gently inserted into the rectum, up to a fixed depth. At day 7 the animals were sacrificed by CO2 hypoxia.

2.3 Sample collection and preparation

Broncho-alveolar lavage fluid (BALF) was collected in the following manner. The mice were dissected to expose the trachea, and a small incision was made. A sterile tube (with an internal diameter of 0.58 mm) was inserted through the incision and connected to a sterile syringe needle. To create an airtight seal, a piece of sterile sur- gical thread was tightly wrapped around the intubated trachea. Two rounds of instillation and retrieval of 1 mL of sterile phosphate-buffered saline (PBS) into the lungs were then performed using the sterile syringe. To ensure the integrity of the procedure, the tubing-needle-syringe setup was rinsed thoroughly with sterile PBS between each sample collection. Sterile PBS (n=2) was used for lavage, and PBS rinses (n=4) of the syringe, needle, and tubing (before and after lavage) were collected as pro- cedural controls. BAL fluid was prepared by pooling the two sequential lavages from each mouse, resulting in up to 2 mL of total BAL fluid per mouse. To prepare perfused lungs for H&E and immuno- fluorescence analysis, a solution of 4% PFA was injected directly into the lung through the trachea, which was then secured with a piece of thread. The lungs were sub- sequently immersed in the same fixative for 24 h. Follow- ing fixation, the lungs were perfused and then immersed in 30% sucrose for 24 h. Finally, the lungs perfused and immersed in OCT for a period of 24 h before the cryostat cutting. Lungs homogenates were obtained from non-PFA fixed lungs. The snap-frozen lungs were thawed, weighed, transferred to different tubes on ice containing hypo- tonic lysis buffer (10 mM 4-(2-hydroxyethyl)-1-pipera- zineethanesulfonic acid (HEPES), 1.5 mM MgCl2, 10 mM KCl, 0.5 mM phenylmethylsulphonylfluoride, 1.5 mg/mL soybean trypsin inhibitor, 7 mg/mL pepstatinA, 5 mg/mL leupeptin, 0.1 mM benzamidine and 0.5 mM dithioth- reitol (DTT)). The samples were centrifuged at 10,000 × g for 10 min and supernatants were transferred to clean microcentrifuge tubes, frozen on dry ice and stored at -80 for the analysis.

2.4 Confirmation of pNAPE-LP lung colonization

BALF collected from groups 1 and 3 as previously described were immediately diluted in serial 1/10 dilu- tions (from 10−1 to 10−5) and plated in MRS agar enriched with

Erythromycin [50 μg/mL] as selection marker. The plates were incubated for 72 h at 37 °C in a microaerophilic environment and then the colonies from each spot were counted to determine the CFU/mL con- tained in the BALF samples. *N*=4 single colonies have been picked up from the 10−5 dilution and inoculated in MRS liquid media enriched with Erythromycin [50 μg/ mL] and growth overnight. According to the procedure previously described [17] with slight modifications, immunofluorescence analysis was performed in both pNAPE-LP and in the cultured pLP as a negative con- trol. Briefly, the cultures undergo spinning and the pellets were washed in phosphate buffer saline (PBS). For immu- nofluorescence staining of both pNAPE-LP and in the pLP, 1 × 107 bacterial cells were placed on polyethylenei- mine-coated coverslips and fixed with 4% PFA. Blocking solution containing 1% bovine serum albumin (BSA) in PBS (w/v) was used. Labelling was performed using poly- clonal rabbit anti-NAPE-PLD antibody (1:100 dil. v/v) (Cell Signaling Technology, Inc., Danvers, MA, USA). Secondary fluorescein isothiocyanate-conjugated anti- rabbit antibodies were incubated at room temperature for 2 h in the dark. Samples were examined by Optika XDS-3L4 microscope (Ponteranica, Bergamo, Italy). Images were captured at 100× by a high-resolution digital camera (Nikon Digital Sight DS-U1).

2.5 HPLC-MS determination of PEA level in mice lungs

Specimens from the lung from every groups of mice were isolated to evaluate PEA concentrations *in vivo*. Tissues were processed according to the method described by the Endocannabinoid Research Group [39]. Extraction and analysis were performed accord- ing to Gachet et al. [40], with slight modifications. Analyses were run on a Jasco Extrema LC-4000 system (Jasco Inc., Easton, MD, USA) coupled to an Advion Expression mass spectrometer (Advion Inc., Ithaca, NY, USA) equipped with an electrospray (ESI) source. Mass spectra were recorded in positive SIM mode. The capillary voltage was set at +180 V, the spray voltage was at 3 kV, the source voltage offset was at +20 V, and the capillary temperature was set at 250 °C. The chromatographic separation was performed on a Kine- tex C18 analytical column (150 × 4.6 mm, id. 3 μm, 100 Å) and security guard column, both supplied by Phe- nomenex (Torrance, CA, USA). The analyses were performed at a flow rate of 0.3 mL/min, with solvent A (water containing 2 mM ammonium acetate) and solvent B (methanol containing 2 mM ammonium acetate and 0.1% formic acid). Elution was performed according to the following linear gradient: 15% B for 0.5 min, 15–70% B from 0.5 to 2.5

min, 7–99% B from 2.5 to 4.0 min and held at 99% B from 4.0 to 8.0 min. From 8 to 11.50 min, the column was equilibrated to 15% B and conditioned from 11.5 to 15.0 min at 15% B. The injection volume was 10 µL and the column temperature was fixed at 40 °C. For quantitative analy- sis, standard curves of PEA (Sigma-Aldrich St. Louis, MO, USA) were prepared over a concentration range of 0.0001–1 ppm with six different concentration lev- els and duplicate injections at each level. All data were collected and processed using JASCO ChromNAV (v2.02.04)andAdvionDataExpress(v4.0.13.8).

2.6 Western blot analysis

Proteins were extracted from lung tissue or bacte- ria pellets and processed by Western blot analysis. For protein extraction by the bacterial pellet, a spe- cific CelLyticTM lysis buffer (Sigma-Aldrich, Milan, Italy) was used according to manufacturer's instruc- tions. Tissue samples were homogenized in ice-cold hypotonic lysis buffer [10 mM 4-(2-hydroxyethyl)- 1-piperazineethanesulfonic acid (HEPES), 1.5 mM MgCl2, 10 mM KCl, 0.5 mM phenylmethylsulphonyl- fluoride, 1.5 µg/ml soybean trypsin inhibitor, 7 mg/ ml pepstatin A, 5 mg/ml leupeptin, 0.1 mM benzami- dine, and 0.5 mM dithiothreitol (DTT)]. Both bacte- rial- and tissue-deriving protein extracts were mixed with a non-reducing gel loading buffer [50 mM Tris (hydroxymethyl)aminomethane (Tris), 10% sodium dodecyl sulfate (SDS), 10% glycerol, 2 mg/ml bromo- phenol] at a 1:1 ratio, and then boiled for 3 min fol- lowed by centrifugation at 10,000×g for 10 min. The protein concentration was determined using Brad- ford assay and equivalent amounts (50 µg) of each homogenate underwent electrophoresis through a polyacrilamide minigel. After the transfer the mem- branes were incubated with 10% nonfat dry milk in PBS overnight at 4 °C and then exposed, depending on the experiments, with the appropriate primary anti- body according to standard experimental protocols (see Table 1). Membranes were then incubated with the specific secondary antibodies conjugated to HRP (Dako, Milan, Italy). Immune complexes were exposed to enhanced chemiluminescence detection reagents, and the blots were analyzed by scanning densitometry (Versadoc MP4000; Bio-Rad, Segrate, Italy). Results were expressed as optical density (OD; arbitrary units = mm2) and normalized against the expression of the housekeeping proteins β-actin for mice samples and GroEL for bacterial pellets.

Antibody	Host	Clonality	Dilution	Brand
Anti-NLRP3	Rabbit	Monoclonal	1:100 *v/v*	Thermo Fisher Scientific, Waltham, MA, USA, Cat #MA5-32255
Anti-cleaved caspase 1	Mouse	Monoclonal	1:100 *v/v*	Santa Cruz Biotechnology, Dallas, TX, USA, sc-56,036
Anti-NAPE-PLD	Rabbit	Polyclonal	1:200 *v/v*	AbCam, Cambridge, UK, ab95397
Anti-TLR4	Rabbit	Polyclonal	1:50 v/v	Bioss Antibodies, Boston, MA, USA, bs-1021R

Table 2 Antibodies for immunofluorescence

Antibody	Host	Clonality	Dilution	Brand
Anti-NLRP3	Rabbit	Monoclonal	1:100 *v/v*	Thermo Fisher Scientific, Waltham, MA, USA, Cat #MA5-32255
Anti-ACE2	Mouse	Monoclonal	1:50 *v/v*	Santa Cruz Biotechnology, Dallas, TX, USA, sc-390,851
Anti-CD68	Goat	Monoclonal	1:200 *v/v*	AbCam, Cambridge, UK, ab289671
Anti-TLR4	Rabbit	Polyclonal	1:50 v/v	Bioss Antibodies, Boston, MA, USA, bs-1021R

Table 1 Antibodies for western blot

2.7 Hematoxylin and Eosin (H&E) staining and lung injury assessment

Frozen sections of the lungs were sectioned using a cryostat at 8 µm and placed onto slides. The sections were stained with H&E according to Ling et al. [35]. The histopathological analysis has been performed in the following manner. Number of epithelial cells, and the number infiltrated neutrophils in alveolar spaces and interstitial space were analyzed by NIH Image J. Ten 40x fields from each group were chosen for the counting of the epithelial and infiltrated neutrophils. Lung injury score was measured as described by Mat- ute-Bello et al. [36] following a scale (see Supplemen- tary Table 2).

2.8 Immunofluorescence

Frozen sections of the lungs were sectioned using a cryostat at 8 µm and placed onto slides. Sections were blocked with bovine serum albumin (BSA) and subsequently stained with the appropriate primary antibody (See Table 2). Slices were then washed with PBS 1X and incubated in the dark with fluorescein isothiocyanate-conjugated anti-rabbit or anti-mouse (Abcam, Cambridge, UK). Nuclei were stained with Hoechst. Sections were analyzed with a microscope (Nikon Eclipse 80i), and images were captured by a high-resolution digital camera (Nikon Digital Sight DS-U1).

2.9 Myeloperoxidase assay

Myeloperoxidase (MPO), a marker of polymorphonuclear leukocyte accumulation, was determined as previously described (Mullane et al., 1985). After removal, lungs tis- sues

were rinsed with a cold saline solution. Then, the tissues were homogenized in a solution containing 0.5% hexadecyltrimethylammonium bromide (Sigma-Aldrich, Milan, Italy), dissolved in 10 mM potassium phosphate buffer, and centrifuged for 30 min at 20,000 × g at 37 °C. An aliquot of the supernatant was mixed with a solution of tetramethylbenzidine (1.6 mM; Sigma-Aldrich, Milan, Italy) and 0.1 mM hydrogen peroxide (Sigma-Aldrich, Milan, Italy). The solution was then spectrophotometri- cally measured at 650 nm. MPO activity was determined as the amount of enzyme degrading 1 mmol/min of per- oxide at 37 °C and was expressed in milliunits (mu) per 100 mg of wet tissue weight.

2.10 Enzyme-linked immunosorbent assay (ELISA)

ELISA for IL-1β, IL-6, TNFα and CRP (all from Thermo Fisher Scientific, MA, USA) was carried out on lungs homogenate according to the manufacturer's protocol. Absorbance was measured on a microtiter plate reader. IL-1β, IL-6, TNFα and CRP levels were determined using standard curve methods.

3. Results

3.1 pNAPE-LP colonizes mice lungs and actively releases PEA in situ

In order to validate the lung colonization by our probi- otic system, we cultured the BALF obtained from groups (1) and (3) on MRS agar supplemented with erythro- mycin [50 μg/mL]. Our findings revealed the presence of erythromycin-resistant colonies exclusively in the samples derived from the group subjected to intranasal administration of pNAPE-LP (Fig. 3, A). Additionally, the samples from group (3) exhibited an average level of 104 CFU/mL (Fig. 3, B), thereby confirming the successful colonization of the lungs by pNAPE-LP. To further cor- roborate our observations, four colonies were selected from each sample and cultured overnight in MRS liquid media supplemented with erythromycin. Subsequently, the resulting cultures underwent Immunofluorescence and western blot analyses to ascertain the expression of the NAPE-PLD enzymes. Our immunofluorescence analysis (Fig. 3, C) and western blot results (Fig. 3, D-E) demonstrated the selective expression of the NAPE-PLD enzyme exclusively in the bacterial cells isolated from the BALF of group (3). Moreover, to validate the capacity of pNAPE-LP to locally produce and release PEA under minimal stimula- tion with

palmitate, homogenates of mouse lung samples from groups (1), (3), and (4) were subjected to HPLS-MS analysis to determine the levels of PEA. Once again, only the samples obtained from animals treated with pNAPE- LP and palmitate exhibited a significant increase in PEA levels ($p < 0.001$ vs. Vehicle group) (Fig. 3, B).

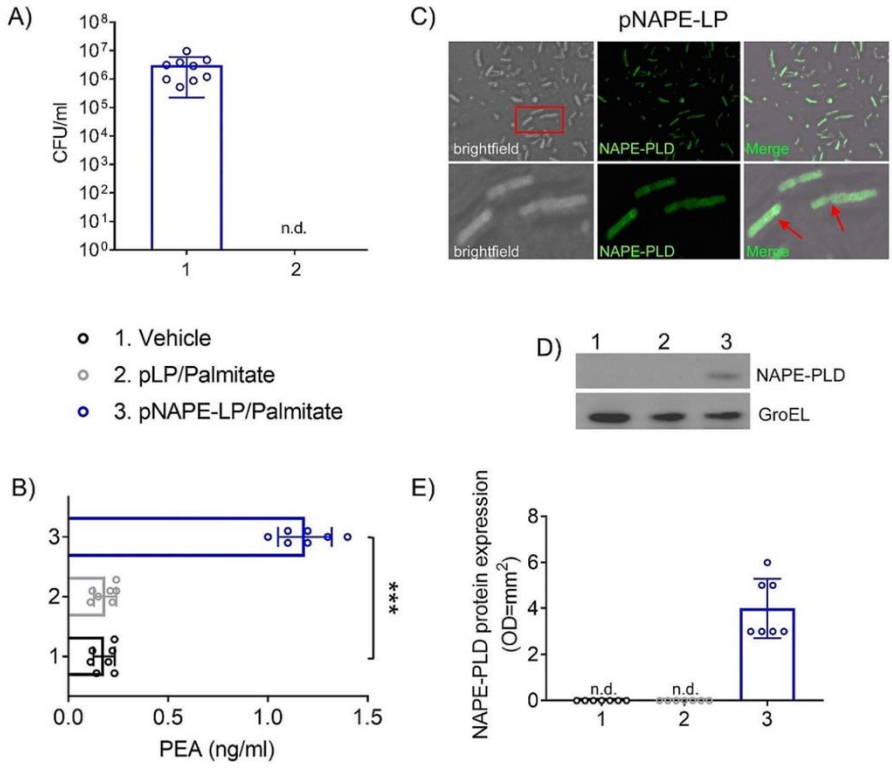

Fig. 3 Confirmation of pNAPE-PLD colonization of the mice lungs. At the end of the experimental protocol the BALF from pNAPE-LP/Palmitate group displays significant levels of erythromycin resistant CFU compared to the Vehicle group (**A**). Once picked and amplified, these cells are revealed to express the NAPE-PLD enzyme as confirmed by immunofluorescence (**C**), and western blot analysis (46 kDa) (housekeeping protein GroEL, 57 kDa) (**D, E**). The HPLC-MS analysis of homogenates of lungs revealed a significant increase in the levels of PEA only in pNAPE-LP/Palmitate group (**B**). Results are expressed as mean ± SD of $n = 7$ or 9 experiments performed in triplicate. *** $p < 0.001$, ** $p < 0.01$, * $p < 0.05$ vs. Vehicle, n.d.=non detectable

3.2 pNAPE-LP protects alveolar morphology and reduces the lung injury score from SARS-CoV-2 SP pro-inflammatory effect

After 7 days of intranasal delivery of SARS-CoV-2 SP, mice in group 2 exhibited a substantial deterioration in their alveolar architecture, indicating significant dam- age to the small air sacs in their lungs. In contrast, the prophylactic administration of pNAPE-LP/Palmitate (3) demonstrated a protective effect, effectively preserving the alveolar morphology in the mice's lungs. It is note- worthy that the combination of the engineered probiotic pNAPE-LP and palmitate played a pivotal role in confer- ring histological protection in our experimental model (Fig. 4, A). The results clearly highlight the efficacy of this specific combination in mitigating the detrimental effects induced by SARS-CoV-2 SP. The observed loss of alveolar architecture in group 2 was accompanied by a significant increase in the infiltra- tion of epithelial cells ($p < 0.001$ vs. Vehicle), as well as a marked elevation in the neutrophil count ($p<0.001$ vs. Vehicle), indicating a pronounced lung injury ($p<0.001$ vs. Vehicle). However, the prophylactic treatment with pNAPE-LP/Palmitate (3) reversed the histological dam- age observed in this group. Specifically, it successfully normalized the percentage of infiltrated epithelial cells ($p < 0.001$ vs. SP [500 μg/Kg]), reduced the neutrophil count ($p<0.01$ vs. SP [500 μg/Kg]), and consequently decreased the overall lung injury score ($p<0.01$ vs. SP [500 μg/Kg]) to levels comparable to those observed in the vehicle group (Fig. 4, B-D). Consistent with expec- tations, the two internal control groups, namely pLP/ Palmitate (4) and Palmitate alone (5), did not show any significant differences compared to the SP [500 μg/Kg] group (2) in terms of deterioration in their alveolar archi- tecture, the percentage of infiltrated epithelial cells, the neutrophil count and the lung injury score (Fig. 4, A-D).

3.3 pNAPE-LP attenuates TLR4-mediated NLRP3 activation in the lungs of mice and reduces global ACE2 expression

To gain insights into the role of SARS-CoV-2 SP agonism on TLR4 *in vivo* and explore the potential protective effect of pNAPE-LP/Palmitate, we conducted immuno-fluorescent analysis on lung sections of mice. Our objec- tive was to examine the expression of TLR4 in alveolar macrophages (CD68 + cells) and its influence on the co-expression of NLRP3 and ACE-2, two important markers of ARDS onset and viral invasion, respectively. Our findings+ revealed a significant upregulation of TLR4 in CD68 cells ($p<0.001$ vs. Vehicle) in samples from the SP [500 μg/Kg] group (2). Similarly, we

observed a parallel increase in the co-expression of NLRP3 and ACE-2 (p<0.001 vs. Vehicle) following daily administra- tion of SARS-CoV-2 SP (Fig. 4E-H). Consistent with previous observations, treatment with pNAPE-LP/Palmitate significantly mitigated the pro- inflammatory environment in the lungs of mice. Notably, the expression levels of TLR4 in CD68+ cells were mark- edly reduced (p<0.001 vs. SP [500 µg/Kg]), as were the overall numbers of CD68+ cells, indicating the beneficial effects of the probiotic system compared to the SARS- CoV-2 SP group (2). Similarly, the global co-expression of NLRP3/ACE-2 was significantly diminished by the engi- neered probiotic (p < 0.001 vs. SP [500 µg/Kg]), further confirming its anti-inflammatory properties (Fig. 4E-H). In contrast, our investigation of the internal control groups, namely pLP/Palmitate (4) and Palmitate alone (5), revealed no significant changes in the expression of the aforementioned markers compared to the SP [500 µg/ Kg] group (2). Specifically, there were no notable dif- ferences observed in the levels of TLR4 expression in CD68+ cells or concerning the co-expression of NLRP3 and ACE-2. These findings suggest that the administra- tion of pLP/Palmitate or Palmitate alone did not exert a significant impact on reducing the expression of these markers when compared to the SP [500 µg/Kg] group (Fig. 4E-H).

3.4 pNAPE-LP reduces the MPO activity in mice lungs

To gain a deeper comprehension of the role of innate immunity in SP-induced lung inflammation and to understand the therapeutic potential of pNAPE-LP/Pal- mitate system, we conducted an MPO assay on samples obtained from all experimental groups. As anticipated, the SP [500 µg/Kg] group (2) exhib- ited an elevated MPO activity, indicative of an inflam- matory state in the lungs of mice (p < 0.001 vs. Vehicle). In contrast, treatment with pNAPE-LP/Palmitate reduced MPO activity to physiological levels (p < 0.001 vs. SP [500 µg/Kg]), thereby confirming the probiotic system's ability to restrain over-activation of the innate immune system.

Once again, the internal control groups, pLP/Pal- mitate (4) and Palmitate alone (5), demonstrated no significant changes in MPO activity levels when com- pared to the SP [500 µg/Kg] group (2) (Fig. 4, I).

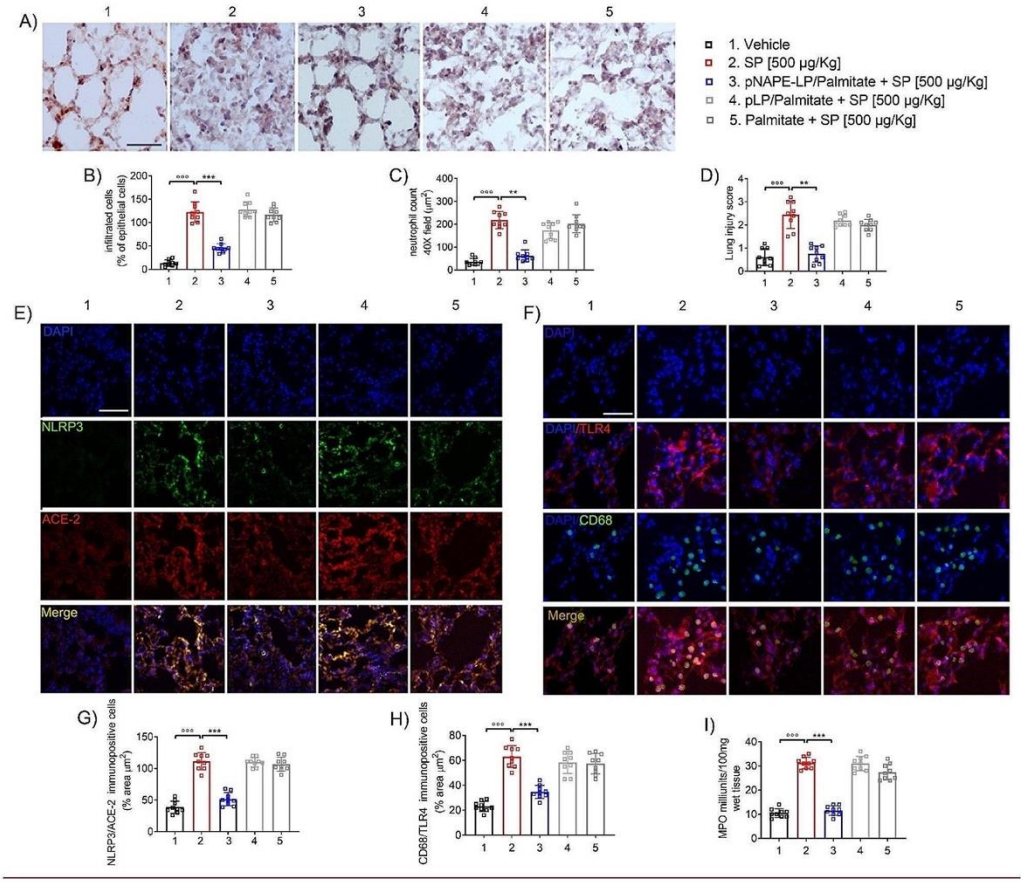

Fig. 4 Prophylactic administration of pNAPE-LP/Palmitate accounts for histological damage attenuation, reduction of pro-inflammatory markers expres- sion and MPO activity in mice lungs. Hematoxylin and eosin (**H** and **E**) stained lung specimens (**A**), relative quantification of infiltrated epithelial cells (**B**), the neutrophil count (**C**) and the global lung damage score (**D**) showing the protective effect of pNAPE-LP/palmitate treatment on SP-induced lung injury. Representative immunofluorescence images showing the co-expression of NLRP3 (green) and ACE-2 (red) and their merge (**E**) on the left and the expression of TLR4 (red) on the surface of CD68+ (green) cells in mice lung specimens with their respective quantifica- tion (**G,H**) display the protective effect of pNAPE-LP/Palmitate treatment on mice lungs following SP-mediated injury. Effect of pNAPE-LP prophilactic treatment in reducing the MPO activity in lung tissue (**I**). Nuclei were also investigated using DAPI staining. Results are expressed as mean ± SEM of n = 5 experiments performed in triplicate. *** $p < 0.001$, ** $p < 0.01$ vs. SP [500 µg/Kg]. Scale bar = 20 µm; magnification 20×

3.5 Western blot analysis confirms pNAPE-LP-mediated modulation of NLRP3, TLR4, and caspase 1 expression in SARS-CoV-2 SP-induced lung injury

To further validate the findings obtained from immunofluorescent analysis and delve into the activation of procaspase 1 upon NLRP3 expression, western blot analysis was conducted on lung homogenates. Corroborating the previous data, our investigation revealed a significant increase in the abundance of TLR4 ($p < 0.001$ vs. Vehicle), NLRP3 ($p < 0.001$ vs. Vehicle), and the cleaved form of caspase1 ($p < 0.001$ vs. Vehicle) in the SP [500 μg/Kg] group (2) when com- pared to the levels observed in the Vehicle group (1). Once again, the prophylactic administration of pNAPE-LP/Palmitate demonstrated its ability to reverse this inflammatory trend. It not only reduced the expression of TLR4 ($p < 0.001$ vs. SP [500 μg/Kg]) and NLRP3 ($p < 0.001$ vs. SP [500 μg/Kg]) but also decreased the levels of the effector protein caspase1 $p < 0.01$ vs. SP [500 μg/Kg]) derived from NLRP3. In contrast, the internal control groups (4,5) did not exhibit any consistent effect in reducing the levels of the aforementioned proteins. The levels observed in these control groups were comparable to those of the SP [500 μg/Kg] group (2) (Fig. 5, A-D).

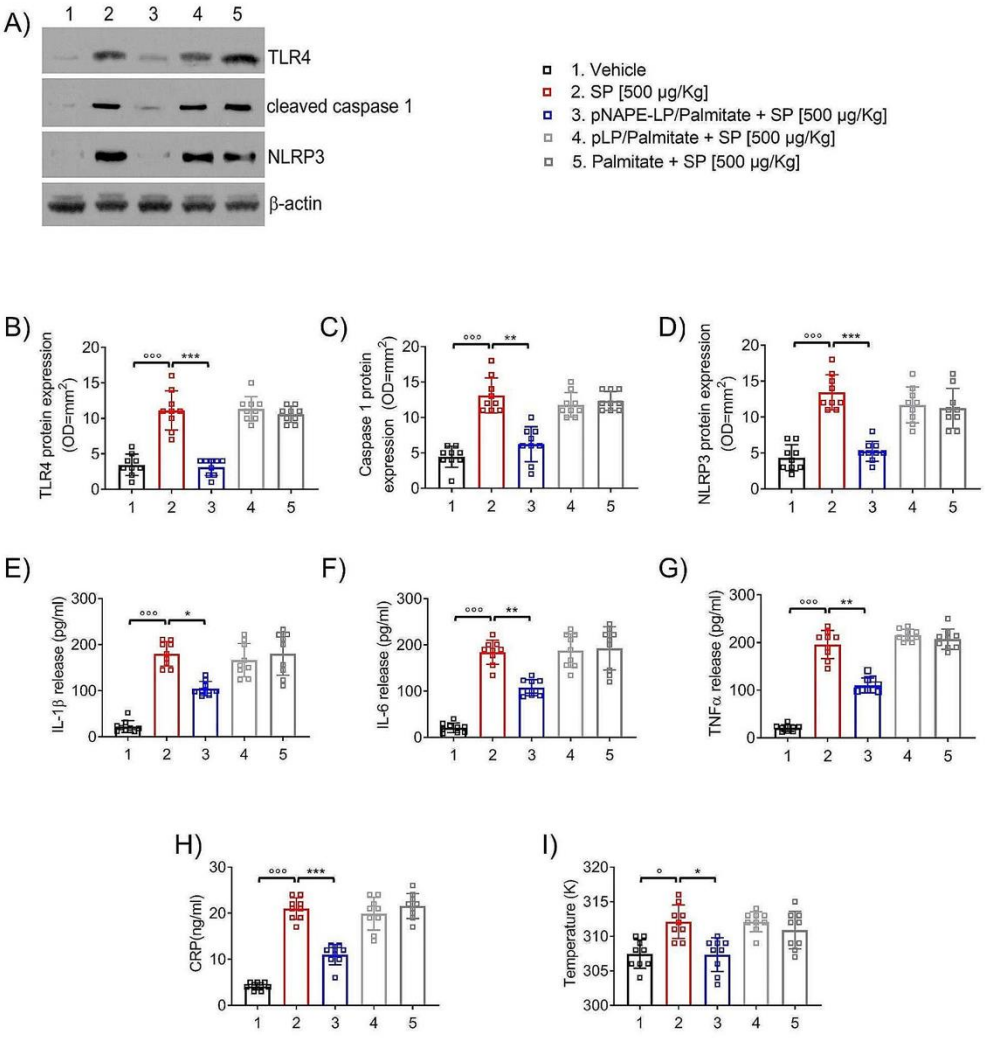

Fig. 5 Prophylactic administration of pNAPE-LP/Palmitate reduces pro-inflammatory markers expression and body temperature in mice. Western blot analysis on lung specimens to detect TLR4 (95 kDa), cleaved Caspase 1 (50 kDa), NLRP3 (120 kDa) and the housekeeping protein β-actin (40 kDa) (**A**), and the relative densitometric quantification (**B, C, D**) showing the protective effect of pNAPE-LP/palmitate treatment on SP-induced lung injury. pNAPE- LP + palmitate treatment reduces ILs (**E, F**), TNF-alpha (**G)** and CRP (**H**), thus reducing the body temperature (**I**) in SP-challenged mice. Results are ex- pressed as mean ± SEM of n = 5 experiments performed in triplicate. *** $p < 0.001$, ** $p < 0.01$, * $p < 0.05$ vs. SP [500 µg/Kg]

3.6 pNAPE-LP/Palmitate treatment reduce the release of IL-1β, IL-6, TNFα and CRP in the lungs of mice

In conjunction with the western blot analysis, we con- ducted ELISA tests to assess the levels of downstream effectors released upon activation of the TLR4-NLRP3 pathway in the lungs of mice, including ILs, TNFα and CRP. Following the same pattern as the previous data, the ELISA test demonstrated a significant increase in the release of IL-1β (p<0.001 vs. Vehicle), IL-6 (p<0.001 vs. Vehicle), TNFα (p<0.001 vs. Vehicle) and CRP (p<0.001 vs. Vehicle) in the SP [500 μg/Kg] group (2) as a result of TLR4/NLRP3 pathway activation. Conversely, the pre-treatment with pNAPE-LP/pal- mitate led to a parallel reduction in the release of IL-1β (p < 0.05 vs. SP [500 μg/Kg]), IL-6 (p < 0.01 vs. SP [500 μg/ Kg]), TNFα (p<0.01 vs. SP [500 μg/Kg]) and CRP (p<0.001 vs. SP [500 μg/Kg]), aligning with the down- regulation observed in the upstream proteins. In con- trast, the pLP/palmitate (4) and Palmitate (5) groups did not exhibit such effects, as they displayed similar levels of IL-1β, IL-6, and TNFα to those observed in the SP [500 μg/Kg] group (2) (Fig. 3, E-H).

3.7 pNAPE-LP mitigates hyperthermia in mice

Because of the pro-inflammatory markers overexpres- sion, the mice from SP [500 μg/Kg] group (2) displayed an increased body temperature during the SP exposition (p < 0.05 vs. Vehicle). Again, the prophylactic pNAPE-LP/ Palmitate treatment was able to mitigate the hyperther- mia to physiological levels (p < 0.05 vs. SP [500 μg/Kg]).

4. Discussion

The present study highlights the remarkable potential of the probiotic system pNAPE-LP in counteracting lung inflammation triggered by SARS-CoV-2 SP. This excep- tional probiotic effectively colonizes mice lungs and releases the anti-inflammatory compound PEA. More- over, pNAPE-LP exhibits a protective effect on alveolar morphology, effectively reducing lung injury induced by SARS-CoV-2 SP. This is achieved by mitigating TLR4- mediated NLRP3 activation and global ACE2 expression in the lungs, while also reining in innate immune system over-activation.

The notion of harnessing probiotics as formidable allies in the battle against COVID-19 has gained momentum due to their remarkable ability to modulate the micro- biota in hollow organs [37, 38]. This modulation, in turn, exerts a positive influence on immune responses [39], resulting in a potential reduction in systemic inflamma- tion [40, 41]—a critical factor in severe COVID-19 cases. Specifically, when probiotics are administered intrana- sally, they have demonstrated the capacity to shape the composition of the respiratory microbiota [42], a pivotal player in determining immune responses [43]. These beneficial microbial agents fortify the respiratory tract's defense mechanisms, fostering a stronger and more bal- anced immune reaction to viral infections [44]. By pro-moting the production of short-chain fatty acids and anti-inflammatory molecules, they have the potential to play a crucial role in quelling the body's inflammatory storm, potentially alleviating the severity of COVID-19 [45, 46]. By integrating the inherent attributes of probiotic strains with the capacity of pNAPE-LP to release PEA on-site, our probiotic system accomplishes the objective of significantly enhancing the anti-inflammatory impact in comparison to the unmodified strain. The majority of PEA's anti-inflammatory characteristics stem from its ability in counteracting the NF-κB signaling pathway via the activation of PPAR receptors, with a strong affinity for PPAR-α [47]. Additionally, PEA has the capability to hinder NF-κB through a dual mechanism: direct interaction with NF-κB p65 or the stimulation of NF-κB inhibitors (IκBs) expression across diverse cell types [48]. In our model, the opposition to the NF-κB signaling pathway was indirectly validated by the observation of diminished levels of upstream (TLR4) and downstream (NLRP3, ILs, etc.) signaling molecules. Through this pathway inhibi- tion, pNAPE-LP effectively governs several genes linked to pro-inflammatory cytokine transcription, culminating in reduced release of IL-6 and TNF-α. Furthermore, in alignment with our prior *in vitro* findings, a significant reduction in NLRP3 expression was demonstrated, consequently lowering inflammasome activation within the cohort subjected to pNAPE-LP and palmitate treatment. This data strongly suggests that pNAPE-LP might hold a pivotal role in the regulation of the inflammatory processes implicated in the initiation of ARDS. By curtailing NLRP3-dependent pathways, this probiotic systematically targets and downregulates downstream products, including IL-1β, a significant mediator in ARDS pathogenesis [49] and a potential pharmacological target in the early phases of COVID- 19 [50]. The inhibition of the NLRP3/caspase-1 pathway within lung tissue also stands to be crucial in preventing the initiation of pyroptosis ‘ [51]. Such prevention could be deemed strategic since, in numerous

pathological conditions and models, extensive pyroptosis triggered by NLRP3/caspase-1 activation has been linked to heightened neutrophil recruitment [52, 53] (See Fig. 6). This scenario was notably observed in our experimental model's group treated with SP, as evidenced by increased neutrophil count and heightened MPO activity. In contrast to resident tissue macrophages, neutrophils exhibit greater immunoreactivity [54], and their activation often results in intensified inflammation. Notably, an excessive recruitment of neutrophils has been reported in severe stages of COVID-19 [55, 56]. The mitigation of pyroptosis facilitated by pNAPE-LP pre-treatment was indirectly confirmed by the reduction in neutrophil count and MPO activity within lung samples. Furthermore, specific probiotic strains, notably from the Lactobacillus family, have exhibited direct antiviral effects [57–59], displaying the capacity to impede viral replication. While the precise mechanisms demand further elucidation, probiotics from the Lactobacillus genus seem adept at lowering viral infection rates by establishing an antiviral state within macrophages [60, 61]. Within our probiotic system, this inherent antiviral activity of Lactobacillus strains harmonizes with PEA's ability to hinder SARS-CoV-2 infection by directly engaging with SP and ACE2 receptors [62], as well as its inhibitory influence on PPAR-α, which curbs viral replication [63]. Recent in vitro studies have indeed indicated that PEA's binding to the SARS-CoV-2 S protein results in approximately 70% reduction in viral infection among Huh-7 cells [62]. Furthermore, a previous research contribution from our team underscored SP's in vitro capability to elevate ACE2 receptor expression by instigating TLR4-mediated inflammatory responses [18]. Once again, this pattern was substantiated in our current *in vivo* study, evident in the ACE2/NLRP3 co-expression within lung tissues. Scientific understanding dictates that proinflammatory elements, such as LPS (lipopolysaccharides) and/or pathological inflammatory states, are linked to elevated ACE-2 expression on tissue macrophages [19, 64]. Numerous investigations have indicated that elevated ACE expression in macrophages accentuates the immune response of these cells, potentially leading to a shift towards the M2 phenotype, indicating a regulatory role in the inflammatory process. It is plausible that SARS-CoV-2's SP potentially fosters viral infection by enhancing ACE2 receptor expression in neighboring cells via the induction of inflammatory conditions in alveolar macrophages [18, 65]. However, the precise mechanism governing this ACE-2 upregulation by SP remains elusive and necessitates further exploration through additional studies. Conversely, our probiotic system effectively reversed the over-expression of ACE2 receptors, likely attributable to its anti-inflammatory impact. This intriguing effect holds

the potential to mitigate the propagation of infection within lung tissue. The findings presented in this study open up several avenues for future research and have significant implications for healthcare practices, particularly in the context of addressing lung inflammation triggered by SARS-CoV-2. Future research could focus on translating these findings into clinical trials to evaluate the safety and efficacy of pNAPE-LP in human subjects with SARS-CoV-2 infections. If proven effective, this probiotic system could be developed as a novel therapeutic strategy for managing COVID-19 and other respiratory infections. On the other hand, considering the complex nature of COVID-19 and its associated inflammatory responses, future investigation may also explore combination therapies. Combining pNAPE-LP with other anti-inflammatory agents or medications commonly used in COVID-19 treatment might enhance therapeutic outcomes. This approach could be explored in preclinical models and, subsequently, in clinical trials.

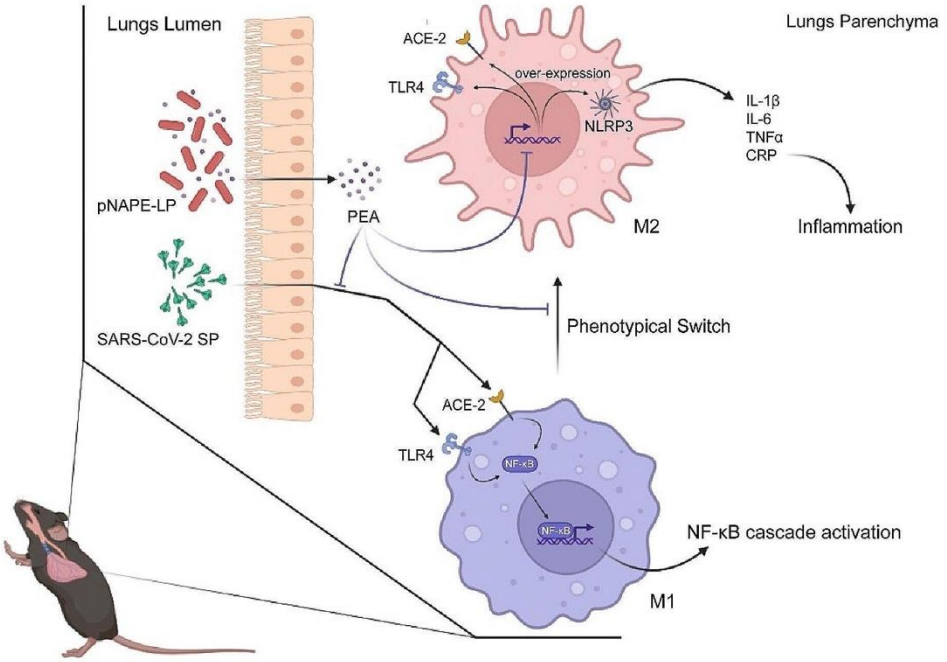

Fig. 6 Graphical representation of the main findings of the present paper

5. Conclusion

In essence, the notion of harnessing probiotics as allies in the battle against COVID-19 is rapidly gaining traction. A number of studies have focused on the preclinical efficacy of recombinant probiotics as potential platform for oral and intranasal vaccines. The probiotic system, known as pNAPE-LP, has exhibited promising potential in addressing the lung inflammation triggered by SARS-CoV-2 SP, leading to a reduction in the excessive expression of the ACE2 receptor and a dampening of the inflammatory reaction. This holds the promise of yielding significant advantages in averting severe symptoms and secondary infections among COVID-19 patients, particularly within diverse demo- graphics such as children and the elderly. Emphasizing the significance of localized PEA release is paramount. Notably, pNAPE-LP not only enhances the accessibility of PEA but also has the unique capability to selectively augment its presence precisely where it is required. This characteristic positions it as a novel and auspicious tool within the realm of precision medicine. Furthermore, the combination of immune-modulatory attributes inherent in a probiotic with the potent anti-inflammatory effects of PEA bestows upon pNAPE-LP a distinct superiority when compared to these two individual components in isolation. In conclusion, the innovative synergy between pro- biotics and the pNAPE-LP system holds potential in reshaping our approach to combating COVID-19 and its associated inflammatory challenges.

Data availability

All data generated or analysed during this study are included in this published article [and its supplementary information files].

Declarations

Ethics approval and consent to participate

The animal study protocol was approved by the Ethics Committee of Sapienza University of Rome (Organizzazione per il benessere animale, OPBA), approval code 890/2021-PR, approved on 17 November 2021. All animal experiments complied with the ARRIVE guidelines and were carried out in accordance with the U.K. Animals (Scientific

Procedures) Act, 1986, and associated guidelines, E.U. Directive 2010/63/EU for animal experiments.

Consent for publication

Not applicable.

Competing interests

The authors declare that they have no competing interests. Giuseppe Esposito, Giovanni Esposito, Walter Sanseverino, and Giovanni Sarnelli are all affiliated with Nextbiomics s.r.l., Naples, Italy. Nextbiomics s.r.l is an academic off-shoot of the University “Federico II” of Naples and should not, therefore, be perceived as a commercial conflict of interest.

6. References

1. Marani M, Katul GG, Pan WK, Parolari AJ. Intensity and frequency of extreme novel epidemics. *Proc. Natl. Acad. Sci* 118, e2105482118 (2021).
2. WHO Coronavirus (COVID. -19) Dashboard. https://covid19.who.int.
3. Lamers MM, Haagmans BL. SARS-CoV-2 pathogenesis. Nat Rev Microbiol. 2022;20:270–84.
4. Nesteruk I. Endemic characteristics of SARS-CoV-2 infection. Sci Rep. 2023;13:14841.
5. Baker RE, et al. Infectious disease in an era of global change. Nat Rev Microbiol. 2022;20:193–205.
6. Agrawal U, et al. Severe COVID-19 outcomes after full vaccination of primary schedule and initial boosters: pooled analysis of national prospective cohort studies of 30 million individuals in England, Northern Ireland, Scotland, and Wales. Lancet. 2022;400:1305–20.
7. Lee J-W, et al. The role of macrophages in the development of Acute and Chronic Inflammatory Lung diseases. Cells. 2021;10:897.
8. Budnevsky AV, et al. Role of mast cells in the pathogenesis of severe lung damage in COVID-19 patients. Respir Res. 2022;23:371.
9. McVey MJ, Steinberg BE, Goldenberg NM. Inflammasome activation in acute lung injury. Am J Physiol -Lung Cell Mol Physiol. 2021;320:L165–78.

10. Jo E-K, Kim JK, Shin D-M, Sasakawa C. Molecular mechanisms regulating NLRP3 inflammasome activation. Cell Mol Immunol. 2016;13:148–59.
11. van den Berg DF, te Velde AA. Severe COVID-19: NLRP3 Inflammasome Dysregulated. Front Immunol. 2020;11:1580.
12. Zhao C, Zhao W. NLRP3 Inflammasome—A key player in antiviral responses. Front Immunol. 2020;11:211.
13. Choudhury A, Mukherjee S. In silico studies on the comparative characterization of the interactions of SARS-CoV-2 spike glycoprotein with ACE-2 recep- tor homologs and human TLRs. J Med Virol. 2020;92:2105–13.
14. Brandão SCS, et al. Is toll-like receptor 4 involved in the severity of COVID-19 pathology in patients with cardiometabolic comorbidities? Cytokine Growth Factor Rev. 2021;58:102–10.
15. Zhao Y, et al. SARS-CoV-2 spike protein interacts with and activates TLR41. Cell Res. 2021;31:818–20.
16. SARS-CoV-2. drives NLRP3 inflammasome activation in human microglia through spike protein | Molecular Psychiatry. https://www.nature.com/ articles/s41380-022-01831-0.
17. Yin M, Marrone L, Peace CG, O'Neill LA. J. NLRP3, the inflammasome and COVID-19 infection. QJM Int J Med. 2023;116:502–7.
18. Del Re A, et al. Ultramicronized Palmitoylethanolamide inhibits NLRP3 inflammasome expression and pro-inflammatory response activated by SARS- CoV-2 spike protein in cultured murine alveolar macrophages. Metabolites. 2021;11:592.
19. Veiras LC, et al. Over expression of ACE in myeloid cells increases immune effectiveness and leads to a new way of considering inflammation in acute and chronic diseases. Curr Hypertens Rep. 2020;22:4.
20. Khan Z, et al. Angiotensin-converting enzyme enhances the oxidative response and bactericidal activity of neutrophils. Blood. 2017;130:328–39.
21. Roncati L, Lusenti B, Pellati F, Corsi L. Micronized / ultramicronized palmitoyle- thanolamide (PEA) as natural neuroprotector against COVID-19 inflammation. Prostaglandins Other Lipid Mediat. 2021;154:106540.
22. Raciti L, De Luca R, Raciti G, Arcadi FA, Calabrò RS. The Use of Palmitoyletha- nolamide in the treatment of long COVID: a real-life Retrospective Cohort Study. Med Sci. 2022;10:37.

23. Pesce M, et al. Phytotherapics in COVID19: why palmitoylethanolamide? Phytother Res. 2021;35:2514–22.
24. Fessler SN, Liu L, Chang Y, Yip T, Johnston CS. Palmitoylethanolamide reduces proinflammatory markers in unvaccinated adults recently diagnosed with COVID-19: a Randomized Controlled Trial. J Nutr. 2022;152:2218–26.
25. Albanese M et al. Effects of Ultramicronized Palmitoylethanolamide (um-PEA) in COVID-19 Early Stages: A Case-Control Study. (2022).
26. Camerlingo C. Randomized clinical trial olfactory dysfunction after COVID-19: olfactory rehabilitation therapy vs. intervention treatment with Palmitoyle- thanolamide and Luteolin: preliminary results. Eur Rev https://www.europeanreview.org/article/26059 (2021).
27. Keppel Hesselink JM, de Boer T, Witkamp RF, Palmitoylethanolamide. A Natural Body-Own Anti-Inflammatory Agent, Effective and Safe against Influenza and Common Cold. *Int. J. Inflamm* 2013, 151028 (2013).
28. Epitech Group SpA. *Efficacy of Palmitoylethanolamide, in add-on to Standard Therapy, on Inflammatory Markers of Patients With Interstitial Pneumonia Due to COVID-19. A Pilot Controlled, Randomized, Open Lable Clinical Study*. https:// clinicaltrials.gov/study/NCT04568876 (2021).
29. Pharma FSD, Randomized IA., *Double-Blind, Placebo-Controlled, Multicenter Phase IIA Study of FSD201 (Ultramicronized PEA) + Standard of Care (SOC) Vs SOC in the Treatment of Hospitalized Patients With COVID-19*. https://clinicaltrials. gov/study/NCT04619706 (2022).
30. Rankin L, Fowler CJ. The basal pharmacology of Palmitoylethanolamide. Int J Mol Sci. 2020;21:E7942.
31. Esposito G, et al. Engineered Lactobacillus paracasei producing Palmitoylethanolamide (PEA) prevents colitis in mice. Int J Mol Sci. 2021;22:2945.
32. Esposito G, et al. A palmitoylethanolamide producing Lactobacillus paracasei improves Clostridium difficile Toxin A-Induced Colitis. Front Pharmacol. 2021;12:639728.
33. Gopal G, Muralidar S, Kamalakkannan A, Ambi SV. Microbiome in Acute Respiratory Distress Syndrome (ARDS). in *Microbiome in Inflam- matory Lung Diseases* (eds. Gupta, G., Oliver, B. G., Dua, K., Singh, A. & MacLoughlin, R.) 117–134Springer Nature, (2022). https://doi.org/10.1007/978-981-16-8957-4_8.

34. Kyo M, et al. Unique patterns of lower respiratory tract microbiota are associated with inflammation and hospital mortality in acute respiratory distress syndrome. Respir Res. 2019;20:246.
35. Ling LH, et al. Comparison of various tissue-Preparation techniques for Cryosectioning of Frozen Mouse tissues. J Histotechnol. 2009;32:186–9.
36. Paidi RK, et al. ACE-2-interacting domain of SARS-CoV-2 (AIDS) peptide suppresses inflammation to reduce fever and protect lungs and heart in mice: implications for COVID-19 therapy. J Neuroimmune Pharmacol. 2021;16:59–70.
37. Brahma S, Naik A, Lordan R, Probiotics. A gut response to the COVID-19 pandemic but what does the evidence show? Clin Nutr Espen. 2022;51:17–27.

38. Tian Y et al. Probiotics improve symptoms of patients with COVID-19 through gut-lung axis: a systematic review and meta-analysis. Front Nutr 10, (2023).

39. Mazziotta C, Tognon M, Martini F, Torreggiani E, Rotondo JC. Probiotics mechanism of action on Immune cells and Beneficial effects on Human Health. Cells. 2023;12:184.

40. Monteros MJM, et al. Probiotic lactobacilli as a promising strategy to ameliorate disorders associated with intestinal inflammation induced by a non-steroidal anti-inflammatory drug. Sci Rep. 2021;11:571.

41. Klaenhammer TR, Kleerebezem M, Kopp MV, Rescigno M. The impact of probiotics and prebiotics on the immune system. Nat Rev Immunol. 2012;12:728–34.

42. Wu Y, et al. Effect of probiotics on nasal and intestinal microbiota in people with high exposure to particulate matter ≤ 2.5 μm (PM2.5): a randomized, double-blind, placebo-controlled clinical study. Trials. 2020;21:850.

43. Yuksel N, Gelmez B, Yildiz-Pekoz A. Lung microbiota: its relationship to Respiratory System diseases and approaches for Lung-targeted probiotic Bacteria delivery. Mol Pharm. 2023;20:3320–37.

44. Li Z, et al. Targeting the Pulmonary Microbiota to Fight against Respiratory diseases. Cells. 2022;11:916.

45. Machado MG, Sencio V, Trottein F. Short-chain fatty acids as a potential treatment for infections: a closer look at the lungs. Infect Immun 89, (2021).

46. Włodarczyk J, Czerwiński B, Fichna J. Short-chain fatty acids–microbiota crosstalk in the coronavirus disease (COVID-19). Pharmacol Rep. 2022;74:1198–207.

47. Lo Verme J, et al. The nuclear receptor peroxisome proliferator-activated receptor-alpha mediates the anti-inflammatory actions of palmitoylethanol- amide. Mol Pharmacol. 2005;67:15–9.

48. Korbecki J, Bobiński R, Dutka M. Self-regulation of the inflammatory response by peroxisome proliferator-activated receptors. Inflamm Res. 2019;68:443–58.

49. Kolb M, Margetts PJ, Anthony DC, Pitossi F, Gauldie J. Transient expression of IL-1β induces acute lung injury and chronic repair leading to pulmonary fibrosis. J Clin Invest. 2001;107:1529–36.

50. van de Veerdonk FL, Netea MG. Blocking IL-1 to prevent respiratory failure in COVID-19. Crit Care. 2020;24:445.

51. Yu P, et al. Pyroptosis: mechanisms and diseases. Signal Transduct Target Ther. 2021;6:1–21.

52. Chen L, et al. Neutrophil extracellular traps promote macrophage pyroptosis in sepsis. Cell Death Dis. 2018;9:1–12.

53. Liu L, Sun B. Neutrophil pyroptosis: new perspectives on sepsis. Cell Mol Life Sci. 2019;76:2031–42.

54. Yang S-C, Tsai Y-F, Pan Y-L, Hwang T-L. Understanding the role of neutrophils in acute respiratory distress syndrome. Biomed J. 2021;44:439–46.

55. Kuri-Cervantes L, et al. Comprehensive mapping of immune perturbations associated with severe COVID-19. Sci Immunol. 2020;5:eabd7114.

56. Ruan Q, Yang K, Wang W, Jiang L, Song J. Clinical predictors of mortality due to COVID-19 based on an analysis of data of 150 patients from Wuhan, China. Intensive Care Med. 2020;46:846–8.

57. Wang Y, Moon A, Huang J, Sun Y, Qiu H-J. Antiviral effects and underlying mechanisms of Probiotics as Promising antivirals. Front Cell Infect Microbiol. 2022;12:928050.

58. Salaris C et al. Lacticaseibacillus Paracasei DG enhances the lactoferrin anti-SARS-CoV-2 response in Caco-2 cells. Gut Microbes 13, 1961970.

59. Montazeri-Najafabady N, Kazemi K, Gholami A. Recent advances in antiviral effects of probiotics: potential mechanism study in prevention and treatment of SARS-CoV-2. Biol (Bratisl). 2022;77:3211–28.

60. Sundararaman A, Ray M, Ravindra PV, Halami PM. Role of probiotics to com- bat viral infections with emphasis on COVID-19. Appl Microbiol Biotechnol. 2020;104:8089–104.

61. Ivec M, et al. Interactions of macrophages with probiotic bacteria lead to increased antiviral response against vesicular stomatitis virus. Antiviral Res. 2007;75:266–74.

62. Fonnesu R, et al. Palmitoylethanolamide (PEA) inhibits SARS-CoV-2 entry by interacting with S protein and ACE-2 receptor. Viruses. 2022;14:1080.

63. Fantacuzzi M, Amoroso R, Ammazzalorso APPAR. Ligands induce antiviral effects targeting perturbed lipid metabolism during SARS-CoV-2, HCV, and HCMV infection. Biology. 2022;11:114.

64. Song X, et al. Little to no expression of angiotensin-converting enzyme-2 on most human peripheral blood immune cells but highly expressed on tissue macrophages. Cytom Part J Int Soc Anal Cytol. 2023;103:136–45.

65. Aboudounya MM, Heads RJ. COVID-19 and Toll-Like Receptor 4 (TLR4): SARS-CoV-2 May Bind and Activate TLR4 to Increase ACE2 Expression, Facilitating Entry and Causing Hyperinflammation. *Mediators Inflamm* 2021, 8874339 (2021).

GENERAL CONCLUSIONS

In conclusion, this doctoral thesis has undertaken a comprehensive examination of the therapeutic potential of ALIAmide-based formulations, particularly highlighting their effects in inflammation-driven diseases such as colitis, colorectal cancer, and SARS-CoV-2-induced lung inflammation. This research stands out for its innovative approach to addressing complex inflammatory pathways and offers significant insights that could reshape therapeutic strategies in the field. Through an extensive investigation of m-PGA administered orally in a DNBS-induced murine model of colitis, this study illuminated the anti-inflammatory effects of m-PGA during both the acute and resolution phases of inflammation (Palenca I. et al., 2022; Palenca I. et al., 2024). Such dual-phase intervention is crucial, as it suggests that m-PGA plays a significant role in not only controlling inflammation but also in facilitating recovery, thus addressing both immediate and long-term inflammatory responses. This aspect of the research underlines the innovative nature of the study, as it expands the current understanding of therapeutic interventions that target inflammation beyond mere symptom relief, proposing a more holistic approach to managing chronic conditions. Additionally, the investigation into the rectally administered gel containing adelmidrol and hyaluronic acid proved effective in reducing inflammation and providing mucosal protection in murine colitis models and ex-vivo biopsy cultures (Palenca I. et al., 2023). This finding underscores the potential of targeted therapies for gastrointestinal mucosal preservation, presenting an innovative delivery method that could enhance patient outcomes in inflammatory bowel diseases. The ability of this gel to effectively mitigate inflammation highlights its promise as a complementary option in conjunction with other treatments like m-PGA, potentially maximizing therapeutic efficacy. Furthermore, findings from an AOM + DSS model of colorectal cancer underscored m-PGA's dual anti-inflammatory and antiproliferative properties. This dual action emphasizes its potential to influence tumor growth by modulating inflammatory pathways essential to tumorigenesis. Importantly, this thesis posits that targeting inflammation should not be limited to its acute stages but must encompass the entire continuum of the inflammatory process, particularly in chronic

conditions like colitis, where sustained inflammation significantly elevates the risk of developing colorectal cancer. This perspective on inflammation management highlights the study's innovative approach to cancer prevention and treatment, positioning it as a significant advancement in the field. In addition to gastrointestinal inflammation, this research also explored the application of pNAPE-LP in mitigating lung inflammation induced by the SP (Del Re A. et al., 2024). Notably, this engineered bacterium had previously been used in our studies on murine models of gastrointestinal inflammation, where it demonstrated significant anti-inflammatory efficacy, contributing to the maintenance of intestinal mucosal integrity and reducing mucosal permeability (Esposito G. et al., 2021; Esposito G. et al., 2021). This investigation aimed to evaluate the efficacy of pNAPE-LP as a localized anti-inflammatory treatment, a novel strategy that could offer a targeted solution in the face of a global pandemic (Brahim Z., 2021). By administering pNAPE-LP/palmitate intranasally in a murine model, the study successfully demonstrated the capacity of pNAPE-LP to effectively colonize pulmonary tissues and deliver the anti-inflammatory compound PEA directly to the site of inflammation. The findings revealed not only a reduction in cellular infiltration but also the preservation of alveolar integrity and the modulation of key pro-inflammatory mediators, including cytokines and myeloperoxidase, in response to the SP challenge. These results are particularly promising, as they suggest a potential therapeutic avenue for controlling lung inflammation associated with viral infections. Altogether, this thesis contributes significantly to the growing body of evidence supporting ALIAmide-based therapies as viable, potentially complementary options to traditional treatments. By offering a trifecta of anti-inflammatory, mucosal-protective, and potentially antiproliferative benefits with a lower side-effect profile, these formulations demonstrate considerable promise in advancing therapeutic strategies for both gastrointestinal and respiratory inflammation. Looking ahead, future research should aim to refine these interventions further and optimize their clinical applications. This includes conducting extensive clinical trials to establish the safety, efficacy, and optimal dosing regimens for ALIAmide-based therapies across various patient populations. Additionally, numerous studies support the use of ALIAmides as adjuncts in pharmacological therapies for inflammatory diseases and pain management (Cocito D. et al., 2024; Nobili S. et al., 2024; Noce A. et al., 2021; Peritore A.F. et al., 2021; Bartolucci M.L. et al., 2018). Researchers should further explore the potential for combination therapies that integrate ALIAmide formulations with existing anti-inflammatory and immunomodulatory agents, which could enhance therapeutic

outcomes and provide more comprehensive treatment strategies. This approach may offer synergistic benefits, improving efficacy while potentially reducing the dosage and side effects associated with conventional treatments. A deeper understanding of the molecular mechanisms underlying ALIAmide-based therapies will be crucial to identifying specific patient subgroups that may benefit the most from these treatments. For instance, biomarker studies could elucidate which inflammatory pathways are most effectively modulated by these formulations, facilitating personalized medicine approaches. Furthermore, considering that the widely studied ALIAmide PEA has been shown to improve intestinal homeostasis and positively influence gut microbiota (Pirozzi C. et al., 2023; Brankovic M. et al., 2024; Esposito G. et al., 2014). it is worth evaluating whether these new synthetic and semi-synthetic compounds might have similar beneficial effects. Future research should investigate the long-term effects of these therapies, particularly concerning their impact on gut microbiota and overall immune function, to ensure sustained benefits and minimize any adverse effects. Understanding these dynamics could also reveal additional therapeutic benefits, enhancing the application of ALIAmides in chronic inflammatory disease management. Moreover, expanding the scope of investigation to include additional inflammatory and autoimmune diseases could reveal broader applications for ALIAmide-based therapies, potentially transforming the landscape of treatment options available for managing complex conditions. As the field evolves, the integration of advanced drug delivery systems, such as nanocarriers or smart polymers, may also enhance the specificity and efficacy of these formulations, paving the way for innovative therapeutic modalities (Howard M.D. et al., 2014). In conclusion, the promising findings of this thesis underscore the need for continued exploration and innovation in ALIAmide-based therapies. By building on this foundational research, we can advance therapeutic strategies to better manage inflammation-driven diseases like colitis, colorectal cancer, and SARS-CoV-2-induced lung inflammation, ultimately improving patient care and outcomes.

OTHER PUBLICATIONS DURING MY THREE-YEARS Ph.D PROGRAM (2021-2024)

Del Re A., Corpetti C., Pesce M., Seguella L., Steardo L., Palenca I., Rurgo S., De Conno B., Sarnelli G., and Esposito G. Ultramicronized palmitoylethanolamide inhibits NLRP3 inflammasome expression and pro-inflammatory response activated by SARS-CoV-2 Spike protein in cultured murine alveolar macrophages. (Metabolites, published article, September 2021).

Corpetti C., Del Re A., Seguella L., Palenca I., Rurgo S., De Conno B., Pesce M., Sarnelli G., and Esposito G. Cannabidiol inhibits SARS-Cov-2 Spike (S) protein-induced cytotoxicity and inflammation through a PPAR□-dependent TLR4/NLRP3/Caspase-1 signaling suppression in Caco-2 cell line. (Phytotherapy Research, published article, October 2021).

De Conno, B., Pesce, M., Chiurazzi, M., Andreozzi, M., Rurgo, S., Corpetti, C., Seguella, L., Del Re, A., Palenca, I., Esposito, G., & Sarnelli, G. (2022). Nutraceuticals and Diet Supplements in Crohn's Disease: A General Overview of the Most Promising Approaches in the Clinic. review, (Basel, Switzerland)

Pesce M, Seguella L, Del Re A, Lu J, Palenca I, Corpetti C, Rurgo S, Sanseverino W, Sarnelli G, Esposito G. Next-Generation Probiotics for Inflammatory Bowel Disease. 2022; 23(10):5466. https://doi.org/10.3390/ijms23105466

Del Re A, Palenca I, Seguella L, Pesce M, Corpetti C, Steardo L, Rurgo S, Sarnelli G, Esposito G. Oral Adelmidrol Administration Up-Regulates Palmitoylethanolamide Production in Mice Colon and Duodenum through a PPAR-γ Independent Action. 12(5):457. https://doi.org/10.3390/metabo12050457

Sarnelli G, Del Re A, Pesce M, Lu J, Esposito G, Sanseverino W, Corpetti C, Basili Franzin S, Seguella L, Rurgo S, De Palma F, Zilli A, Esposito G. Oral immunization

with escherichia coli Nissel 1917 expressing SARS-CoV-2 Spike Protein induces mucosal and ssystemic antibody responses in mice. 2023 Feb (Biomolecules).

Seguella, L., Palenca, I., Franzin, S. B., Zilli, A., & Esposito, G. (2023). Mini-review: Interaction between intestinal microbes and enteric glia in health and disease. Neuroscience letters, 806, 137221. https://doi.org/10.1016/j.neulet.2023.137221

Sharma, V., Madia, V. N., Tudino, V., Nguyen, J. V., Debnath, A., Messore, A., Ialongo, D., Patacchini, E., Palenca, I., Basili Franzin, S., Seguella, L., Esposito, G., Petrucci, R., Di Matteo, P., Bortolami, M., Saccoliti, F., Di Santo, R., Scipione, L., Costi, R., & Podust, L. M. (2023). Miconazole-like Scaffold is a Promising Lead for -Specific CYP51 Inhibitors. Journal of medicinal chemistry, 66 (24), 17059–17073. https://doi.org/10.1021/acs.jmedchem.3c01898

Sarnelli G, Del Re A, Palenca I, Franzin SB, Lu J, Seguella L, Zilli A, Pesce M, Rurgo S, Esposito G, Sanseverino W, Esposito G. Intranasal administration of Escherichia coli Nissle expressing the spike protein of SARS-CoV-2 induces long-term immunization and prevents spike protein-mediated lung injury in mice. Biomed Pharmacother. 2024 May;174:116441. doi: 10.1016/j.biopha.2024.116441. Epub 2024 Mar 21. PMID: 38518597.

Aurino, A., et al. Clinical and nutritional correlates associated with weight changes in achalasia patients and the impact of laparoscopic Heller myotomy. (Digestive and Liver Disease, article accepted on August 01, 2024)

Seguella L., et al. Oleoylethanolamide-producing Lactobacillus paracasei F19 improves metabolic and behavioral disorders by restoring intestinal permeability and microbiota-gut-brain axis in high-fat diet-induced obese male mice. Brain, Behaviour, and Immunity Journal (Under revision) .

REFERENCES

Agrawal M, Jess T. Implications of the changing epidemiology of inflammatory bowel disease in a changing world. United European Gastroenterol J. 2022 Dec;10(10):1113-1120. doi: 10.1002/ueg2.12317. Epub 2022 Oct 17. PMID: 36251359; PMCID: PMC9752308.

Baidoun F, Elshiwy K, Elkeraie Y, Merjaneh Z, Khoudari G, Sarmini MT, Gad M, Al-Husseini M, Saad A. Colorectal Cancer Epidemiology: Recent Trends and Impact on Outcomes. Curr Drug Targets. 2021;22(9):998-1009. doi: 10.2174/1389450121999201117115717. PMID: 33208072.

Bartolucci ML, Marini I, Bortolotti F, Impellizzeri D, Di Paola R, Bruschetta G, Crupi R, Portelli M, Militi A, Oteri G, Esposito E, Cuzzocrea S. Micronized palmitoylethanolamide reduces joint pain and glial cell activation. Inflamm Res. 2018 Oct;67(10):891-901. doi: 10.1007/s00011-018-1179-y. Epub 2018 Aug 18. PMID: 30121836.

Beggiato S., Tomasini M.C., Ferraro L. Palmitoylethanolamide (PEA) as a Potential Therapeutic Agent in Alzheimer's Disease. Front. Pharmacol. 2019;24:821. doi: 10.3389/fphar.2019.00821.

Bilia A.R., Piazzini V., Guccione C., Risaliti L., Asprea M., Capecchi G., Bergonzi M.C. Improving on nature: The role of nanomedicine in the development of clinical natural drugs. Planta Med. 2017;83:366–381. doi: 10.1055/s-0043-102949.

Brahim Z, EL RK (2021) Strategy Management of COVID-19 Pandemic: An Integrative Review. J Healthcare 4(1):91-104.

Branković M, Gmizić T, Dukić M, Zdravković M, Daskalović B, Mrda D, Nikolić N, Brajković M, Gojgić M, Lalatović J, Kralj Đ, Pantić I, Vojnović M, Milovanović T, Đurašević S, Todorović Z. Therapeutic Potential of Palmitoylethanolamide in Gastrointestinal Disorders. Antioxidants (Basel). 2024 May 14;13(5):600. doi: 10.3390/antiox13050600. PMID: 38790705; PMCID: PMC11117950.

Clayton P, Hill M, Bogoda N, Subah S, Venkatesh R. Palmitoylethanolamide: A Natural Compound for Health Management. Int J Mol Sci. 2021 May 18;22(10):5305. doi: 10.3390/ijms22105305. PMID: 34069940; PMCID: PMC8157570.

Cocito D, Peci E, Torrieri MC, Clerico M. Ultramicronized Palmitoylethanolamide in the Management of Neuropathic Pain Related to Chronic Inflammatory Demyelinating Polyneuropathy: A Proof-of-Concept Study. J Clin Med. 2024 May 9;13(10):2787. doi: 10.3390/jcm13102787. PMID: 38792328; PMCID: PMC11122609.

Cordaro M, Siracusa R, Impellizzeri D, D' Amico R, Peritore AF, Crupi R, Gugliandolo E, Fusco R, Di Paola R, Schievano C, Cuzzocrea S. Safety and efficacy of a new micronized formulation of the ALIAmide palmitoylglucosamine in preclinical models of inflammation and osteoarthritis pain. Arthritis Res Ther. 2019 Nov 28;21(1):254. doi: 10.1186/s13075-019-2048-y. PMID: 31779692; PMCID: PMC6883534.

Crittenden, R., Saarela, M., Mätto, J., Ouwehand, A. C., Salminen, S., Pelto, L., Vaughan, E. E., de Vos, W. M., von Wright, A., Fondén, R., & Mattila-Sandholm, T. (2002). Lactobacillus paracacei subsp. paracasei F19 : Survival, Ecology and Safety in the Human Intestinal Tract-A Survey of Feeding Studies within the PROBDEMO Project. Microbial Ecology in Health and Disease, 53, 22-26. https://edepot.wur.nl/184898

D'Amico R, Impellizzeri D, Cuzzocrea S, Di Paola R. ALIAmides Update: Palmitoylethanolamide and Its Formulations on Management of Peripheral Neuropathic Pain. Int J Mol Sci. 2020 Jul 27;21(15):5330. doi: 10.3390/ijms21155330. PMID: 32727084; PMCID: PMC7432736.

Del Re A, Corpetti C, Pesce M, Seguella L, Steardo L, Palenca I, Rurgo S, De Conno B, Sarnelli G, Esposito G. Ultramicronized Palmitoylethanolamide Inhibits NLRP3 Inflammasome Expression and Pro-Inflammatory Response Activated by SARS-CoV-2 Spike Protein in Cultured Murine Alveolar Macrophages. Metabolites. 2021 Sep 2;11(9):592. doi: 10.3390/metabo11090592. PMID: 34564408; PMCID: PMC8472716.

Del Re A, Palenca I, Seguella L, Pesce M, Corpetti C, Steardo L, Rurgo S, Sarnelli G, Esposito G. Oral Adelmidrol Administration Up-Regulates Palmitoylethanolamide

Production in Mice Colon and Duodenum through a PPAR-γ Independent Action. Metabolites. 2022 May 19;12(5):457. doi: 10.3390/metabo12050457. PMID: 35629962; PMCID: PMC9144287.

Del Re, A., Franzin, S.B., Lu, J. et al. Intranasal delivery of PEA-producing Lactobacillus paracasei F19 alleviates SARS-CoV-2 spike protein-induced lung injury in mice. transl med commun 9, 9 (2024). https://doi.org/10.1186/s41231-024-00167-x

Della Rocca G, Re G. Palmitoylethanolamide and Related ALIAmides for Small Animal Health: State of the Art. Biomolecules. 2022 Aug 26;12(9):1186. doi: 10.3390/biom12091186. PMID: 36139024; PMCID: PMC9496254.

Della Rocca G, Schievano C, Di Salvo A, Conti MB, Della Valle MF. Palmitoyl-glucosamine co-micronized with curcumin for maintenance of meloxicam-induced pain relief in dogs with osteoarthritis pain. BMC Vet Res. 2023 Feb 7;19(1):37. doi: 10.1186/s12917-023-03594-4. PMID: 36747264; PMCID: PMC9903516.

Di Marzo V., Melck D., Orlando P., Bisogno T., Zagoory O., Bifulco M., Vogel Z., De Petrocellis L. Palmitoylethanolamide Inhibits the Expression of Fatty Acid Amide Hydrolase and Enhances the Anti-Proliferative Effect of Anandamide in Human Breast Cancer Cells. Biochem. J. 2001;358:249–255. doi: 10.1042/bj3580249.

Di Paola R, Fusco R, Impellizzeri D, Cordaro M, Britti D, Morittu VM, Evangelista M, Cuzzocrea S. Adelmidrol, in combination with hyaluronic acid, displays increased anti-inflammatory and analgesic effects against monosodium iodoacetate-induced osteoarthritis in rats. Arthritis Res Ther. 2016 Dec 12;18(1):291. doi: 10.1186/s13075-016-1189-5. PMID: 27955699; PMCID: PMC5153857.

Esposito G, Capoccia E, Turco F, Palumbo I, Lu J, Steardo A, Cuomo R, Sarnelli G, Steardo L. Palmitoylethanolamide improves colon inflammation through an enteric glia/toll like receptor 4-dependent PPAR-α activation. Gut. 2014 Aug;63(8):1300-12. doi: 10.1136/gutjnl-2013-305005. Epub 2013 Sep 30. PMID: 24082036.

Esposito G, Corpetti C, Pesce M, Seguella L, Annunziata G, Del Re A, Vincenzi M, Lattanzi R, Lu J, Sanseverino W, Sarnelli G. A Palmitoylethanolamide Producing Lactobacillus paracasei Improves Clostridium difficile Toxin A-Induced Colitis. Front Pharmacol. 2021 Apr 27;12:639728. doi: 10.3389/fphar.2021.639728. PMID: 33986673; PMCID: PMC8111445.

Esposito G, Pesce M, Seguella L, Lu J, Corpetti C, Del Re A, De Palma FDE, Esposito G, Sanseverino W, Sarnelli G. Engineered Lactobacillus paracasei Producing Palmitoylethanolamide (PEA) Prevents Colitis in Mice. Int J Mol Sci. 2021 Mar 14;22(6):2945. doi: 10.3390/ijms22062945. PMID: 33799405; PMCID: PMC7999950.

Fooladi S, Rabiee N, Iravani S. Genetically engineered bacteria: a new frontier in targeted drug delivery. J Mater Chem B. 2023 Nov 1;11(42):10072-10087. doi: 10.1039/d3tb01805a. PMID: 37873584.

Fusco R, Cordaro M, Genovese T, Impellizzeri D, Siracusa R, Gugliandolo E, Peritore AF, D'Amico R, Crupi R, Cuzzocrea S, Di Paola R. Adelmidrol: A New Promising Antioxidant and Anti-Inflammatory Therapeutic Tool in Pulmonary Fibrosis. Antioxidants (Basel). 2020 Jul 9;9(7):601. doi: 10.3390/antiox9070601. PMID: 32660140; PMCID: PMC7402091.

Grabacka M, Pierzchalska M, Płonka PM, Pierzchalski P. The Role of PPAR Alpha in the Modulation of Innate Immunity. International Journal of Molecular Sciences. 2021; 22(19):10545. https://doi.org/10.3390/ijms221910545

Guida F, Rocco M, Luongo L, Persiani P, Vulpiani MC, Nusca SM, Maione S, Coluzzi F. Targeting Neuroinflammation in Osteoarthritis with Intra-Articular Adelmidrol. Biomolecules. 2022 Oct 11;12(10):1453. doi: 10.3390/biom12101453. PMID: 36291664; PMCID: PMC9599300.

Iannotta M, Belardo C, Trotta MC, Iannotti FA, Vitale RM, Maisto R, Boccella S, Infantino R, Ricciardi F, Mirto BF, Ferraraccio F, Panarese I, Amodeo P, Tunisi L, Cristino L, D'Amico M, Di Marzo V, Luongo L, Maione S, Guida F. N-palmitoyl-D-glucosamine, a Natural Monosaccharide-Based Glycolipid, Inhibits TLR4 and Prevents LPS-Induced

Inflammation and Neuropathic Pain in Mice. Int J Mol Sci. 2021 Feb 2;22(3):1491. doi: 10.3390/ijms22031491. PMID: 33540826; PMCID: PMC7867376.

Impellizzeri D, Di Paola R, Cordaro M, Gugliandolo E, Casili G, Morittu VM, Britti D, Esposito E, Cuzzocrea S. Adelmidrol, a palmitoylethanolamide analogue, as a new pharmacological treatment for the management of acute and chronic inflammation. Biochem Pharmacol. 2016 Nov 1;119:27-41. doi: 10.1016/j.bcp.2016.09.001. Epub 2016 Sep 4. Erratum in: Biochem Pharmacol. 2024 May;223:116105. doi: 10.1016/j.bcp.2024.116105. PMID: 27599446.

Jaana Mättö, Rangne Fondén, Tiina Tolvanen, Atte von Wright, Terttu VilpponenSalmela, Reetta Satokari, Maria Saarela, Intestinal survival and persistence of probiotic Lactobacillus and Bifidobacterium strains administered in triple-strain yoghurt, Volume 16, Issue 10, 2006, Pages 1174-1180, ISSN 0958-6946,https://doi.org/10.1016/j.idairyj.2005.10.007.

Korbecki J., Bobiński R., Dutka M. Self-Regulation of the Inflammatory Response by Peroxisome Proliferator-Activated Receptors. Inflamm. Res. 2019;68:443–458. doi: 10.1007/s00011-019-01231-1.

Kuipers EJ, Grady WM, Lieberman D, Seufferlein T, Sung JJ, Boelens PG, van de Velde CJ, Watanabe T. Colorectal cancer. Nat Rev Dis Primers. 2015 Nov 5;1:15065. doi: 10.1038/nrdp.2015.65. PMID: 27189416; PMCID: PMC4874655.

Labianca R, et al. Early colon cancer: ESMO Clinical Practice Guidelines for diagnosis, treatment and follow-up. Ann Oncol. 2013;24(Suppl 6):vi64–72. doi: 10.1093/annonc/mdt354.

Leleux J., Williams R.O. Recent advancements in mechanical reduction methods: Particulate systems. Drug. Dev. Ind. Pharm. 2014;40:289–300. doi: 10.3109/03639045.2013.828217.

Leyang Wu, Feifei Bao, Lin Li, Xingpeng Yin, Zichun Hua, Bacterially mediated drug delivery and therapeutics: Strategies and advancements,Advanced Drug Delivery

Reviews,Volume 187,2022,114363, ISSN 0169 409X,https://doi.org/10.1016/j.addr.2022.114363.

Lo Verme J., La Rana G., Russo R., Calignano A., Piomelli D. The Search for the Palmitoylethanolamide Receptor. Life Sci. 2005;77:1685–1698. doi: 10.1016/j.lfs.2005.05.012.

Maggiori L, Panis Y. Surgical management of IBD--from an open to a laparoscopic approach. Nat Rev Gastroenterol Hepatol. 2013 May;10(5):297-306. doi: 10.1038/nrgastro.2013.30. Epub 2013 Feb 19. PMID: 23419288.

Noce A, Albanese M, Marrone G, Di Lauro M, Pietroboni Zaitseva A, Palazzetti D, Guerriero C, Paolino A, Pizzenti G, Di Daniele F, Romani A, D'Agostini C, Magrini A, Mercuri NB, Di Daniele N. Ultramicronized Palmitoylethanolamide (um-PEA): A New Possible Adjuvant Treatment in COVID-19 patients. Pharmaceuticals (Basel). 2021 Apr 6;14(4):336. doi: 10.3390/ph14040336. PMID: 33917573; PMCID: PMC8067485.

Pagano E, Venneri T, Lucariello G, Cicia D, Brancaleone V, Nanì MF, Cacciola NA, Capasso R, Izzo AA, Borrelli F, Romano B. Palmitoylethanolamide Reduces Colon Cancer Cell Proliferation and Migration, Influences Tumor Cell Cycle and Exerts In Vivo Chemopreventive Effects. Cancers (Basel). 2021 Apr 16;13(8):1923. doi: 10.3390/cancers13081923. PMID: 33923494; PMCID: PMC8073478.

Palenca I, Basili Franzin S, Zilli A, Seguella L, Troiani A, Pepi F, Vincenzi M, Giugliano G, Catapano V, Di Filippo I, Sarnelli G, Esposito G. N-palmitoyl-d-glucosamine limits mucosal damage and VEGF-mediated angiogenesis by PPARα-dependent suppression of pAkt/mTOR/HIF1α pathway and increase in PEA levels in AOM/DSS colorectal carcinoma in mice. Phytother Res. 2024 Sep 5. doi: 10.1002/ptr.8303. Epub ahead of print. PMID: 39235753.

Palenca I, Seguella L, Del Re A, Franzin SB, Corpetti C, Pesce M, Rurgo S, Steardo L, Sarnelli G, Esposito G. N-Palmitoyl-D-Glucosamine Inhibits TLR-4/NLRP3 and Improves DNBS-Induced Colon Inflammation through a PPAR-α-Dependent Mechanism.

Biomolecules. 2022 Aug 22;12(8):1163. doi: 10.3390/biom12081163. PMID: 36009057; PMCID: PMC9405927.

Palenca I, Seguella L, Zilli A, Basili Franzin S, Del Re A, Pepi F, Troiani A, Pesce M, Rurgo S, De Palma FDE, Luglio G, Tropeano FP, Sarnelli G, Esposito G. Intrarectal Administration of Adelmidrol plus Hyaluronic Acid Gel Ameliorates Experimental Colitis in Mice and Inhibits Pro-Inflammatory Response in Ex Vivo Cultured Biopsies Derived from Ulcerative Colitis-Affected Patients. Int J Mol Sci. 2023 Dec 21;25(1):165. doi: 10.3390/ijms25010165. PMID: 38203336; PMCID: PMC10778920.

Patel SG, Karlitz JJ, Yen T, Lieu CH, Boland CR. The rising tide of early-onset colorectal cancer: a comprehensive review of epidemiology, clinical features, biology, risk factors, prevention, and early detection. Lancet Gastroenterol Hepatol. 2022 Mar;7(3):262-274. doi: 10.1016/S2468-1253(21)00426-X. Epub 2022 Jan 26. PMID: 35090605.

Peritore AF, D'Amico R, Siracusa R, Cordaro M, Fusco R, Gugliandolo E, Genovese T, Crupi R, Di Paola R, Cuzzocrea S, Impellizzeri D. Management of Acute Lung Injury: Palmitoylethanolamide as a New Approach. Int J Mol Sci. 2021 May 24;22(11):5533. doi: 10.3390/ijms22115533. PMID: 34073872; PMCID: PMC8197255.

Petrosino S., Cordaro M., Verde R., Schiano Moriello A., Marcolongo G., Schievano C., Siracusa R., Piscitelli F., Peritore A.F., Crupi R., et al. Oral ultramicronized palmitoylethanolamide: Plasma and tissue levels and spinal anti-hyperalgesic effect. Front Pharmacol. 2018;9:249. doi: 10.3389/fphar.2018.00249.

Pirozzi C, Coretti L, Opallo N, Bove M, Annunziata C, Comella F, Turco L, Lama A, Trabace L, Meli R, Lembo F, Mattace Raso G. Palmitoylethanolamide counteracts high-fat diet-induced gut dysfunction by reprogramming microbiota composition and affecting tryptophan metabolism. Front Nutr. 2023 Aug 1;10:1143004. doi: 10.3389/fnut.2023.1143004. PMID: 37599675; PMCID: PMC10434518.

Pithadia AB, Jain S. Treatment of inflammatory bowel disease (IBD). Pharmacol Rep. 2011;63(3):629-42. doi: 10.1016/s1734-1140(11)70575-8. PMID: 21857074.

Rankin L., Fowler C.J. The Basal Pharmacology of Palmitoylethanolamide. Int. J. Mol. Sci. 2020;21:7942. doi: 10.3390/ijms21217942.

Rao S., Song Y., Peddie F., Evans A.M. Particle size reduction to the nanometer range: A promising approach to improve buccal absorption of poorly water-soluble drugs. Int. J. Nanomed. 2011;6:1245–1251. doi: 10.2147/IJN.S19151.

Re G., Barbero R., Miolo A., Di Marzo V. Palmitoylethanolamide, Endocannabinoids and Related Cannabimimetic Compounds in Protection against Tissue Inflammation and Pain: Potential Use in Companion Animals. Vet. J. 2007;173:21–30. doi: 10.1016/j.tvjl.2005.10.003.

Sarnelli G, Gigli S, Capoccia E, Iuvone T, Cirillo C, Seguella L, Nobile N, D'Alessandro A, Pesce M, Steardo L, Cuomo R, Esposito G. Palmitoylethanolamide Exerts Antiproliferative Effect and Downregulates VEGF Signaling in Caco-2 Human Colon Carcinoma Cell Line Through a Selective PPAR-α-Dependent Inhibition of Akt/mTOR Pathway. Phytother Res. 2016 Jun;30(6):963-70. doi: 10.1002/ptr.5601. Epub 2016 Mar 1. PMID: 26929026.

Sarnelli G, Pesce M, Seguella L, Lu J, Efficie E, Tack J, Elisa De Palma FD, D'Alessandro A, Esposito G. Impaired Duodenal Palmitoylethanolamide Release Underlies Acid-Induced Mast Cell Activation in Functional Dyspepsia. Cell Mol Gastroenterol Hepatol. 2021;11(3):841-855. doi: 10.1016/j.jcmgh.2020.10.001. Epub 2020 Oct 14. PMID: 33065341; PMCID: PMC7858681.

Stefania Nobili, Laura Micheli, Elena Lucarini, Alessandra Toti, Carla Ghelardini, Lorenzo Di Cesare Mannelli, Ultramicronized N-palmitoylethanolamine associated with analgesics: Effects against persistent pain, Pharmacology & Therapeutics,Volume 258,2024,108649,ISSN 0163-7258,https://doi.org/10.1016/j.pharmthera.2024.108649.

Takano R., Furumoto K., Shiraki K., Takata N., Hayashi Y., Aso Y., Yamashita S. Rate-limiting steps of oral absorption for poorly water-soluble drugs in dogs; prediction from a

miniscale dissolution test and a physiologically-based computer simulation. Pharm. Res. 2008;25:2334–2344. doi: 10.1007/s11095-008-9637-9.

Van Cutsem E, Cervantes A, Nordlinger B, Arnold D. Metastatic colorectal cancer: ESMO Clinical Practice Guidelines for diagnosis, treatment and follow-up†. Ann Oncol. 2014;25(Suppl 3):iii1–9. doi: 10.1093/annonc/mdu260. European Society of Medical Oncology guidelines for management of metastatic colorectal cancer.

Willett CG, et al. Direct evidence that the VEGF-specific antibody bevacizumab has antivascular effects in human rectal cancer. Nat Med. 2004;10:145–7. doi: 10.1038/nm988.

Windsor JW, Kaplan GG. Evolving Epidemiology of IBD. Curr Gastroenterol Rep. 2019 Jul 23;21(8):40. doi: 10.1007/s11894-019-0705-6. PMID: 31338613.

Yang XY, Wang LH, Farrar WL. A Role for PPARgamma in the Regulation of Cytokines in Immune Cells and Cancer. PPAR Res. 2008;2008:961753. doi: 10.1155/2008/961753. Retraction in: PPAR Res. 2015;2015:982750. doi: 10.1155/2015/982750. PMID: 18566687; PMCID: PMC2430015.